EFFECT OF IRON AND BISMUTH ADDITION ON THE MICROSTRUCTURE AND MECHANICAL PROPERTIES OF SAC105 SOLDER UNDER SEVERE THERMAL ENVIRONMENT

BAKHTIAR ALI

FACULTY OF ENGINEERING
UNIVERSITY OF MALAYA
KUALA LUMPUR

2017

EFFECT OF IRON AND BISMUTH ADDITION ON THE MICROSTRUCTURE AND MECHANICAL PROPERTIES OF SAC105 SOLDER UNDER SEVERE THERMAL ENVIRONMENT

BAKHTIAR ALI

DISSERTATION SUBMITTED IN FULFILMENT OF THE REQUIREMENTS FOR THE DEGREE OF MASTER OF ENGINEERING SCIENCE

FACULTY OF ENGINEERING
UNIVERSITY OF MALAYA
KUALA LUMPUR

2017

UNIVERSITY OF MALAYA

ORIGINAL LITERARY WORK DECLARATION

Name of Candidate: **Bakhtiar Ali**

Registration/Matric No: **KGA150023**

Name of Degree: **MASTER OF ENGINEERING SCIENCE**

Title of Project Paper/Research Report/Dissertation/Thesis ("this Work"):

EFFECT OF IRON AND BISMUTH ADDITION ON THE MICROSTRUCTURE AND MECHANICAL PROPERTIES OF SAC105 SOLDER UNDER SEVERE THERMAL ENVIRONMENT

Field of Study: **Mechanical Engineering**

I do solemnly and sincerely declare that:

(1) I am the sole author/writer of this Work;
(2) This Work is original;
(3) Any use of any work in which copyright exists was done by way of fair dealing and for permitted purposes and any excerpt or extract from, or reference to or reproduction of any copyright work has been disclosed expressly and sufficiently and the title of the Work and its authorship have been acknowledged in this Work;
(4) I do not have any actual knowledge nor do I ought reasonably to know that the making of this work constitutes an infringement of any copyright work;
(5) I hereby assign all and every rights in the copyright to this Work to the University of Malaya ("UM"), who henceforth shall be owner of the copyright in this Work and that any reproduction or use in any form or by any means whatsoever is prohibited without the written consent of UM having been first had and obtained;
(6) I am fully aware that if in the course of making this Work I have infringed any copyright whether intentionally or otherwise, I may be subject to legal action or any other action as may be determined by UM.

Candidate's Signature Date:

Subscribed and solemnly declared before,

Witness's Signature Date:

Name:

Designation:

ABSTRACT

The transition to lead-free soldering for the electronic industry has been necessitated by the health and environmental concerns over the usage of lead and lead-containing products. Many lead-free solders have been extensively researched for this purpose. Amongst all, the near-eutectic Sn-3.0Ag-0.5Cu (SAC305) and Sn-4.0Ag-0.5Cu (SAC405) solders were termed as the most suitable replacements for lead-tin (Sn-Pb) solder, particularly in surface mount technology (SMT), owing to the excellent electrical and thermal properties of Ag and Cu. However, due to their low reliability during high strain rate exposures, like drop and shock and the high cost of Ag, various SAC solder alloys with lower-Ag-content have been suggested, including 98.5Sn-1.0Ag-0.5Cu (SAC105). Nevertheless, their low mechanical performance as well as low stability during thermal exposures limit their range of applications. A limited number of studies have indicated that the addition of alloying elements to the low-Ag-content SAC solders can improve their mechanical properties as well as stabilize their properties under high temperature exposures. This work aims to investigate the effect of iron (Fe) and bismuth (Bi) addition on the microstructural and mechanical properties of Sn-1Ag-0.5Cu (SAC105) solder alloy under severe thermal exposures. The isothermal aging was done at 200 °C for 100 h, 200 h, and 300 h. The average grain size significantly reduced with Fe/Bi addition to the base alloy Sn-1Ag-0.5Cu and remained literally the same after thermal aging. Fe/Bi added Sn-1Ag-0.5Cu showed a significant reduction in the IMCs size (Ag_3Sn and Cu_6Sn_5), especially the Cu_6Sn_5 IMCs and a refinement in the microstructure, which is due to the presence of Bi in the alloys. Moreover, their microstructure remained much more stable under severe thermal aging conditions, which is due to the presence of both Fe and Bi in the alloy. The tensile testing results showed that Fe/Bi addition to Sn-1Ag-0.5Cu significantly improved the tensile properties. Likewise, the impact absorbed energy increased by about 20% with the 0.05 wt.% Fe and

1 wt.% Bi addition to the Sn-1Ag-0.5Cu alloy and literally no further improvement was observed by increasing the Bi content in the alloy. The addition of Fe/Bi to Sn-1Ag-0.5Cu increased the hardness of the alloy by more than two fold. Shear strength almost doubled for the Fe/Bi added Sn-1Ag-0.5Cu, as compared to the base alloy. Improvements in these mechanical properties is due to the Bi solid solution strengthening mechanism. Under severe thermal aging, the Fe/Bi added Sn-1Ag-0.5Cu showed more stable mechanical properties than the base alloy, owing to the presence of both Fe and Bi in the alloys. The Fe/Bi added Sn-1Ag-0.5Cu solder alloys showed a potential for the severe thermal environments' applications of as high as 200 °C, along with low cost and much improved microstructure and mechanical properties.

ABSTRAK

Peralihan kepada pematerian bebas plumbum dalam industri elektronik diperlukan berikutan masalah kesihatan dan alam sekitar berhubung kebimbangan penggunaan plumbum dan produk yang mengandungi plumbum. Banyak pateri bebas plumbum telah dikaji untuk tujuan ini. Diantaranya, pateri Sn-3.0Ag-0.5Cu (SAC305) hampir eutektik dan Sn-4.0Ag-0.5Cu (SAC405) telah disebut sebagai pengganti yang paling sesuai untuk pateri plumbum timah (Sn-Pb), terutamanya dalam teknologi peletakan permukaan (SMT), oleh kerana sifat-sifat elektrik dan haba yang sangat baik daripada Ag dan Cu. Walau bagaimanapun, disebabkan kebolehpercayaan yang rendah semasa didedahkan kadar terikan yang tinggi, seperti jatuh dan kejutan dan kos yang tinggi untuk Ag, pelbagai aloi pateri SAC dengan kandungan rendah-Ag telah dicadangkan, termasuk 98.5Sn-1.0Ag-0.5Cu (SAC105) . Namun, prestasi mekanikal yang rendah serta kestabilan yang rendah semasa dedahan haba menghadkan aplikasi mereka. Beberapa kajian telah menunjukkan bahawa penambahan unsur-unsur pengaloian kepada pateri SAC kandungan rendah-Ag boleh menambahbaik sifat-sifat mekanikal mereka serta menstabilkan sifat-sifat mereka di bawah dedahan suhu yang tinggi. Kerja ini bertujuan untuk mengkaji kesan tambahan besi (Fe) dan bismut (Bi) kepada sifat-sifat mikrostruktur dan mekanikal pateri aloi Sn-1Ag-0.5Cu (SAC105) di bawah pendedahan haba yang teruk. Penuaan isoterma dilakukan pada suhu 200 °C untuk 100 jam, 200 jam, dan 300 jam. Purata saiz butiran berkurangan mendadak dengan tambahan Fe/Bi ke dalam aloi asas Sn-1Ag-0.5Cu dan kekal selepas penuaan haba. Sn-1Ag-0.5Cu ditambah Fe/Bi menunjukkan pengurangan saiz IMC (Ag_3Sn dan Cu_6Sn_5) yang ketara, terutama IMC Cu_6Sn_5 dan perbaikan dalam mikrostruktur, yang disebabkan oleh kehadiran Bi di dalam aloi. Selain itu, mikrostruktur mereka kekal lebih stabil di bawah keadaan penuaan haba yang teruk, yang mana disebabkan oleh kehadiran kedua-dua Fe dan Bi dalam aloi. Keputusan ujian tegangan menunjukkan bahawa tambahan Fe/Bi dalam Sn-1Ag-0.5Cu

meningkatkan sifat tegangan dengan ketara. Begitu juga, penyerapan tenaga hentakan meningkat kira-kira 20% dengan tambahan 0.05. wt.% Fe dan 1 wt.% Bi kepada aloi Sn-1Ag-0.5Cu dan tiada penambahbaikan diperhatikan lagi dengan meningkatkan kandungan Bi dalam aloi. Penambahan Fe/Bi dalam Sn-1Ag-0.5Cu meningkat kekerasan aloi lebih daripada dua kali ganda. Kekuatan ricih hampir dua kali ganda bagi Sn-1Ag-0.5Cu ditambah Fe/Bi, berbanding dengan aloi asas. Penambahbaikan dalam sifat-sifat mekanikal adalah disebabkan oleh mekanisme pengukuhan larutan pepejal Bi. Di bawah penuaan haba yang teruk, Sn-1Ag-0.5Cu ditambah Fe/Bi menunjukkan sifat-sifat mekanikal yang lebih stabil daripada aloi asas, oleh kerana kehadiran kedua-dua Fe dan Bi dalam aloi. Aloi pateri Sn-1Ag-0.5Cu ditambah Fe/Bi berpotensi untuk aplikasi persekitaran haba yang teruk sehingga setinggi 200 °C, juga dengan kos yang rendah dan mikrostruktur dan sifat-sifat mekanik yang ditambahbaik.

ACKNOWLEDGEMENTS

First of all, countless thanks to Almighty Allah Who is the most merciful. He enabled me to complete my research work successfully. I would express a deep sense of gratitude to my parents for their unending support and love from childhood to now, who taught me to do what I like and gave me the confidence and determination to achieve my goals. I also warmly acknowledge the unconditional love and blessings showed by my brother and sisters.

I feel honored to thank my respected research supervisor Assoc. Prof. Dr. Mohd Faizul Mohd Sabri for his support, motivation and constant encouragement during this work. His sincere guidance, sound advices and expertise always helped me in doing my research work. His dedication and enthusiasm for research will be a continuous source of inspiration for me. I would like to extend my sincere thanks and appreciation to my Co-supervisor Dr. Nazatul Liana Sukiman for her support and valuable suggestions during this work.

I deeply acknowledge the research facilities provided by Department of Mechanical Engineering in NME, Material Science and Electronic Packaging labs. I would like to thank the LCD and EM lab members who helped me in everything to make my work more interesting and enjoyable.

TABLE OF CONTENTS

Abstract iii

Abstrak v

Acknowledgements vii

Table of Contents viii

List of Figures xi

List of Tables xiv

List of Symbols and Abbreviations xv

CHAPTER 1: INTRODUCTION 1

1.1 Background 1

1.2 Aim, objectives and scope of the research 3

1.2.1 Aim of the research 3

1.2.2 Research objectives 3

1.2.3 Scope of study 4

1.3 Organization of the dissertation 4

CHAPTER 2: LITERATURE REVIEW 6

2.1 SAC solder series 6

2.2 Influence of Ag content on SAC solder alloy microstructure and mechanical properties 7

2.3 Influence of alloying elements on the microstructure and mechanical properties of low Ag Content SAC solder Alloys 9

2.4 Influence of alloying elements on the high temperature performance of Sn-based solder alloys 18

2.5 Microstructure coarsening 29

2.5.1 Coarsening Mechanism 29
2.5.2 Ostwald Ripening 30
2.5.3 Phase coarsening in SAC solder alloys 32
2.6 High temperature solders applications 34
2.6.1 Die-Attach Material 35
2.6.2 BGA Technology 35
2.6.3 Flip-Chip Technology 36
2.6.4 MCM Technology 37
2.6.5 CSP Technology 37
2.7 Summary 38

CHAPTER 3: METHODOLOGY 39

3.1 Introduction 39
3.2 Bulk solder specimen preparation 41
3.3 Isothermal aging treatment 43
3.4 Microstructural characterization 43
3.5 Tensile testing of specimens 46
3.6 Charpy impact testing of specimens 47
3.7 Microhardness tests of specimens 48
3.8 Shear testing of specimens 49
3.9 Summary 50

CHAPTER 4: RESULTS AND DISCUSSION 52

4.1 Qualitative microstructure study 52
4.2 Grains size evaluation 60
4.3 Quantitative microstructure study 62
4.4 Tensile Properties 63

4.5 Impact performance 67
4.6 Microhardness 71
4.7 Shear performance 75
4.8 Cost analysis 77
4.9 Summary 79

CHAPTER 5: CONCLUSION AND RECOMMENDATIONS 80

5.1 Conclusion 80
5.2 Recommendations 82

REFERENCES 83

LIST OF PUBLICATIONS 91

LIST OF FIGURES

Figure 2.1: The market share of different lead-free solders (Ma & Suhling, 2009) 6

Figure 2.2: Schematic diagram of Sn-rich region in the Sn-Ag-Cu solder ternary phase diagram (D. Kim et al., 2007; Suh et al., 2007) 7

Figure 2.3: Scheil solidification simulation of SAC305 and SAC105 (H. Kim et al., 2007) 8

Figure 2.4: Initial microstructure of SAC105 and SAC305 bulk solders (Terashima et al., 2003) 10

Figure 2.5: Effect of Zn addition to SAC105 on: (a) UTS, (b) yield stress, (c) percent elongation (H. Y. Song et al., 2010) 12

Figure 2.6: Effect of addition of Bi to Sn-0.3Ag-0.7Cu on: (a) melting reaction, (b) mechanical properties, and (c) aging resistance (Y. Liu, Sun, Yan, & Hu, 2008)..... 13

Figure 2.7: Micrographs of SAC105, SAC105-0.15Mn, SAC105-0.15Ti (Lin et al., 2009) 14

Figure 2.8: Effect of Ti and Mn on the mechanical properties of SAC105 (Lin et al., 2009) 15

Figure 2.9: Effect of Al addition to SAC105 on (a) drop-impact test and (b) bulk hardness (Y. W. Lee et al., 2010)..... 16

Figure 2.10: Effect of addition of Pd to Sn-1.2Ag-0.5Cu-0.4In on the (a) drop test, (b, c) mechanical properties, and (d) wetting properties (A. M. Yu et al., 2010) 18

Figure 2.11: SEM micrographs of cross-sectional view of Sn-3.5Ag-0.7Cu-xBi solder joints aged at 190 "C for 400 h: (a) x=0; (b) x=1.0; (c) x=2.0; (d) x=3.0; (e) x= 4.0; (f) x= 5.0 (G.-y. Li & Shi, 2006)..... 19

Figure 2.12: Average IMC thickness against aging time at aging temperature of 120 °C (G.-y. Li & Shi, 2006)..... 20

Figure 2.13: Grain size as a function of La content (Pei & Qu, 2008) 21

Figure 2.14: Particle size as a function of thermal aging condition (Pei & Qu, 2008)... 21

Figure 2.15: Average grain size versus La content for: (a) as-cast and (b) thermally aged samples (Sadiq et al., 2013) 22

Figure 2.16: Average IMC particle size versus La content for: (a) as-cast and (b) thermally aged samples (Sadiq et al., 2013)..... 23

Figure 2.17: Microhardness of Ti-bearing: (a) Sn-Ag and (b) Sn-Cu solder alloys aged at 200 °C up to 8 h (W. M. Chen et al., 2012) 24

Figure 2.18: Cross-polarized optical images of Ti-added solder alloys aged at 200 °C for 0 h, 2 h, 4 h and 8 h (W. M. Chen et al., 2012) 25

Figure 2.19: Micrographs of Sn–5Sb/Cu couple reacted at 260 °C for (a) 30 min, and (b) 180 min (C. Lee et al., 2007) 27

Figure 2.20: Effects of temperature on the average grain size of Sn–5Sb (Harry Schoeller, 2008) 28

Figure 2.21: Microstructure Evolution of SAC405 Solder Joints (S. L. Allen, Notis, M. R., Chromik, R. R., Vinci, R. P., 2004): (a) as soldering, (b) aged for 4 weeks at 152 °C. 33

Figure 2.22: Schematic diagram of BGA packaging (Intel-Corporation, 2010) 36

Figure 2.23: Chip level packaging using Au wire bonding (Kang et al., 2009) 38

Figure 3.1: Flow chart of the research work 40

Figure 3.2: Dimensions of the dog-bone shape tensile specimen 42

Figure 3.3: Prepared sample for microscopic study 44

Figure 3.4: IMCs particles analysis through ImageJ software 45

Figure 3.5: Schematic diagram for calculating the percent elongation and reduction in area 46

Figure 3.6: Schematic diagram showing the setup and principle of Charpy impact tester 48

Figure 3.7: Schematic diagram showing the shear testing setup and principle 50

Figure 4.1: FESEM micrographs for as-cast samples of: (a) SAC105, (b) SAC105-Fe-1Bi, (c) SAC105-Fe-2Bi 53

Figure 4.2: XRD analysis results for: (a) SAC105, (b) SAC105-Fe-1Bi and (c) SAC105-Fe-2Bi 54

Figure 4.3: EDX elemental mapping analysis of SAC105-Fe-2Bi solder alloy 55

Figure 4.4: FESEM micrographs of SAC105 after thermal aging at 200 °C for: (a) 100 h, (b) 200 h, (c) 300 h 57

Figure 4.5: FESEM micrographs of SAC105-Fe-1Bi after thermal aging at 200 °C for: (a) 100 h, (b) 200 h, (c) 300 h 58

Figure 4.6: FESEM micrographs of SAC105-Fe-2Bi after thermal aging at 200 °C for: (a) 100 h, (b) 200 h, (c) 300 h 59

Figure 4.7: Grains size of as-cast samples and thermally aged samples at 200 °C for 300 h: (a) SAC105 as-cast, (b) SAC105 aged, (c) SAC105-Fe-1Bi as-cast, (d) SAC105-Fe-1Bi aged, (e) SAC105-Fe-2Bi as-cast, and (f) SAC105-Fe-2Bi aged 61

Figure 4.8: Effect of thermal aging at 200 °C of SAC105, SAC105-Fe-1Bi and SAC105-Fe-2Bi on the tensile properties: (a) yield stress, (b) tensile strength, (c) total percent elongation, (d) percent reduction in area..... 65

Figure 4.9: Impact absorbed energy of the solder specimens during Charpy impact tests under severe thermal aging at 200 °C 68

Figure 4.10: Effect of thermal aging at 200 °C of SAC105, SAC105-Fe-1Bi and SAC105-Fe-2Bi on: (a) yield stress, (b) tensile strength, (c) total percent elongation, (d) modulus of toughness 69

Figure 4.11: Effect of thermal aging at 200 °C on the hardness of SAC105, SAC105-Fe-1Bi and SAC105-Fe-2Bi 72

Figure 4.12: The indentations made during Vickers hardness test on the surface of: (a) SAC105, (b) SAC105-Fe-1Bi and (c) SAC105-Fe-2Bi..... 74

Figure 4.13: Effect of thermal aging at 200 °C on the shear strength of SAC105, SAC105-Fe-1Bi and SAC105-Fe-2Bi..... 76

LIST OF TABLES

Table 2.1: The particle size exponent n values for coarsening processes with different rate-controlling mechanisms (S. L. Allen, Notis, M.R., Chromik, R.R., Vinci, R.P., 2004). 30

Table 2.2: Activation Energies for Diffusion and the Heats of Solution for Sn, Ag , Cu (S. L. Allen, Notis, M. R., Chromik, R. R., Vinci, R. P., 2004) 34

Table 3.1: Chemical composition of the alloys (wt.%)..... 42

Table 4.1: Effect of thermal aging 200°C on the average IMCs particles size of SAC105, SAC105-Fe-1Bi and SAC105-Fe-2Bi 63

Table 4.2: Two-sample t-test results comparing various tested samples 73

Table 4.3: Comparison of strength and hardness of SAC105, SAC105-Fe-1Bi and SAC105-Fe-2Bi 74

Table 4.4: Cost analysis of various solder alloys 78

Table 4.5: Summary of the key experimental findings 79

LIST OF SYMBOLS AND ABBREVIATIONS

RoHS	:	Restriction of Hazardous Substances
WEEE	:	Waste electronic and electrical equipment
SAC	:	Sn-Ag-Cu (Tin-Silver-Copper)
Wt.%	:	Weight percent
SAC405	:	Sn-4 wt.% Ag-0.5 wt.% Cu
SAC305	:	Sn 3 wt.% Ag-0.5 wt.% Cu
Sn–Pb	:	Tin-lead
SAC105	:	Sn-1 wt.% Ag-0.5 wt.% Cu
I/O	:	Input/ Output
IMCs	:	Intermetallic compounds
Sn-1Ag-0.5Cu	:	Sn-1 wt.% Ag-0.5 wt.% Cu
RE	:	Rare-earth
Sn-1.2Ag-0.5Cu-0.4In	:	Sn-1 wt.% Ag-0.5 wt.% Cu-0.4 wt.% In
Sn-1.2Ag-0.7Cu-.4In-.03Pd	:	Sn-1wt.% Ag-0.5 wt.% Cu-0.4 wt.% In--0.03wt.% Pd
Sn-3.5Ag	:	Sn-3.5 wt.% Ag
Sn3.6Ag0.9Cu	:	Sn-3.6 wt.% Ag-0.9 wt.% Cu
MEMS	:	Microelectromechanical systems
Sn–5Sb	:	Sn-5 wt.% Sb
Sn–10Sb	:	Sn–10 wt. % Sb
Tm	:	Melting temperature
Sn-25Ag-10Sb	:	Sn-25 wt. % Ag-10 wt. % Sb
CTE	:	Co-efficient of thermal expansion
Sn-4Cu	:	Sn-4 wt. % Cu
d	:	Particle size

t	:	Time
R	:	Average particles radius
υ	:	Molar volume
C_∞	:	Particle material solubility
γ	:	Surface energy or surface tension
T	:	Absolute temperature
Rg	:	Ideal gas constant
D	:	Diffusion coefficient
Q	:	Activation energy
K	:	Constant
Q_S	:	Heat of solution
Q_D	:	Activation energy for diffusion
FESEM	:	Field emission scanning electron microscope
EDX	:	Energy dispersive X-ray spectroscopy
XRD	:	X-ray diffraction
SAC105-Fe-1Bi	:	Sn-1 wt.% Ag-0.5 wt.% Cu-0.05 wt.% Fe--1 wt.% Bi
SAC105-Fe-2Bi	:	Sn-1 wt.% Ag-0.5 wt.% Cu-0.05 wt.% Fe--2 wt.% Bi
AES	:	Atomic emission spectrometry
ppm	:	Parts per million
h	:	Hour
SiC	:	Silicon carbide
UTS	:	Ultimate tensile strength
L_o	:	Gage length
L_f	:	Final gage length
A_o	:	Original cross sectional areas
A_f	:	Final cross sectional areas

E_1	:	Initial potential energy
E	:	Energy
H	:	Initial height
h	:	Final height
E_2	:	Final potential energy
U_t	:	Modulus of toughness
ε	:	Strain to failure
σ_{yp}	:	Yield stress
σ_{ult}	:	Ultimate tensile strength
HV	:	Vickers hardness number
F	:	Applied load
d	:	Mean diagonal of indentation

CHAPTER 1: INTRODUCTION

1.1 Background

The electronic industry has been pushed by strict government legislations on Restriction of Hazardous Substances (RoHS) and on the disposal of waste electronic and electrical equipment (WEEE), and consumers' demands towards lead-free solders due to the toxicity of lead (Pb). Thus, Pb-free solders require extensive development to replace Pb-containing solders in microelectronic applications. Near-eutectic Sn-Ag-Cu (SAC) lead-free solders, such as Sn-4 wt.% Ag-0.5 wt.% Cu (SAC405) and Sn- 3 wt.% Ag-0.5 wt.% Cu (SAC305), have been considered as good replacements for Sn–Pb solder alloy due to their favorable thermo-mechanical fatigue properties and their relatively low melting temperatures as compared to other lead-free solders. However, the portable electronic products containing these high Ag SAC solder joints are more susceptible to failure in drop and high impact applications (El-Daly, Fawzy, Mansour, & Younis, 2013). Furthermore, the high-Ag-content in SAC alloys makes these solders relatively more costly.

For economic viability and good reliability during high strain rate exposures, like drop and shock, various SAC solder alloys with lower-Ag-content have been suggested, including Sn-1 wt.% Ag-0.5 wt.% Cu (SAC105) (Cai, Suhling, Lall, & Bozack, 2012). However, the coarse microstructure, higher melting temperature and poor mechanical properties of these solder alloys limit their application (Shih & Lin, 2006; Wu, Yu, Law, & Wang, 2002). Various alloying elements, including Fe, Ag, Ni, Co, Au, Sb, Zn, Ce, La, Pd, Ca and Cr have been added to these Sn-based solder alloys to refine their microstructures, and improve their mechanical properties and wettability.

As a microelectronic package progressively demands smaller pitch, smaller solder bumps, more input/ output (I/O) counts and higher electric current per solder bump, flip–chip solder joints experience very high temperatures and thermal stresses (Seo, Kang, Shih, & Lee, 2009). The miniaturization of solder joints also leads to significant increase in the volume ratio of intermetallic compounds (IMCs), which could affect the reliability of the solder joint (Choudhury & Ladani, 2015). In addition, Sn–based solders, used in microelectronics, generally undergo microstructural coarsening during service (Dutta, Kumar, & Subbarayan, 2009). This microstructural coarsening results in continuous degradation of mechanical properties of the solder joint over time, and thus affects the long-term reliability of a microelectronic package (Dutta et al., 2009; C.-Y. Liu et al., 2014; Shen, Pu, Yin, Luo, & Chen, 2014). Moreover, the operating conditions of several new electronic systems demand service at high temperatures and thermal stress levels, particularly for industrial and automotive applications (Anderson & Harringa, 2004). These more challenging operating environments, combined with the push for enhanced reliability of all electronic packaging systems, demand continued studies of elevated aging effects of the emerging lead-free solders to replace Sn-Pb solders (Miller, Anderson, & Smith, 1994). Solder alloy properties can be improved by modifying the microstructure of the alloy by changing the number and/or character of the phases. The microstructure of the solder and the response of the alloy to heat treatment as well as the resulting mechanical properties are crucial to the evaluation of solder joint reliability. Owing to the high service temperature, it is imperative to characterize these properties at high temperatures.

In order to stabilize the microstructural and mechanical properties of these solders under severe thermal environments, iron (Fe) addition to these alloys has been suggested (D. A. Shnawah et al., 2012). Fe also improves the drop impact reliability of these solder alloys (D. A. Shnawah et al., 2012). Likewise, bismuth (Bi) addition has also been

reported to suppress the degradation of microstructure and mechanical properties with aging (Cai et al., 2012). Bi addition also improves the mechanical properties and the wetting/spreading behavior (Xiaowu Hu, Li, Liu, & Min, 2015; Huang & Wang, 2005; Vianco & Rejent, 1999b). In this work, we prepared iron (Fe) and bismuth (Bi) added SAC105 lead-free solder alloys and extensively investigated their microstructure and mechanical properties, including tensile properties, impact toughness, hardness and shear strength, under severe thermal environments, and compared the results with the base alloy SAC105.

1.2 Aim, objectives and scope of the research

1.2.1 Aim of the research

The aim of the research is to come up with solder alloy that can work at high temperature and is suitable for portable electronic products, as well as is economically viable and environmentally friendly.

1.2.2 Research objectives

The objectives of the research are as follows:

1. To develop the cost-effective low-Ag-content Sn-1Ag-0.5Cu (SAC105) by the addition of Fe and Bi.
2. To study the effect of Fe and Bi addition on the microstructure of SAC105 solder alloys.
3. To study the effect of Fe and Bi addition on the mechanical properties of SAC105 solder alloys.
4. To study the effect of high thermal aging on the microstructure and various mechanical properties of Fe/Bi-bearing SAC105 solders and to correlate the mechanical behavior of the alloys with their microstructure.

1.2.3 Scope of study

The scope of this research is to study the high temperature performance of Fe/Bi bearing SAC105 solder alloys in terms of its microstructure and mechanical properties. This study only focuses on the bulk solder and does not include the interfacial properties of the solder joints with different substrates. Also, in this study, only the experimental results are discussed, and the molecular modelling and simulation is not in the scope of this study.

1.3 Organization of the dissertation

This dissertation is organized in the following structure:

Chapter one: Introduction

This chapter presents the background of the research, research objectives and the organization of the dissertation.

Chapter two: Literature review

This chapter presents a thorough literature review relevant to the study. The literature review focuses on the effect of alloying elements on the microstructure and mechanical properties as well as on the high temperature performance of Sn-based solder alloys.

Chapter three: Research Methodology

This chapter elucidates the experimental procedure of alloys fabrication, samples preparation, thermal aging treatments as well as the evaluation of microstructural and mechanical properties.

Chapter four: Results and discussion

This chapter presents the findings of the research related to the microstructure, mechanical properties and high temperature reliability of Fe/Bi bearing SAC105 as well as an extensive discussion to interpret the results.

Chapter five: Conclusion and recommendations

This chapter provides the concluding remarks based on the results and discussion in the previous chapter and also the recommendations for future research.

CHAPTER 2: LITERATURE REVIEW

2.1 SAC solder series

The Sn-Ag-Cu (SAC) series of solder alloys has emerged as the most widely accepted among the numerous lead-free solder alloys proposed over the last decade, as shown in Figure 2.1 (Ma & Suhling, 2009). A variety of SAC solder alloys with different Ag contents, such as SAC105, SAC305 and SAC405, have been investigated and are currently in use in the electronics industry for a wide range of applications. Nevertheless, a particular Ag content can be either an advantage or a disadvantage depending on the application, packaging and reliability requirements (Kariya, Hosoi, Terashima, Tanaka, & Otsuka, 2004; D. Kim et al., 2007; Suh et al., 2007; Terashima, Kariya, Hosoi, & Tanaka, 2003). Obviously, using low-Ag-content makes the solder quite economical and vice versa, due to the high cost of Ag.

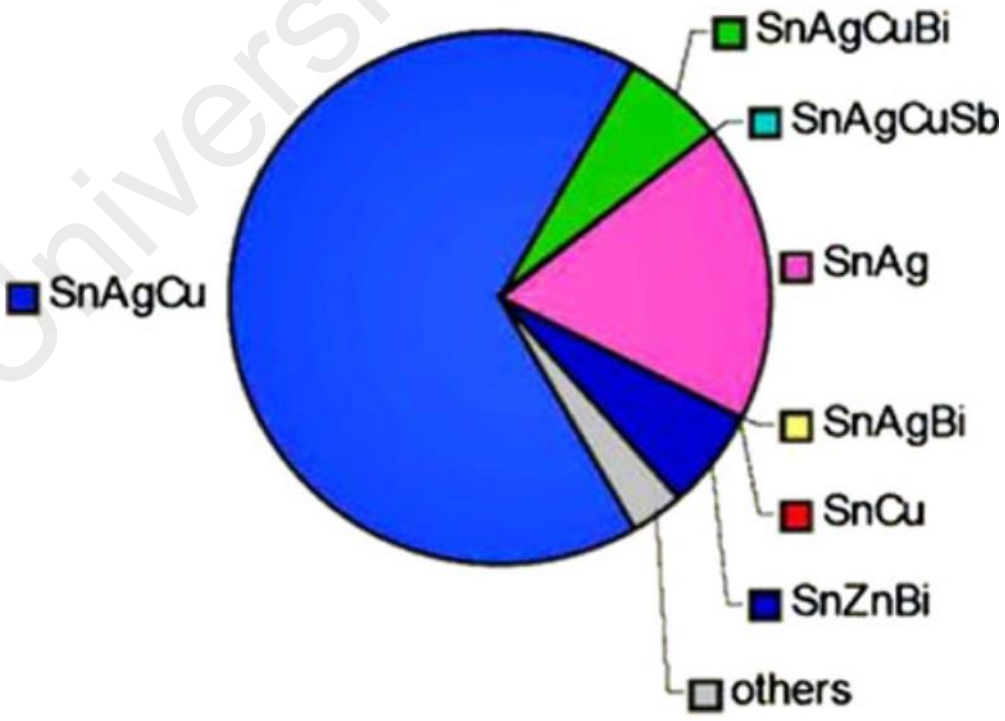

Figure 2.1: The market share of different lead-free solders (Ma & Suhling, 2009)

2.2 Influence of Ag content on SAC solder alloy microstructure and mechanical properties

As we know that microstructure features of an alloy play important role in its mechanical reliability (Anderson & Harringa, 2004). Therefore, the microstructural characteristics of SAC alloys is crucial for understanding their mechanical performance. It has been reported that the microstructures of the bulk SAC solder alloys consists of a primary β-Sn phase and two IMCs phases of Ag_3Sn and Cu_6Sn_5 distributed within an Sn-rich matrix (Kariya et al., 2004; J.-M. Song, Wu, & Huang, 2007; Terashima et al., 2003). The low-Ag-content SAC alloys make more primary β-Sn phase (Kariya et al., 2004; D. Kim et al., 2007; Suh et al., 2007; Terashima et al., 2003) as shown in Figure 2.2, i.e. the fraction of β-Sn in SAC105 was found to be 35%, while it was merely 11% in the SAC305 alloy (Figure 2.3).

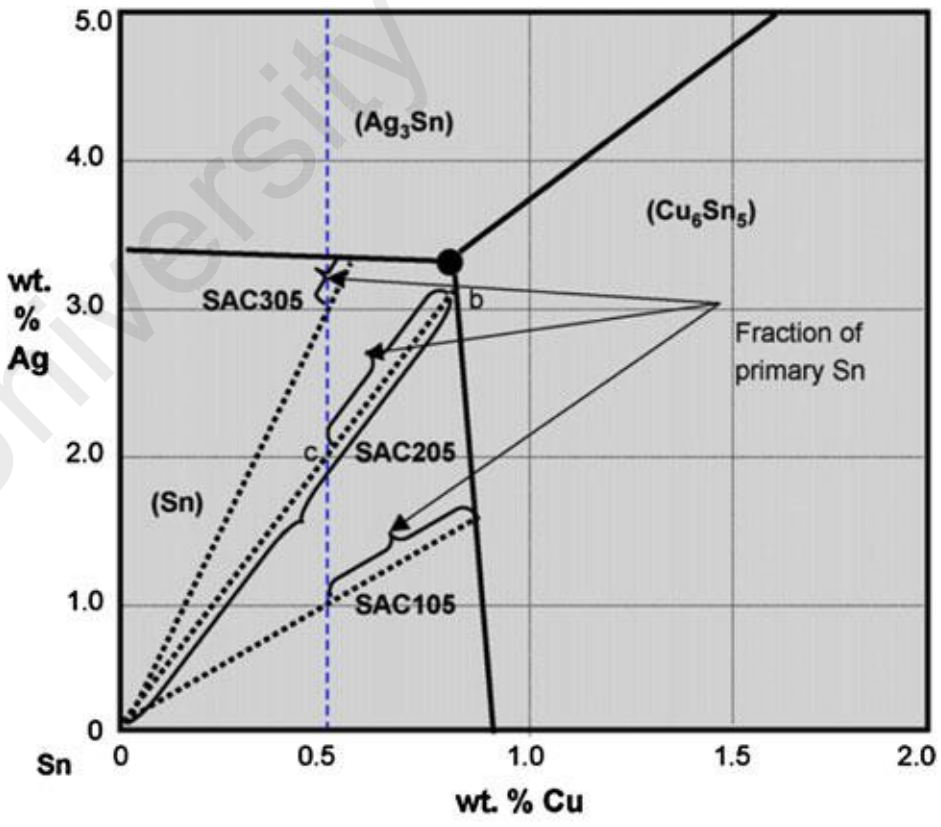

Figure 2.2: Schematic diagram of Sn-rich region in the Sn-Ag-Cu solder ternary phase diagram (D. Kim et al., 2007; Suh et al., 2007)

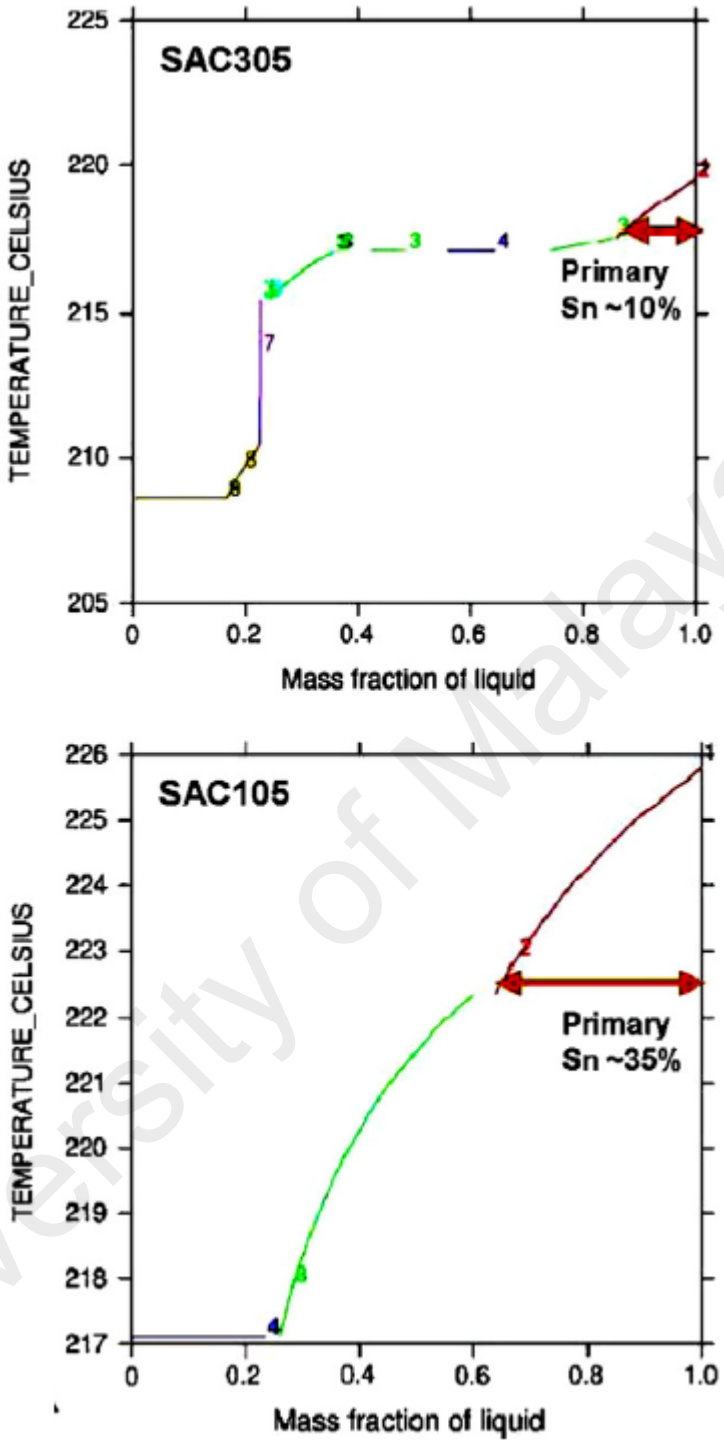

Figure 2.3: Scheil solidification simulation of SAC305 and SAC105 (H. Kim et al., 2007)

Furthermore, with an increase of the Ag content in the SAC solders, the amount of Ag_3Sn IMCs increases (Kariya et al., 2004; Terashima et al., 2003). This is because the Ag_3Sn is the only Ag-containing phase in the SAC solder alloy. Therefore, variation in Ag content also varies the whole microstructure of the SAC solders. It has been reported that the microstructure of the low-Ag-content SAC105 solder alloy consists of large primary β-Sn dendrites and fine Ag_3Sn IMCs sparsely dispersed within the inter-dendritic regions (Figure 2.4). On the other hand, the microstructure of the high-Ag-content SAC305 alloy is comprised of fine primary β-Sn dendrites and a large number of Ag_3Sn IMCs finely distributed within the interdendritic regions (Figure 2.4) (Kariya et al., 2004; Terashima et al., 2003). The primary β-Sn phase possesses lower elastic modulus and lower strength than the IMCs particles Cu_6Sn_5 and Ag_3Sn, which have much higher strength than the bulk material in the SAC alloys (D. Kim et al., 2007; Suh et al., 2007). As a result, the proportion of IMCs particles within the microstructure of a solder determines its overall mechanical performance. This means that the presence of a high fraction of the primary β-Sn phase reduces the strength and elastic modulus while improves the ductility of the alloy, whereas a large amount of Ag_3Sn and Cu_6Sn_5 phases increases the strength and elastic modulus while embrittles the solder.

2.3 Influence of alloying elements on the microstructure and mechanical properties of low Ag Content SAC solder Alloys

Various studies have shown that the addition of alloying elements, such as Zn, Co, Fe, Bi, Mn, Ti, Ni, Al, Ce, In and Pd to low-Ag SAC solder alloys can significantly improve their microstructural and mechanical properties and thus these elements have attracted considerable attention.

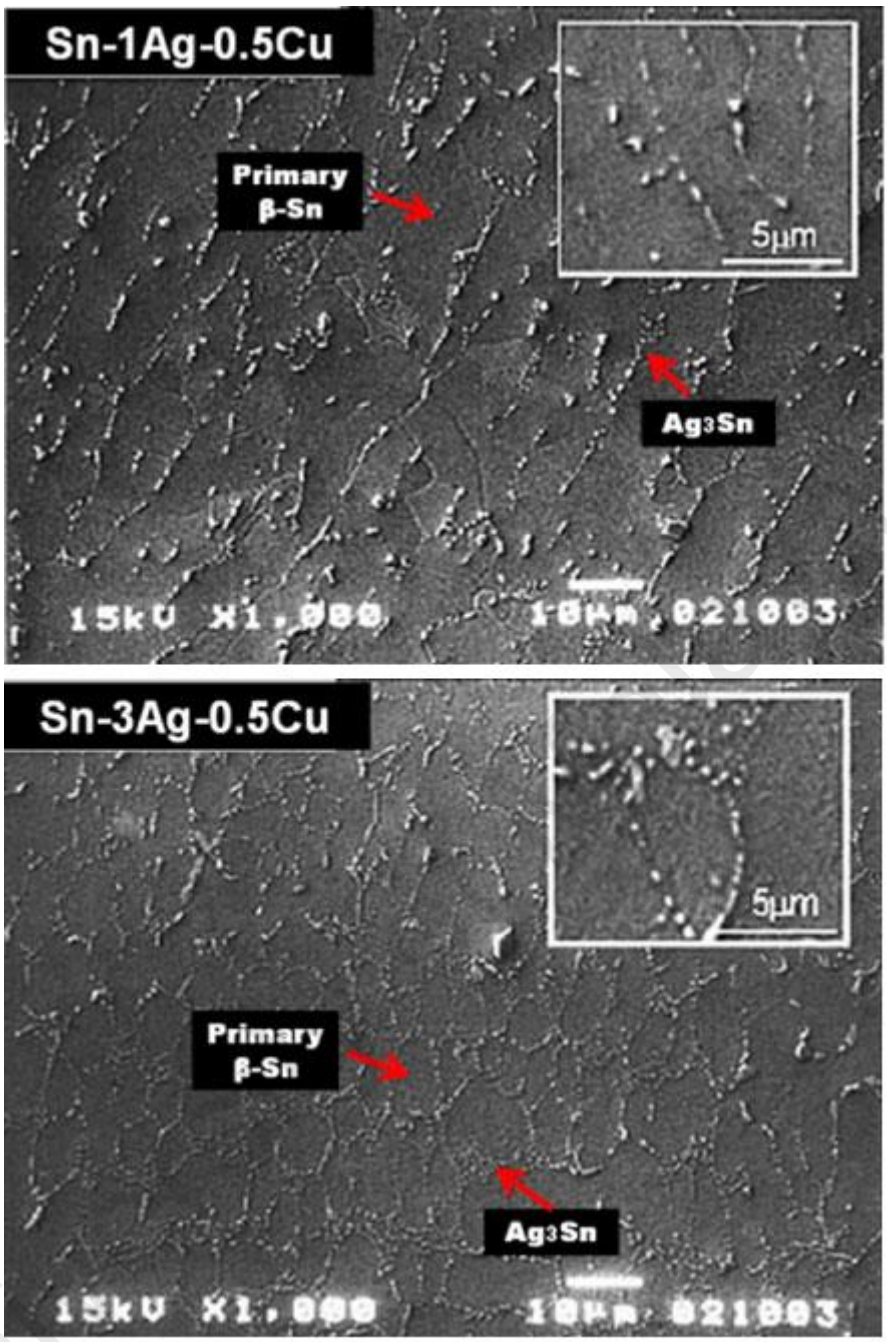

Figure 2.4: Initial microstructure of SAC105 and SAC305 bulk solders (Terashima et al., 2003)

Zinc (Zn) has got considerable attention due to its ability to slow down the growth of the IMCs layers and hinder the Kirkendall voids formation (T.-H. Chuang & Lin, 2008; F.-J. Wang, Gao, Ma, & Qian, 2006; H. Wang, Fang, Xu, & Zhang, 2015). Furthermore, it has been reported that Zn addition to Sn-based solders can also enhance the strength

and creep resistance of the solder alloys (Fawzy, 2007; McCormack, Jin, Kammlott, & Chen, 1993). (H. Y. Song, Zhu, Wang, Shang, & Lu, 2010) studied the effect of Zn on the tensile properties of SAC105 alloy and reported an improvement in strength but a decrease in ductility with the addition of Zn (Figure 2.5).

Studies have shown that the addition of Co or Fe to SAC solder alloys significantly improve the microstructure features and mechanical properties of the alloy. Co improves the impact reliability of the alloy by enhancing its ductility (Syed, Kim, Cho, Kim, & Yoo, 2006) as well as results in higher nucleation rate (Anderson & Harringa, 2004) and modifies the growth rate of the IMC layer between the solder and the circuit board metallization. Fe is reported to enhance the shear strength (Anderson & Harringa, 2004) as well as decrease the number of Kirkendall voids (K. S. Kim, Huh, & Suganuma, 2003). Fe also improves the drop impact reliability of these solder alloys (D. A. Shnawah et al., 2012).

(Weiping, Bachorik, & Ning-Cheng, 2008) found that the addition of 1 to 4.5 wt.% Bi to SAC solder alloys reduces the melting temperature of the alloy (Figure 2.6a). The Bi addition also results in an increase in the strength and a decrease the ductility (Figure 2.6b). Thus, the Bi content in the alloy needs to be optimum as an excess amount of Bi would reduce the bulk compliance as well as increase the melting range of the alloy. It was also found that Bi addition improves the aging resistance of the alloy (Weiping et al., 2008) (Figure 2.6c).

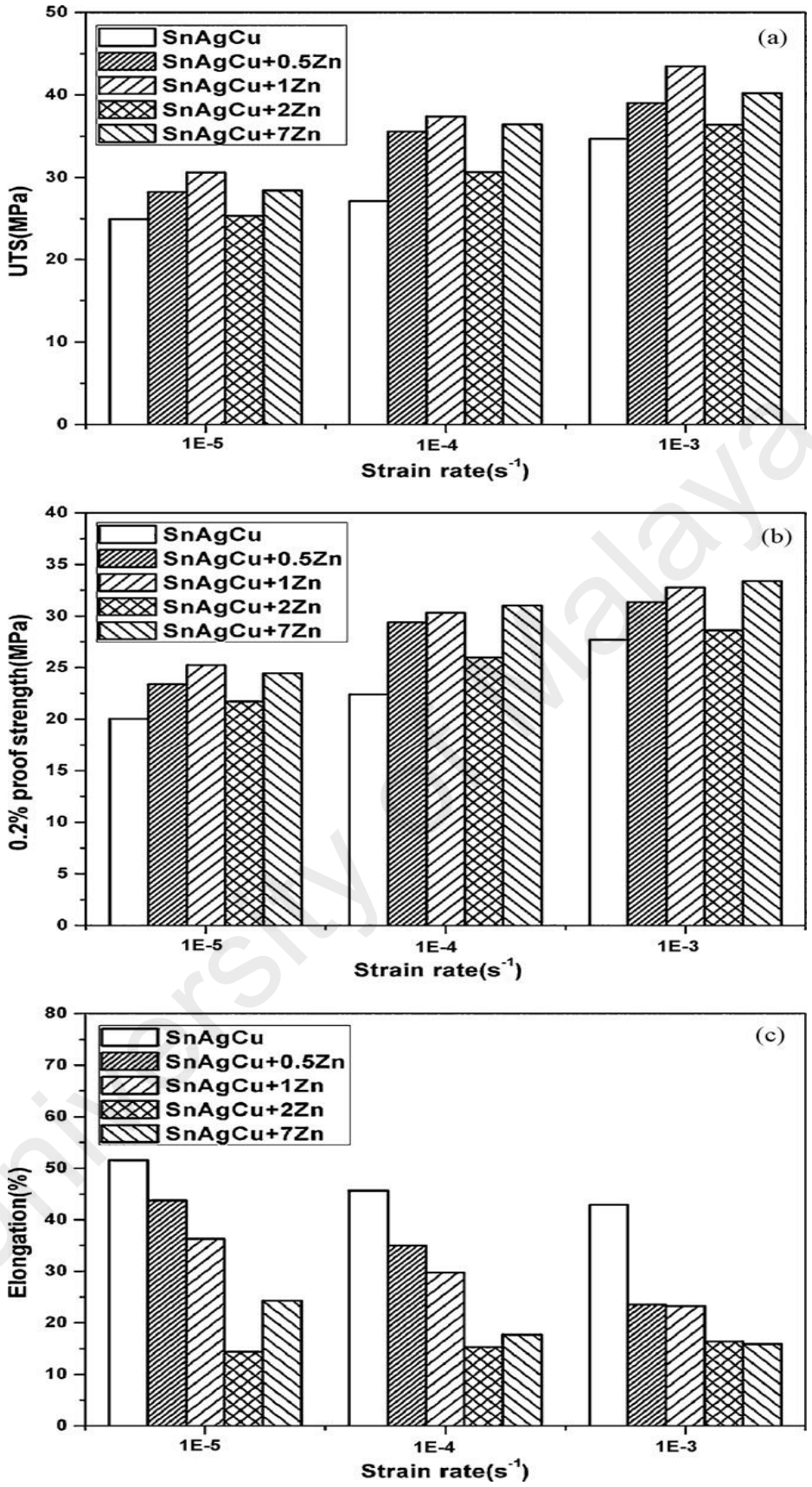

Figure 2.5: Effect of Zn addition to SAC105 on: (a) UTS, (b) yield stress, (c) percent elongation (H. Y. Song et al., 2010)

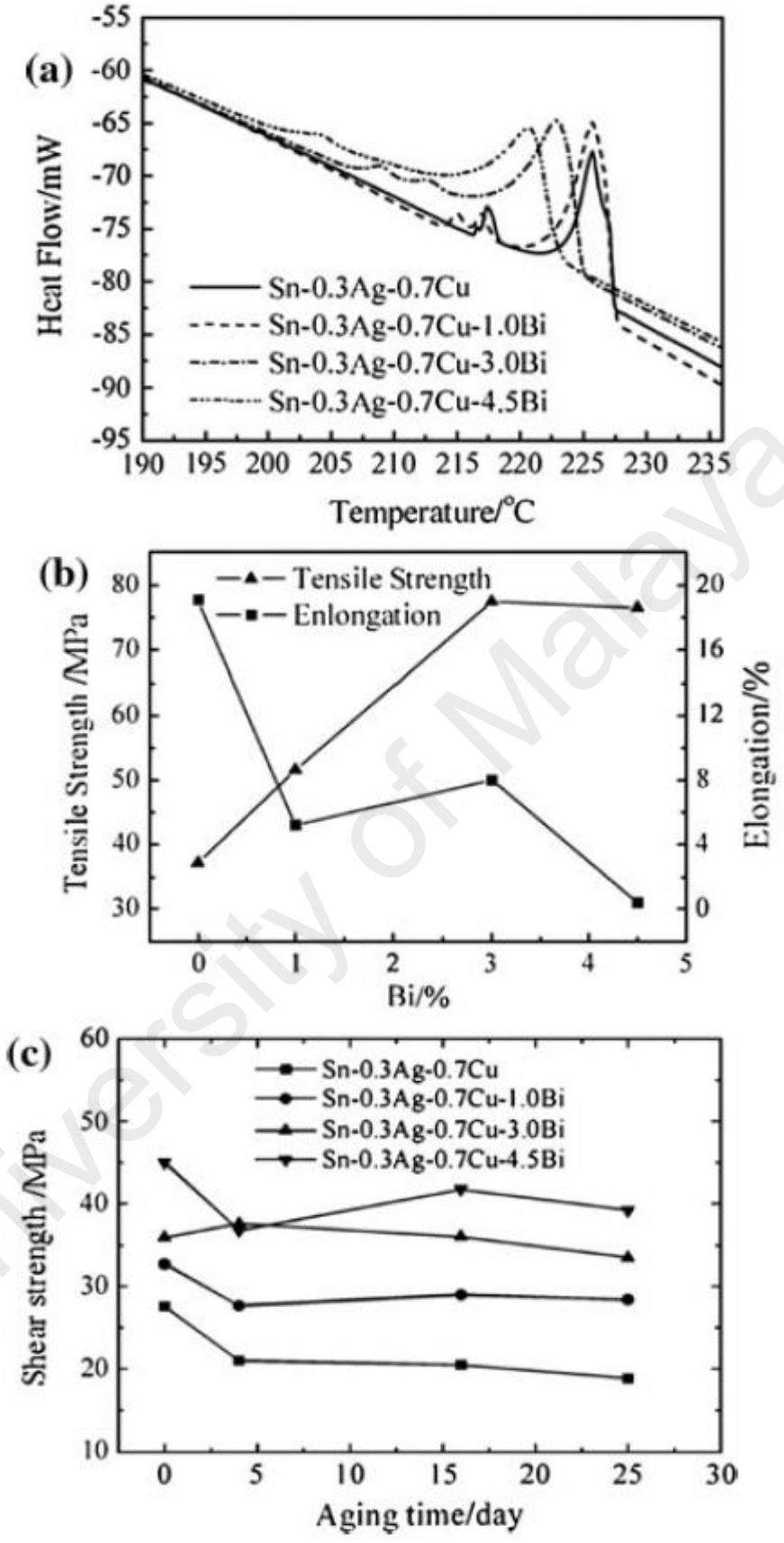

Figure 2.6: Effect of addition of Bi to Sn-0.3Ag-0.7Cu on: (a) melting reaction, (b) mechanical properties, and (c) aging resistance (Y. Liu, Sun, Yan, & Hu, 2008)

Transition metals such as Mn and Ti have also been reported to significantly improve the microstructural and mechanical properties of SAC105 solder alloys. (Lin et al., 2009) reported that Mn and Ti additions lead to a rapidly reduced undercooling as well as an extended volume fraction of pro-eutectic Sn with a refined dendritic size. These microstructural and thermal changes were ascribed to the formation of $MnSn_2$ and Ti_2Sn_3 IMCs, which are present in the Mn and Ti modified solder alloys, respectively (Figure 2.7). The addition of Mn and Ti were also reported to improve the ductility but decease the strength of the alloy (Fig. 2.8).

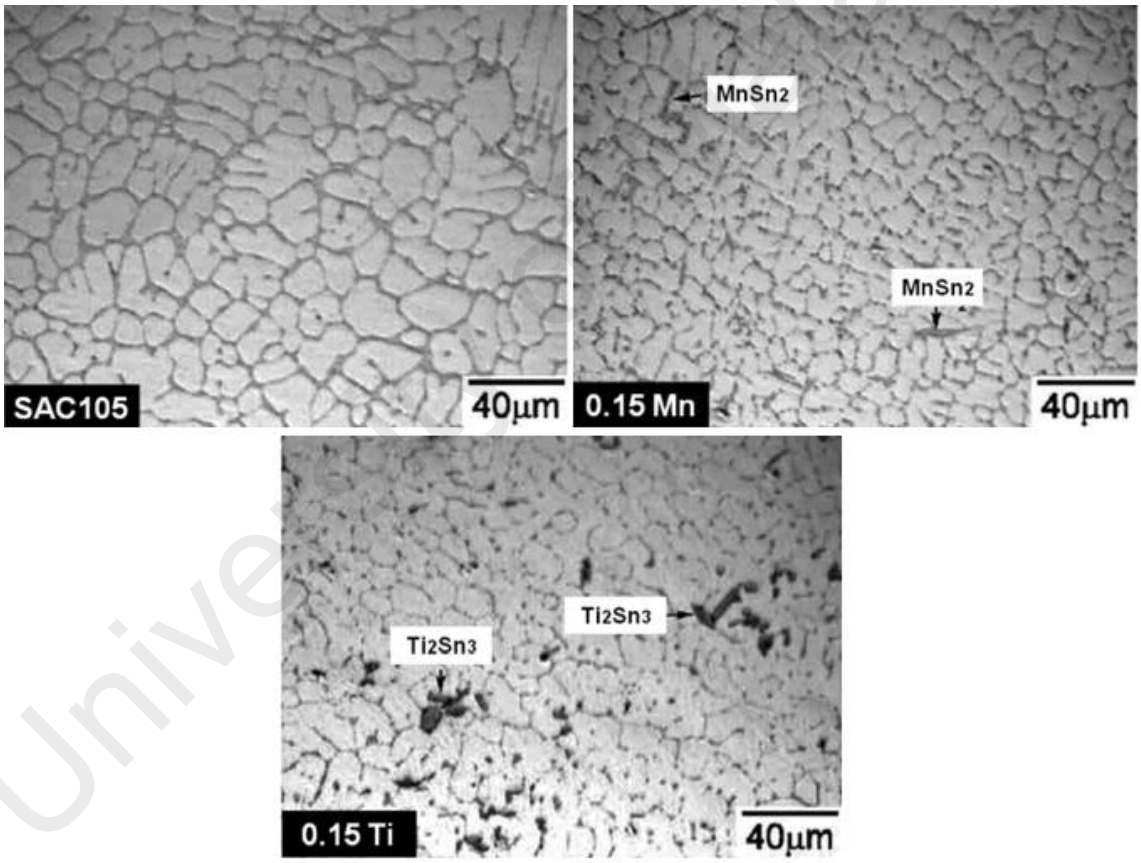

Figure 2.7: Micrographs of SAC105, SAC105-0.15Mn, SAC105-0.15Ti (Lin et al., 2009)

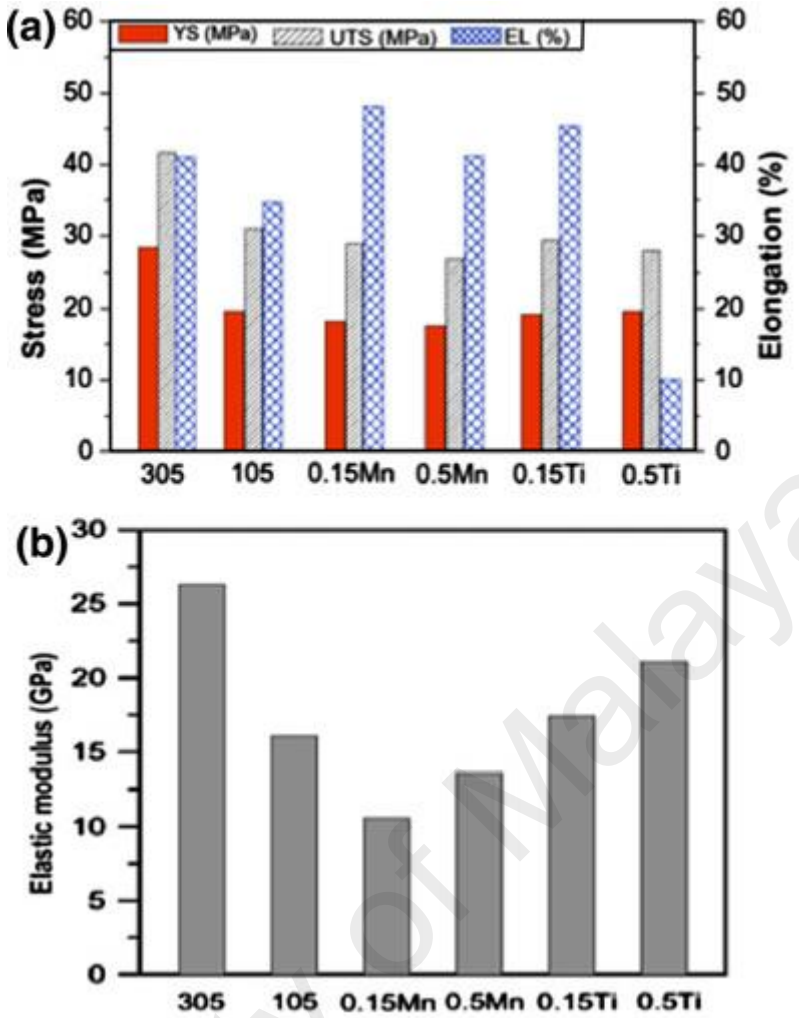

Figure 2.8: Effect of Ti and Mn on the mechanical properties of SAC105 (Lin et al., 2009)

Nickel (Ni) is one of the most widely used doping elements for SAC solders. Ni addition to SAC solder alloys gives the alloy a microstructure stability and controls its IMCs layer growth as well as increases its drop reliability (Anderson & Harringa, 2006; C.-M. Chuang & Lin, 2003; Gao, Takemoto, Nishikawa, & Komatsu, 2006).

Aluminum (Al) addition can enhance the bulk compliance and creep resistance of the solder alloy as well as change the composition and morphology of the IMC layer phases formed at the interface (Y. W. Lee, Kim, Kim, Lee, & Moon, 2010). Moreover, Al

addition can further improve the drop-impact performance of the SAC105 solder alloy, which is due to the higher bulk ductility of the Al-supplemented bulk solders (Figure 2.9).

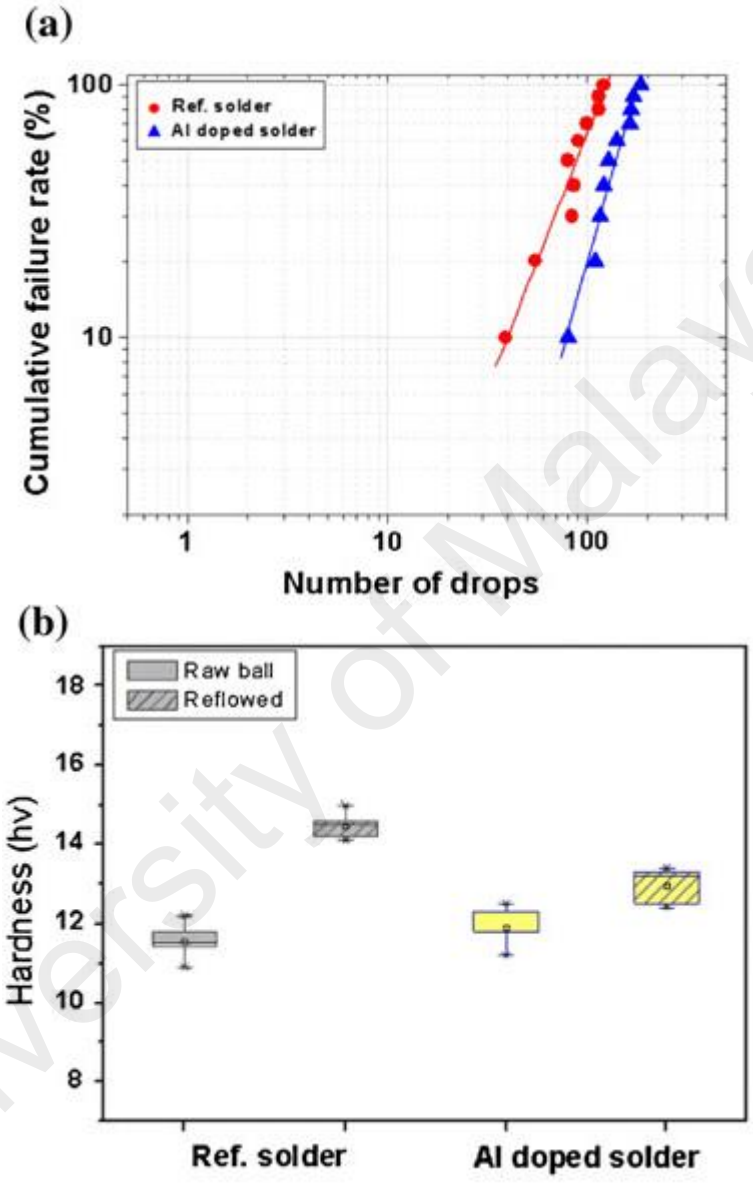

Figure 2.9: Effect of Al addition to SAC105 on (a) drop-impact test and (b) bulk hardness (Y. W. Lee et al., 2010)

Rare-earth (RE) elements are considered the ‘‘vitamins of metals,’’ which in small amount may significantly improve the properties of metals or alloys (B. Li et al., 2005). Cerium (Ce) addition was reported to lower the amount of undercooling for the β-Sn as well as refine the microstructure, which enhances the tensile strength of the alloy. RE elements tend to be absorbed at the grain boundary and decrease the boundary movement and, thus, increase the tensile strength of a solder joint (Wu, Yu, Law, & Wang, 2004).

Indium (In) addition to various lead-free solders was also studied by various researchers. However, its main disadvantages are due to its high cost and scarcity of supply. Nevertheless, all studies to date regarding addition of In to lead-free solder alloys showed superior solder performance, such as stable interfacial reaction and excellent wettability. Sn-1.2Ag-0.5Cu-0.4In solder joints were found to exhibit drop impact reliability that was better than that of SAC305 solder joints but lower than SAC105. Thus, In-bearing low-Ag SAC solder alloys tend to be strong candidates for use in portable electronic applications. The addition of fifth dopant palladium (Pd) was studied by (A. M. Yu, Kim, Lee, & Kim, 2010). It was reported that a small amount of Pd addition to Sn-1.2 Ag-0.7Cu-0.4In solder improved its drop-impact reliability, which was better than that of SAC105 alloy (Figure 2.10a) due to the higher plastic deformation capability of the Sn-1.2Ag-0.7Cu-0.4In-0.03Pd solder alloy. Figure 2.10b, c shows that the Sn-1.2Ag-0.7Cu-0.4In-0.03Pd alloy possesses the best tensile strength as well as elongation, and thus the highest impact energy. Nonetheless, Sn-1.2Ag-0.7Cu-.4In-.03Pd solder alloy showed a decrease in wettability as compared with Sn-1.2Ag- 0.7Cu-0.4In alloy at temperature lower than 240 °C. However, its wettability was still comparable with SAC305 solder alloy (Figure 2.10d).

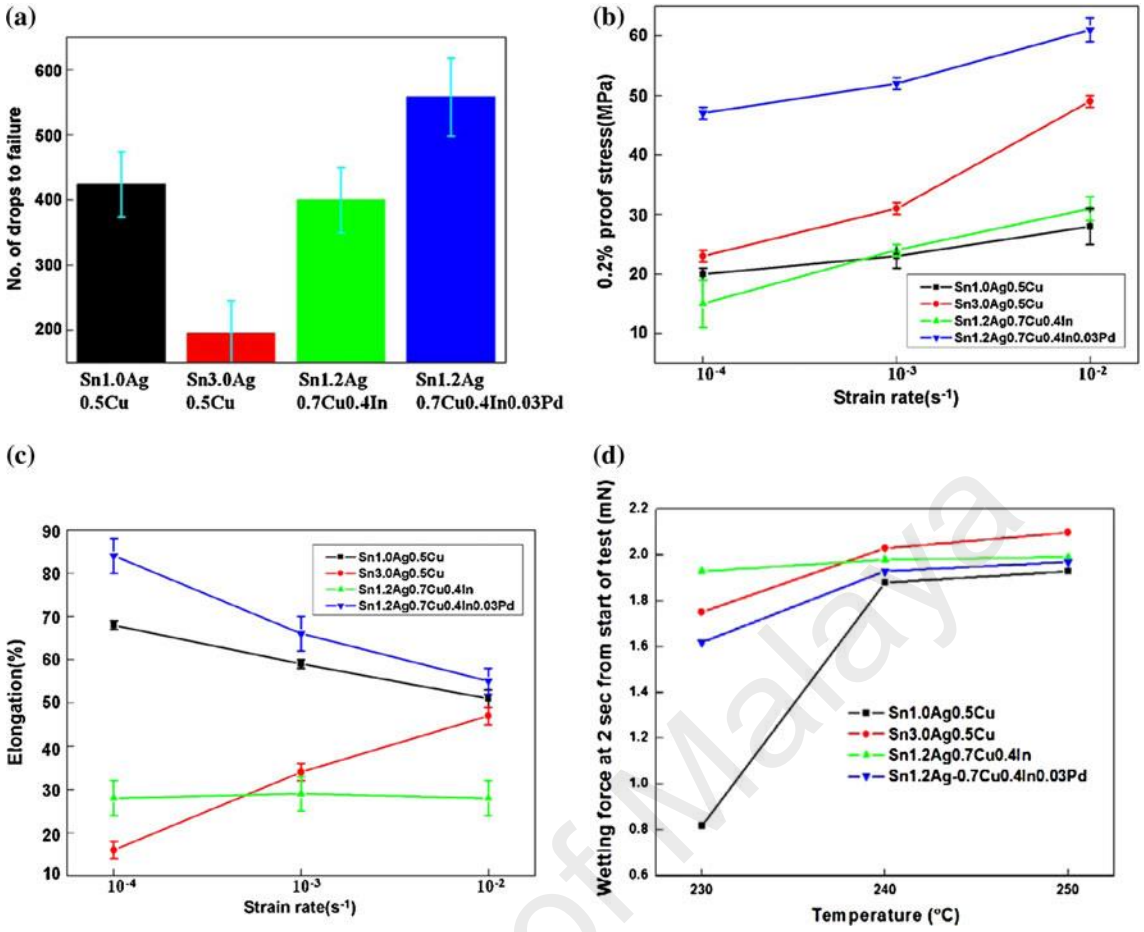

Figure 2.10: Effect of addition of Pd to Sn-1.2Ag-0.5Cu-0.4In on the (a) drop test, (b, c) mechanical properties, and (d) wetting properties (A. M. Yu et al., 2010)

2.4 Influence of alloying elements on the high temperature performance of Sn-based solder alloys

Various studies have been reported with an aim to develop the Sn-based solder alloys for elevated temperature applications (150-200 °C) by improving their high temperature performance with various alloying elements addition to them. (G.-y. Li & Shi, 2006) studied the bismuth (Bi)-bearing Sn-Ag-Cu solders under thermal aging at 190 °C and reported that the grain sizes become smaller and the IMC layers become thinner with the l % Bi addition (Figure 2.11). Moreover, it was reported that with about 1 % Bi addition, the activation energy of Sn-3.8Ag-0.7Cu solder alloy system gets to the highest value,

which results in reduction in the atomic diffusion rate so as to inhibit the excessive IMCs growth (Figure 2.12) (G.-y. Li & Shi, 2006). (Cai et al., 2012) also reported that Bi addition to Sn-based solders suppresses the degradation of microstructure and mechanical properties with aging.

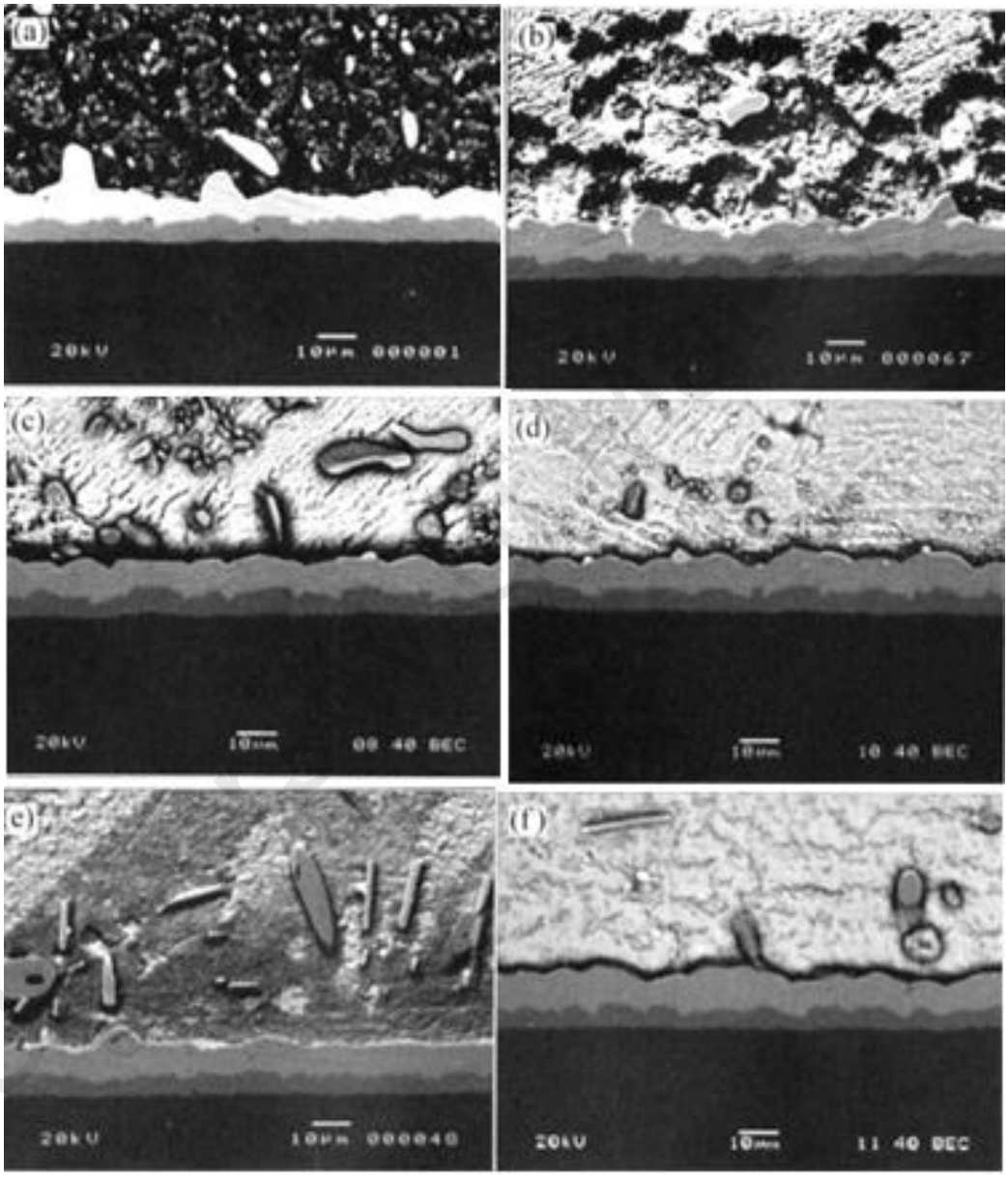

Figure 2.11: SEM micrographs of cross-sectional view of Sn-3.5Ag-0.7Cu-xBi solder joints aged at 190 "C for 400 h: (a) x=0; (b) x=1.0; (c) x=2.0; (d) x=3.0; (e) x= 4.0; (f) x= 5.0 (G.-y. Li & Shi, 2006)

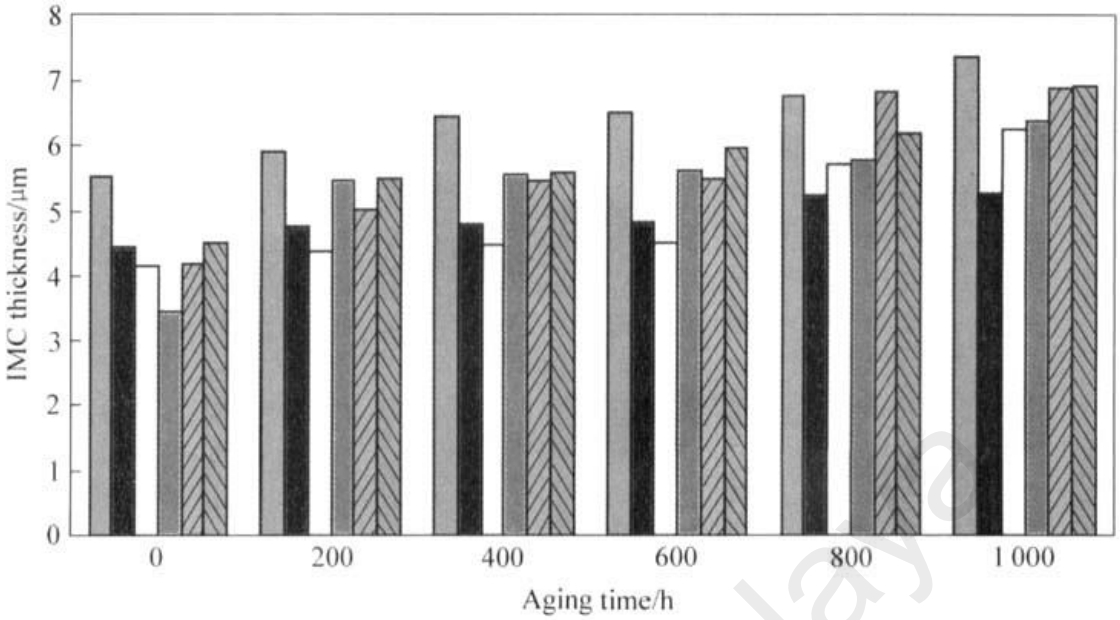

Figure 2.12: Average IMC thickness against aging time at aging temperature of 120 °C (G.-y. Li & Shi, 2006)

Shnawah et al. (D. A. Shnawah et al., 2012) studied the iron (Fe)-bearing Sn-1Ag-0.5Cu (SAC105) solder alloys under aging at up to 180 °C and reported that the addition of Fe stabilized the microstructure of SAC105, which in turn provided a mechanical stability to the Fe-modified alloy. Small amount of Fe is incorporated in Ag_3Sn and Cu_6Sn_5 IMC particles, which reduces the vacancy diffusion rate-a crucial mechanism for IMCs coarsening with aging (D. A. Shnawah et al., 2012). Therefore, the Fe-bearing SAC105 solder alloys are more resistant to microstructural coarsening, which contributes to their mechanical stability during aging.

(Pei & Qu, 2008) studied the impact of addition of lanthanum (La) on the properties of Sn-3.5Ag solder under thermal aging at up to 170 °C and reported that La addition greatly reduces grain size and that during thermal aging, the reduced grain size stays

stable (Figure 2.13). Likewise, La addition significantly reduces the Ag_3Sn IMCs particles size and sharply reduces the coarsening rate of IMCs particles (Figure 2.14).

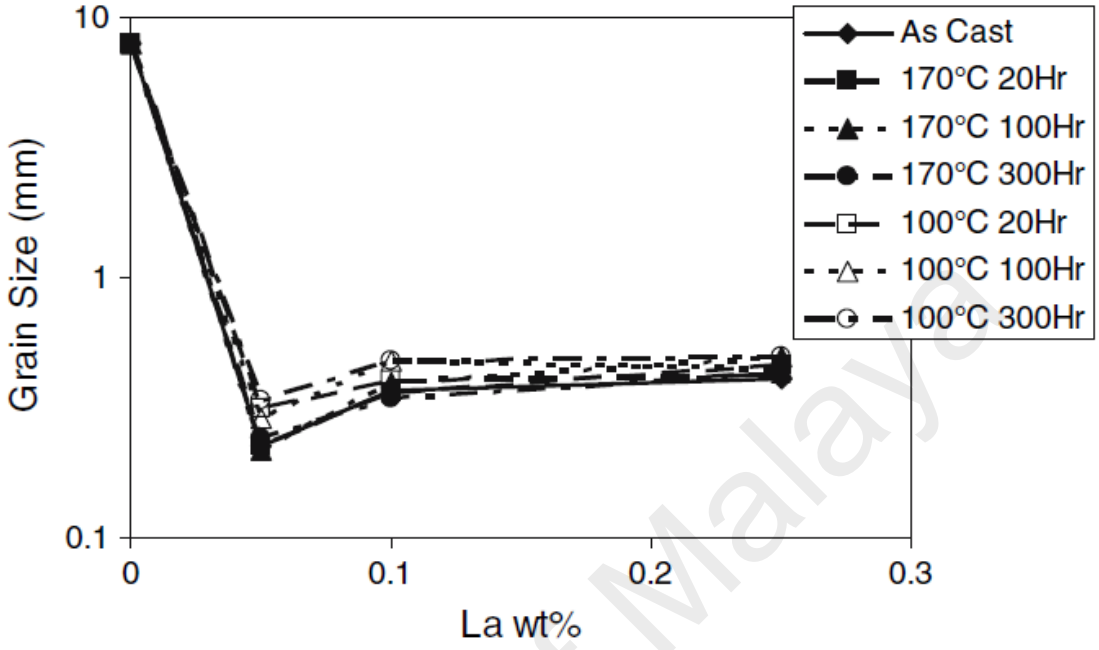

Figure 2.13: Grain size as a function of La content (Pei & Qu, 2008)

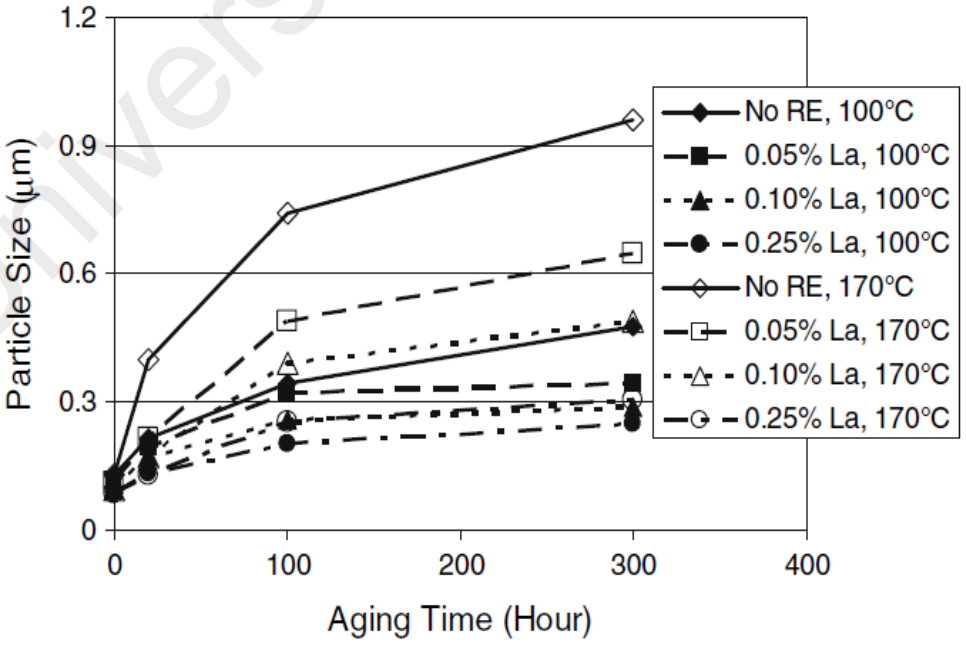

Figure 2.14: Particle size as a function of thermal aging condition (Pei & Qu, 2008)

(Sadiq, Pesci, & Cherkaoui, 2013) studied the La addition to Sn-Ag-Cu solders under thermal aging at 150 °C temperature and reported a huge refinement in grains size and the grains size remained stable during aging (Figure 2.15). Moreover, the average IMCs particles size was decreased by about 40% for the as-cast samples, whereas, for the aged samples, the IMCs coarsening rate was lowered by about 70% (Figure 2.16).

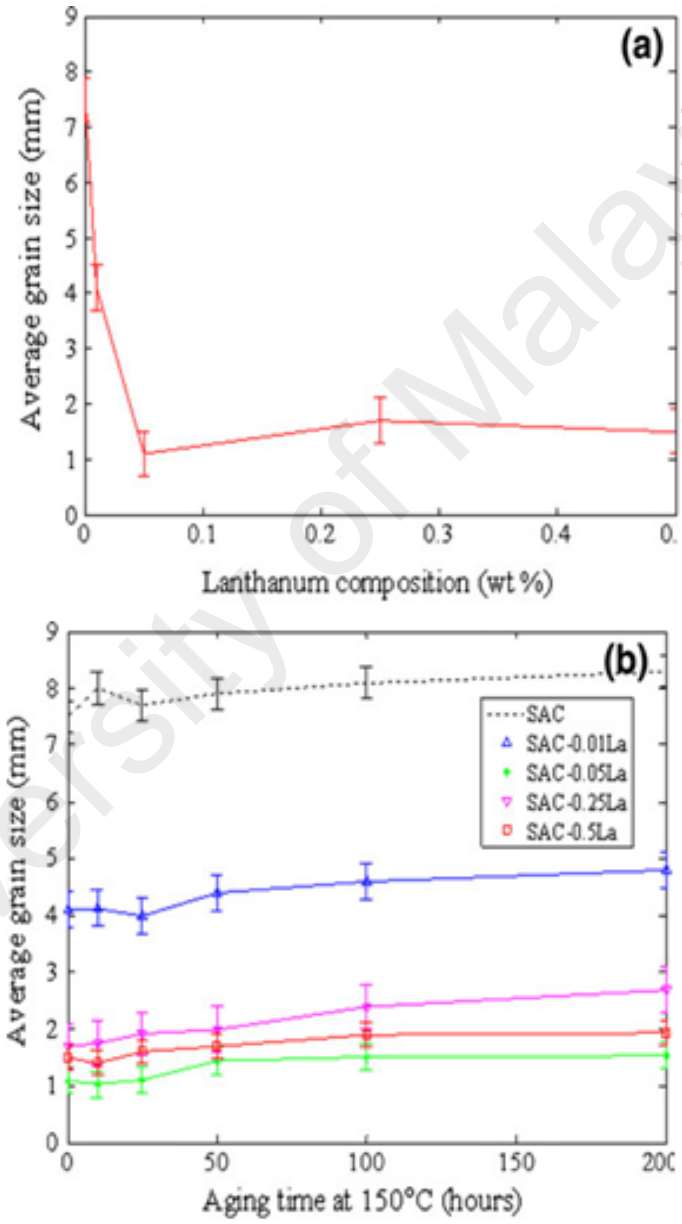

Figure 2.15: Average grain size versus La content for: (a) as-cast and (b) thermally aged samples (Sadiq et al., 2013)

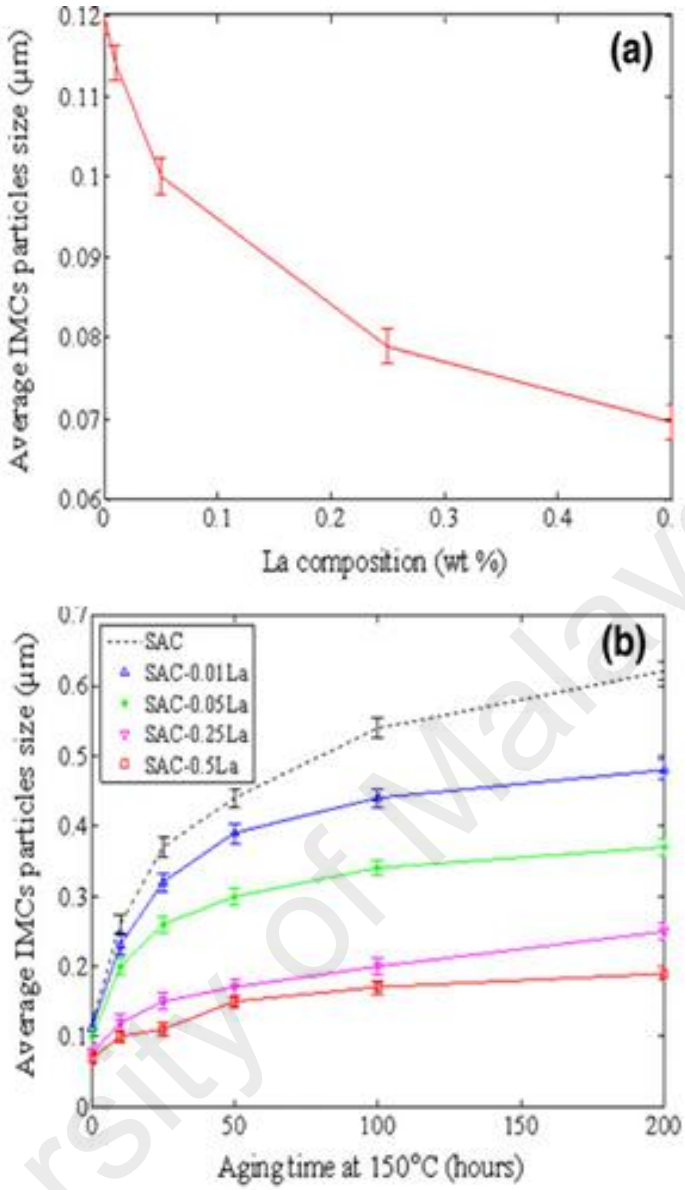

Figure 2.16: Average IMC particle size versus La content for: (a) as-cast and (b) thermally aged samples (Sadiq et al., 2013)

(W. M. Chen, Kang, & Kao, 2012) studied the influence of titanium (Ti) addition on the properties of Sn-Ag and Sn-Cu solder alloys under thermal aging at up to 200 °C and reported that as compared with the base alloy Sn-1Ag, Sn-1Ag-0.2Ti showed very stable hardness under thermal aging (Figure 2.17 (a)), which shows consistency with the microstructural stability shown in Figure 2.18. The effect of the addition of Ti on Sn-Cu solder alloys was similar to its effect on Sn-Ag solders (Figure 2.17 (b)). Ti addition

stabilized the microstructure and hardness of Sn-0.7Cu during thermal aging as well (W. M. Chen et al., 2012).

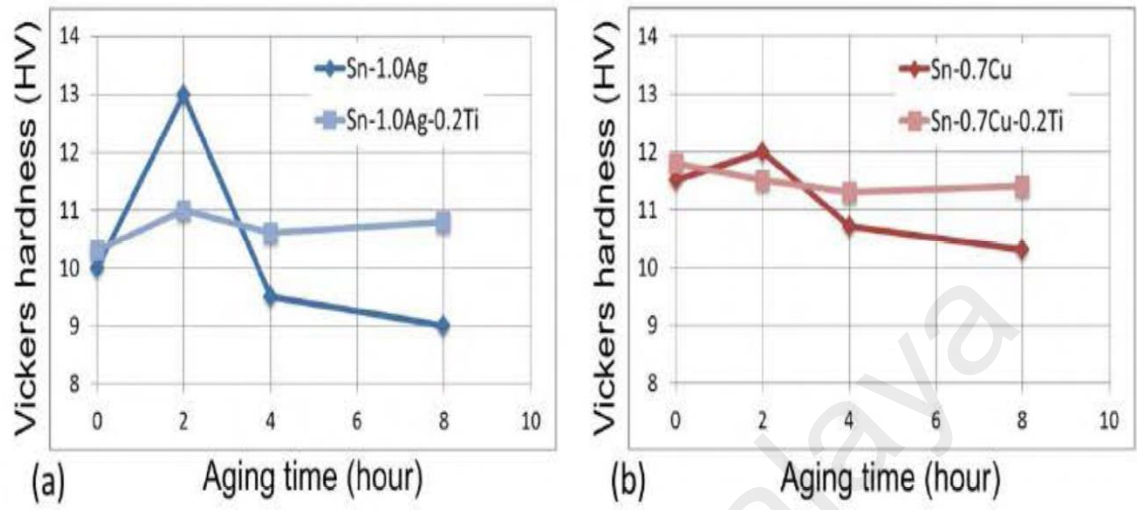

Figure 2.17: Microhardness of Ti-bearing: (a) Sn-Ag and (b) Sn-Cu solder alloys aged at 200 °C up to 8 h (W. M. Chen et al., 2012)

Sn–Sb solder alloys have been considered for many high temperature applications including Microelectromechanical systems (MEMS) microphones and gyroscopes and for attaching I/P pins to ceramic substrates as well as a solder used in air conditioning and refrigeration etc., owing to their microstructural stability, excellent wettability, good mechanical properties and similar electrical resistance to that of Pb-Sb solders (El-Daly, Fawzy, Mohamad, & El-Taher, 2011). The near-peritectic Sn–5Sb solder has a melting point of 245 °C and a contact angle between solder and substrate of 43° (El-Daly, Swilem, & Hammad, 2009). The melting point of Sn–10Sb solder alloy can be increased further by increasing Sb content in the alloy, however high Sb concentration makes the solder hard and brittle due to the formation of more IMCs (Jong Hoon Kim, 2002).

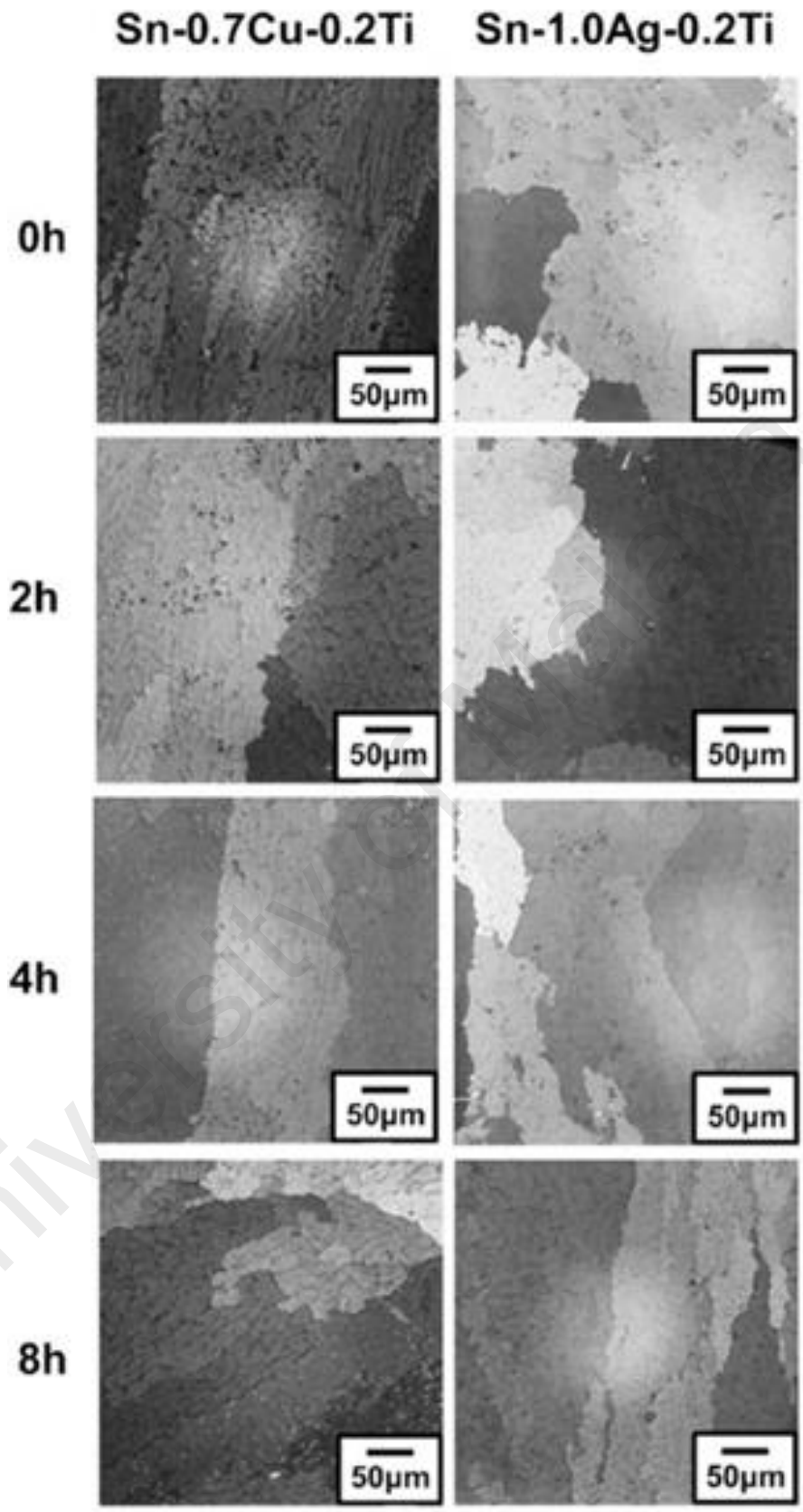

Figure 2.18: Cross-polarized optical images of Ti-added solder alloys aged at 200 °C for 0 h, 2 h, 4 h and 8 h (W. M. Chen et al., 2012)

Many researchers have studied the Sn–Sb solders for their solidification behavior (S.-W. Chen, Chen, et al., 2008), mechanical properties (Geranmayeh, Mahmudi, & Kangooie, 2011; Mahmudi, Geranmayeh, Bakherad, & Allami, 2007) and interfacial reaction with the substrates (C. Lee, Lin, & Yen, 2007). (C. Lee et al., 2007) reported that in interfacial reactions between Sn-5Sb/Cu, SnSb IMCs were not formed and microstructure contained Cu_6Sn_5 and β–Sn phases, as shown in Figure 2.19. In addition, the total thickness of IMCs layer was not significantly effected with up to 7 % addition of Sb into Sn and the behavior of SnSb/Cu and Sn/Cu couples was very similar in terms of phase formations. (S.-w. Chen, Zi, et al., 2008) studied the interfacial reaction in the Sn–Sb/Cu and Sn– Sb/Ag couples and found that the interfacial IMCs linearly grow with the square root of interfacial reaction time indicating that the interfacial reactions are controlled by diffusion mechanism.

The grains of Sn-5Sb did not grow up to 433 K (160 °C) temperature, as shown in Figure 2.20 (Harry Schoeller, 2008), because of the grain boundary pinning caused by the intermediate phase. A rapid growth in the average grains size was observed when the solidus line for Sn–Sb was crossed, which indicates that Sn– 5Sb solders will have good reliability below 160 °C owing to their more microstructural stability. (Harry Schoeller, 2008) found that yield strength and tensile strength as well as elastic modulus of Sn–5Sb was much higher below 0.7Tm temperature. According to (Harry Schoeller, 2008), the presence of the Sn–Sb phase, which is dispersed within the Sn-rich matrix significantly influenced the deformation behavior of Sn–5Sb solders under high temperature. The Sn–Sb precipitates were observed to dissolve into the Sn-rich phase above 453 K (180 °C) temperature, which changed the solder alloy into a single-phase alloy and thus its deformation mechanism was also changed. Moreover, the dissolved Sb in solution do not significantly affect the creep resistance, however higher Sb content can improve the creep resistance due to Sn– Sb precipitation in the solder (El-Daly et al., 2009).

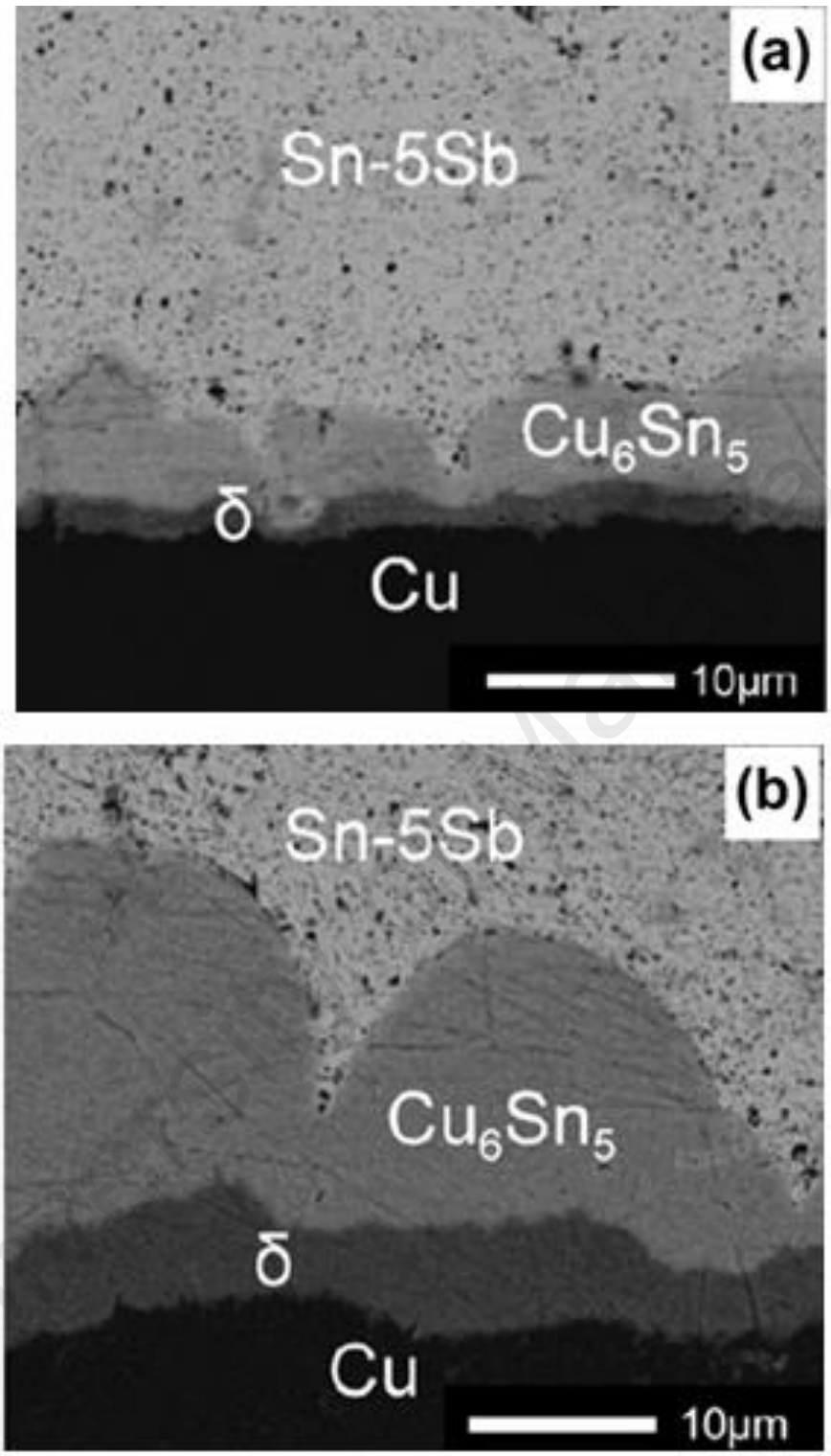

Figure 2.19: Micrographs of Sn–5Sb/Cu couple reacted at 260 °C for (a) 30 min, and (b) 180 min (C. Lee et al., 2007)

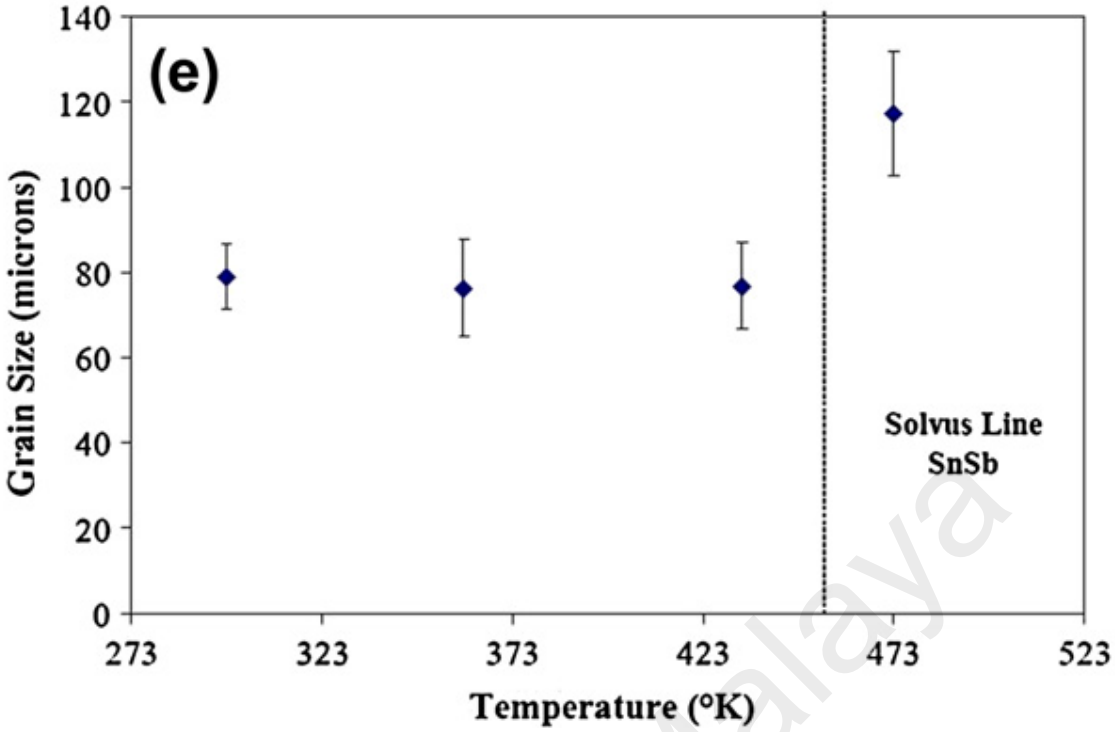

Figure 2.20: Effects of temperature on the average grain size of Sn–5Sb (Harry Schoeller, 2008)

(Hammad, 2008) added Au and Ag to Sn–Sb solders and reported that the addition of Au and Ag significantly increases creep resistance and the rupture time. It has also been reported that the Au addition to Sn–5Sb solder can raise the melting temperature as well increase the fusion heat of the alloy (El-Daly et al., 2009). Sn-25Ag-10Sb solder was also designed, however excessive Ag and Sb make coarse IMCs, which degrades its mechanical properties (Rettenmayr, Lambracht, Kempf, & Graff, 2005). (Shalaby, 2009) reported that small addition of In to Sn–10Sb can improve the yield stress, elastic modulus, fracture strength and hardness of the alloy, while increase its electrical resistivity owing to In_3Sn and Sn–Sb IMCs formation, which serve as scattering centers for the conduction electrons. (Beyer, Sivasubramaniam, Hajas, Nanser, & Brem, 2014) reported that Sn-5Sb demonstrated good shear strength with superior ductility and is suited for connections having large co-efficient of thermal expansion (CTE) mismatch

(e.g. Cu baseplates with Al_2O_3 substrate), whereas the higher Sb-content SnSb showed the higher shear strength with acceptable ductility to suit more to Al-SiC baseplates with Al-N or Si_3N_4 substrates with lower CTE mismatch. Sn-Sb solder systems have stable properties below 160 °C, however their properties degrade drastically beyond 160 °C and are considered somewhat toxic because of the presence of Sb (Jee-Hwan Bae, 2015).

The Sn-based solder can also achieve a high liquidus temperature of over 260 °C, with the addition of transition elements, like nickel, copper and cobalt (Suganuma, Kim, & Kim, 2009). For example, Sn-4Cu binary solder alloy possesses a liquidus temperature of about 300 °C. However, this solder makes massive IMCs, which would degrade its mechanical properties. Moreover, it has a very high liquid fraction at reflow temperature, which would severely damage the package due to high volume expansion. Although there have been various studies to modify the Sn-based solder alloys for high temperature applications between 150-200 °C, more investigations need to be conducted to minimize the coarsening of their microstructure and stabilize their properties during high thermal exposures.

2.5 Microstructure coarsening

2.5.1 Coarsening Mechanism

The increase in the average diameter of the IMCs due to high temperature aging is known as coarsening. This happens because of continuous diffusion of Ag and Cu into Sn due to which the as-cast particles size increases and the particle size "d" for various polycrystalline materials varies with time "t" as per the following relationship (Callister, 1985):

$$< d >^n - < d_o >^n = K^* t \quad \ldots\ldots\ldots\ldots\ldots\ldots\ldots\ldots\ldots\ldots\ldots\ldots\ldots\ldots\ldots\ldots\ldots\ldots.. (2.1)$$

Where, K and n are time-independent constants, <d> is the average particle size at time t, <do> is the average initial particle size before coarsening initiation.

The particle size exponent "n" has different values as there are many coarsening mechanisms as provided in Table 2.1 (S. L. Allen, Notis, M.R., Chromik, R.R., Vinci, R.P., 2004). In different studies over the Sn-Ag solders, it has been noticed that for the particle coarsening, the dominant process is volume diffusion and thus 3 is generally used for the exponent "n" (S. L. Allen, Notis, M.R., Chromik, R.R., Vinci, R.P., 2004; Dutta, Park, & Choi, 2004; Gibson, 1997; Senkov & Myshlyaev, 1986).

Table 2.1: The particle size exponent n values for coarsening processes with different rate-controlling mechanisms (S. L. Allen, Notis, M.R., Chromik, R.R., Vinci, R.P., 2004).

n	**Rate Controlling Mechanism**
5	Diffusion along dislocations or triple junctions
4	Diffusion along interfaces or grain boundaries
3	Volume diffusion
2	Solute atoms transfer across the interface between the matrix and particle

2.5.2 Ostwald Ripening

Ostwald ripening is a thermodynamic driven process that takes place during the thermal aging of solder joints. Generally the larger IMCs particles are energetically more favored to this process, as compared to the smaller IMCs particles (Ratke, 2002). This happens with the fact that the molecules present at the surface of these IMCs particles have less stability (energetically) as compared to the molecules at the interior.

If a simple cubic crystal system is considered to understand this fact, then the atoms present at the interior are engaged/bonded to 6 other atoms but the atoms at the exterior or surface are connected to only 5 atoms and are hence less stable. Continuing to the same example, larger particles are energetically more favorable as more atoms are bonded to 6 atoms at the interior and less atoms are bonded to the exterior and hence the unfavorable locations. Thus if the process continues, the molecules at the surface of the smaller particles (and connected at the unfavorable locations to almost 4 or 5 atoms in their neighborhood) would detach from their respective IMCs particles and would diffuse into the solution following the Kelvin equation. This would be carried out for almost all smaller particles. It would cause an increase in the concentration of free atoms in the solution till a saturation of the free atoms is reached in the solution. It would condense the free atoms on the surface of the bigger particles (Ratke, 2002). Therefore, the larger particles would continue to grow at the cost of the smaller ones and hence the overall (average) size of the IMCs particles would grow. After a long time, all the particles would combine to form a big, ideally spherical shape, single particle to surround the entire surface area.

In case of diffusion of material during thermal coarsening, (Lifshitz & Slyozov, 1961) carried out a mathematical investigation of the ripening process. Their study explained how the shrinking of smaller particles continues and how the larger particles grow at almost a uniform rate till complete saturation. According to their work, the average particle size <R> grows as follows:

$$< R >^3 - < R >_o^3 = \frac{8\gamma C_\infty \ v^2 D}{9 R_g T} \ t \ldots\ldots\ldots\ldots\ldots\ldots\ldots\ldots\ldots\ldots\ldots\ldots\ldots\ldots (2.2)$$

Where, <R> = Average particles radius, v = Molar volume of the particle material, C_∞ = particle material solubility, γ = Surface energy or surface tension of the particles,

T = Absolute temperature, t = Time, Rg = Ideal gas constant, D = Diffusion coefficient of the particle material, Thus, after simplifying the above equation,

$$< R >^3 - < R >_o^3 = \frac{K_o}{T}\, t \exp\left[-\frac{Q}{RT}\right] \ldots\ldots\ldots\ldots\ldots\ldots\ldots\ldots\ldots\ldots\ldots\ldots\ldots\ldots (2.3)$$

Where, Q is the activation energy for the rate-controlling process, K_0 is a time and temperature independent constant. Activation energy is described as the minimum amount of energy required for a chemical reaction to occur.

2.5.3 Phase coarsening in SAC solder alloys

The microstructure of SAC solders progressively coarsens during service. (S. L. Allen, Notis, M. R., Chromik, R. R., Vinci, R. P., 2004) investigated phase coarsening in SAC alloy from a kinetics aspect. They concluded that phase coarsening is governed by $r^3 \propto t$ relationship:

$$\rho^{-\frac{3}{2}} - \rho_o^{-\frac{3}{2}} = \frac{Kt}{RT} exp\left[-\frac{Q_s + Q_D}{RT}\right] \ldots\ldots\ldots\ldots\ldots\ldots\ldots\ldots\ldots\ldots\ldots\ldots\ldots\ldots (2.1)$$

Where, *K* is a constant having terms such as the volume fraction effects and matrix/particle interfacial energy, Q_S is the heat of solution for the rate-controlling species, Q_D is the activation energy for diffusion of the rate-controlling species. The sum of Q_S and Q_D, however, is assumed to be the effective activation energy. By measuring the volume fraction of Cu_6Sn_5 IMC particles in each of the light optical micrographs shown in Figure 2.21, they estimated the effective activation energy to be 69±5 kJ/mol, which perfectly matches the results from other researchers (as tabulated in Table 2.2), indicating that the coarsening of the Cu_6Sn_5 rods was the dominant process ($Q_S + Q_D$ = 36 + 33 = 69 kJ/mol).

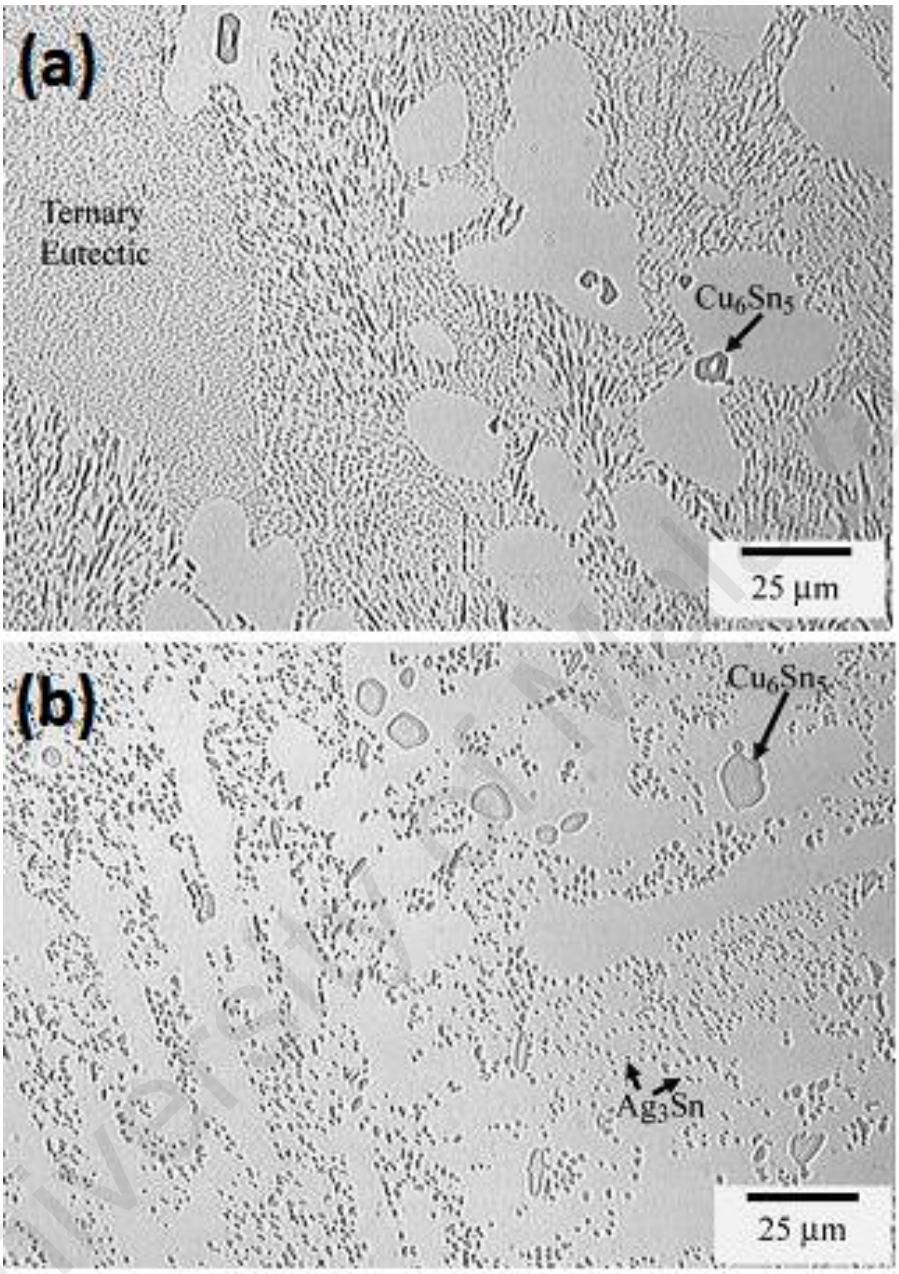

Figure 2.21: Microstructure Evolution of SAC405 Solder Joints (S. L. Allen, Notis, M. R., Chromik, R. R., Vinci, R. P., 2004): (a) as soldering, (b) aged for 4 weeks at 152 °C.

Table 2.2: Activation Energies for Diffusion and the Heats of Solution for Sn, Ag , Cu (S. L. Allen, Notis, M. R., Chromik, R. R., Vinci, R. P., 2004)

Solute	Solvent	Q (kJ/mol)
Ag	Sn (a axis)	77 (D)
Ag	Sn (c axis)	55 (D)
Cu	Sn (a axis)	33 (D)
Sn	Sn (a axis)	123 (D)
Sn	Sn (c axis)	107 (D)
Sn	Sn (Grain Boundaries)	40 (D)
Ag	Sn (Grain Boundaries)	28 (D)
Cu	Sn	36 (S)
Ag	Sn	26 (S)

2.6 High temperature solders applications

The demand for high temperature solders is increasing rapidly in the electronics industry (Kang, Na, Kim, & Kang, 2009). Currently, the high-lead (Pb) solders are being employed as high-temperature solders for first level packaging applications. These applications require solders to operate at over 150 °C temperature and this operating temperature can even exceed 200 °C. There are limited number of studies on the development of high-temperature Pb-free solders. This is owing to the fact that solders used in Level 1 packaging are in low volume, as compared to Level 2 packaging. Nevertheless, solders used in level 1 packaging are increasing rapidly with the emergence of area array packaging concept (Abtew & Selvaduray, 2000). Power semiconductor packaging uses high-temperature solders as die-attach solders (S. Kim, Kim, Kim, Suganuma, & Izuta, 2009). Power-electronics are increasingly being used in a variety of

aerospace, energy production and automotive industries. The power electronics and the miniaturization drive increased the demand for high-temperature operation solder. Advanced packaging technologies are the main applications within the electronics industry for high-temperature solders. The main applications for high-temperature solders within the electronics industry are for advanced packaging technologies, which are needed because electronic products becoming lighter, smaller and faster. Consequently, many advanced packaging technologies use high temperature solders, like chip-scale package (CSP), Ball Grid Array (BGA), multi-chip module (MCM) and flip-chip technology.

2.6.1 Die-Attach Material

A die-attach material needs to bear high operating temperatures as well as thermal loading. Moreover, it needs to be adequately thermally conducting for transferring heat away. In die-attach applications, high-lead solders are usually used in power circuits, which requires high conductivity level. For instance, these solders are used in automotive under-bonnet applications because the car batteries generate high current and low voltages. High-lead solder alloys are also being used for the miniaturization of the inverter that converts DC power to three phases AC power to control the motor system in hybrid vehicles and fuel cell vehicles. These hybrid vehicles and fuel cells perform a vital role in minimizing the carbon dioxide emissions exhausted by automobile engines (Yamada et al., 2006).

2.6.2 BGA Technology

A ball grid array (BGA) is a surface-mount technology (SMT) employed for integrated circuits. BGA is a solution to the issue of making a miniature package for the integrated circuit having many hundreds pins. Pin grid array packages were made with increasingly more pins with decreasing spacing between them. Thus, there was a risk of bridging

adjacent pins with solder. BGAs do not encounter this issue due to the replacement of pins by solder balls. Certain kinds of BGA packaging employ high-lead content solders. Figure 2.22. depicts a BGA packaging involving high lead alloys (Intel-Corporation, 2010).

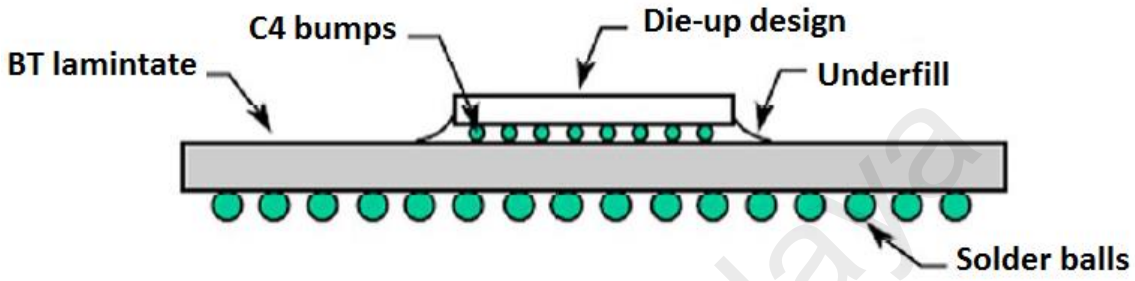

Figure 2.22: Schematic diagram of BGA packaging (Intel-Corporation, 2010)

2.6.3 Flip-Chip Technology

Flip-chip packaging employ a two level packaging plan i.e. first chip is joined to ceramic and then ceramic is joined to polymer. High-lead solder alloys are used in level 1 packaging, in which it is employed to join the chip to the ceramic module. To join the chip to a ceramic module, the chip is flipped upside down. It is named as flip-chip technology. Then the ceramic module is attached to a printed circuit board (PCB) employing a second set of eutectic Sn-Pb solder bumps. The bump size is generally much larger in second level packaging, as compared to the first level packaging. Eutectic Sn-Pb solder alloy is being employed in the second set owing to its much lower melting temperature (183°C) than high-lead content solders. Thus, while the joining of eutectic bumps, the high-lead content solder bumps will not melt (Braun et al., 2006; Tu, Gusak, & Li, 2003). This kind of packaging concept is mainly used in mainframe computers. The solder bumps array is usually positioned on the silicon die generally by vapor deposition or plating (Juergen Wolf, Engelmann, Dietrich, & Reichl, 2006).

2.6.4 MCM Technology

The multi-chip module (MCM) is an advanced form of electronic packaging. It comprises of highly functional electronic components, which are interconnected to the substrate using a fine-line circuitry in the form of multilayers. This module has the ability to handle an entire function. In MCM, there is a single component, which contains several components connected to perform some function (C-Mac-Technology, 2010). The main advantage of MCM is the improved performance resulting from the greatly reduced interconnection length between integrated circuit components (chips), low capacitance loading, low power supply inductance, low offchip driver power and less cross talk (Palomar-Technologies, 2010). MCM technology is being employed for storage array systems, servers, aerospace applications and network management for telecommunications (Ogunseitan, 2007).

2.6.5 CSP Technology

Chip scale package (CSP) possess an area of less than 1.2 times that of the die. It has a single die, direct surface mountable package and their ball pitch is no more than 1mm. The advantages of CSP technology include small size (reduced thickness and footprint), easy assembly process), less weight, improvement in electrical performance and low overall production costs. The significant weight and size reduction makes the CSP ideal to be used in mobile devices like digital cameras, cell phones, laptops and palmtops (Intel-Corporation, 2010). High-lead solder alloys are widely used in CSP technology because it eliminates cooling system, wiring and connectors required in an electronic system and thereby, facilitate the miniaturization drive. A CSP packaging using the traditional Au wiring is shown in Figure 2.23 (Kang et al., 2009).

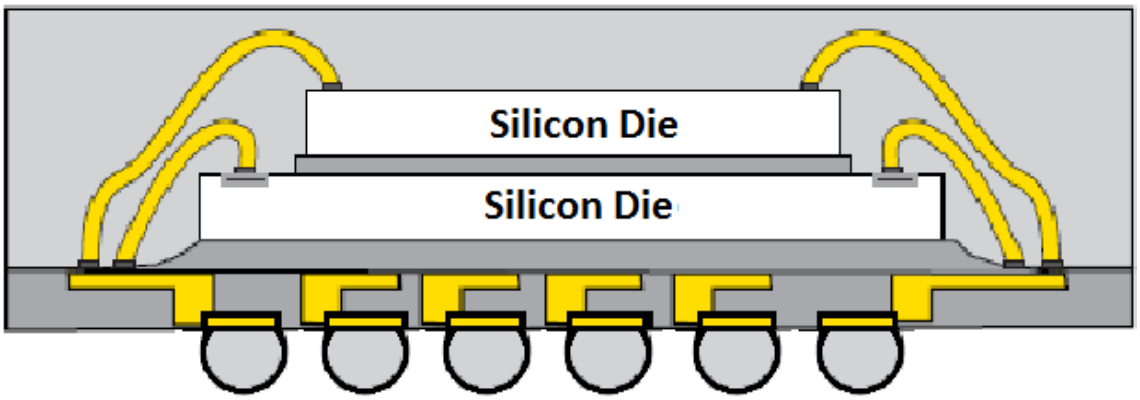

Figure 2.23: Chip level packaging using Au wire bonding (Kang et al., 2009)

2.7 Summary

The SAC solder alloys are the most popular solders in electronic industry. Recently, the low-silver-content SAC solder are increasingly becoming popular due to their low cost and better drop impact performance. Nevertheless, they have inferior mechanical properties and lower stability under high temperature exposures, as compared to high-Ag SAC solder alloys. However, the literature indicates that the addition of Fe and Bi to low-Ag SAC solder alloys can improve their mechanical properties as well as the high temperature performance (150-200 °C). Fe was selected as additive since it improves the high temperature reliability of the alloy. Bi was also selected as additive since it refines the microstructure, improves the mechanical properties and stabilizes the microstructure and mechanical properties during high temperature exposures. The microstructure plays a crucial role in determining the mechanical properties of the alloy. The microstructure of SAC solder alloys progressively coarsens during service resulting in continuous degradation of mechanical properties of the solder joint over time, and thus affects the long-term reliability of a microelectronic package. The mechanisms, which are responsible for such microstructure coarsening are also discussed in this chapter.

CHAPTER 3: METHODOLOGY

3.1 Introduction

This chapter illustrates the methodology of the research work in detail. The details about the samples fabrication and experimental setups as well as sample preparations and characterization are provided. Figure 3.1 depicts the flow chart of the research work. The microstructure has been studied using field emission scanning electron microscope (FESEM), energy dispersive X-ray spectroscopy (EDX) and X-ray diffraction (XRD) analysis techniques. Moreover, various mechanical properties, including tensile properties, impact reliability, microhardness and shear performance, have also been characterized in this work. The microstructure and various mechanical properties have been followed under high thermal aging treatments with progressively increasing aging time.

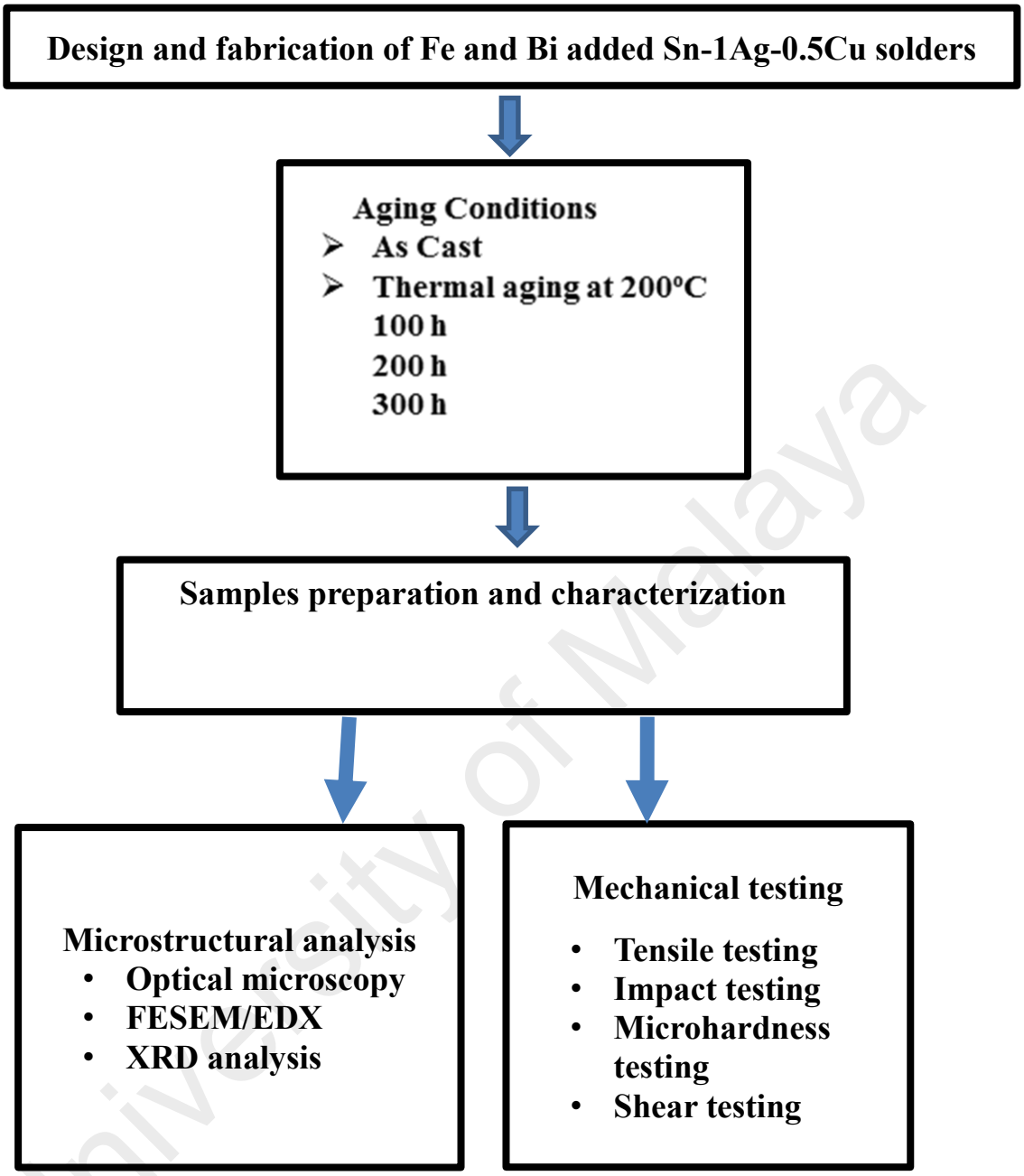

Figure 3.1: Flow chart of the research work

3.2 Bulk solder specimen preparation

Solder alloy specimens of Sn-1Ag-0.5Cu (SAC105), Sn-1Ag-0.5Cu-0.05Fe-1Bi (SAC105-Fe-1Bi) and Sn-1Ag-0.5Cu-0.05Fe-2Bi (SAC105-Fe-2Bi) were prepared from pure metals (99.99% pure) of Sn, Ag, Cu, Fe and Bi. These metals were obtained from Accurus Scientific Co. LTD (Tainan, Taiwan) and some dog-bone shaped tensile specimens were made as shown in Figure 3.2. First, the constituent metals were weighed in proper weight proportions and then melted at more than 1000 °C for 40 min in an induction furnace. Subsequently, the molten materials were mixed with liquid pure Sn for 60 min at 300 °C using a melting furnace. Nitrogen gas was used in the furnace to provide an oxygen-free atmosphere and thus avoid the oxidation of the molten materials. Then, the molten alloys were cast to disk shaped ingots and the exact compositions of the casting ingots were determined by atomic emission spectrometry (AES) with nominally ppm accuracy using a Spectrolab equipment (see Table 3.1). The purpose of doing this was to ensure that the percentages of Sn, Ag, Cu, Fe, Bi and impurities in the alloy complied with the standard specifications (per JIS-Z-3282:1999 standard). Following this, the stainless steel molds, preheated at 130 °C, were used to pour the molten alloys into them. Then, the molds were air cooled naturally to room temperature (25 °C). A K-type thermocouple was used to measure the cooling rate during casting. A cooling rate of 0.45 °C s^{-1} was obtained, which is close to the cooling rate for soldering in electronic assemblies, especially for soldering large components on printed wiring boards (K. S. Kim, Huh, & Suganuma, 2002). Finally, the stainless steel molds were disassembled, and the samples were removed from them and inspected visually for assuring that their surfaces were free of any voids or damage. To release some of the residual stresses,

induced during casting, the solidified samples were kept at room temperature (about 25°C) for one whole day.

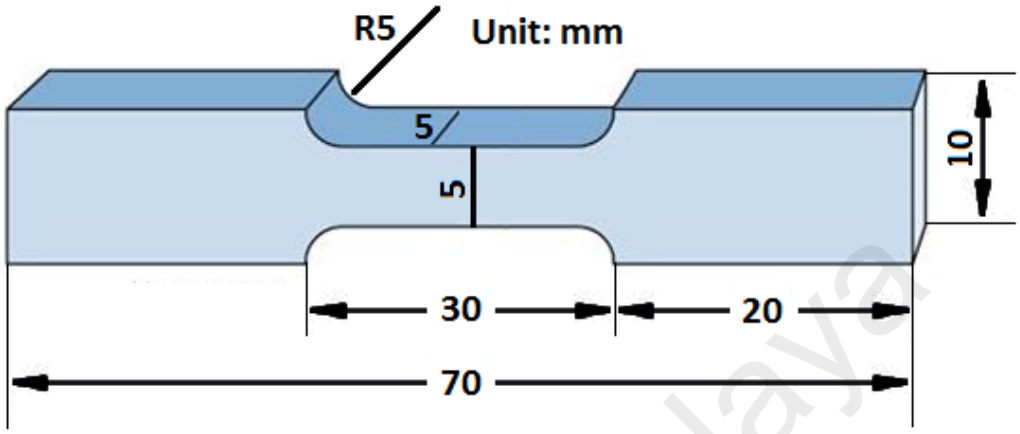

Figure 3.2: Dimensions of the dog-bone shape tensile specimen

Table 3.1: Chemical composition of the alloys (wt.%)

Elements	SAC105	SAC105-Fe-1Bi	SAC105-Fe-2Bi
Sn	98.5524	97.4232	96.5962
Ag	0.9401	1.0105	0.9159
Cu	0.4947	0.4960	0.4747
Fe	0.0005	0.0460	0.0503
Bi	0.0016	1.0124	1.9510
Pb	0.0039	0.0047	0.0045
Al	0.0005	0.0005	0.0005
As	0.0008	0.0008	0.0008
Cd	0.0001	0.0001	0.0002
Co	0.0004	0.0006	0.0006
In	0.0013	0.0013	0.0013
Ni	0.0002	0.0000	0.0000
Sb	0.0034	0.0038	0.0039
Zn	0.0001	0.0001	0.0001

3.3 Isothermal aging treatment

In order to study the effect of severe thermal aging on the bulk alloys' microstructure and mechanical properties, the specimens were aged in Memmert oven (Beschickung-Loading Model 100-800) at constant temperature of 200 °C for 100 h, 200 h and 300 h. Safety gloves were used to avoid any injury during removal of samples from the oven. All the analyses, including microscopy and mechanical testing, were carried out for as-cast samples as well as for samples with these aging conditions.

3.4 Microstructural characterization

Samples were first diced with a dicing saw and then mounted in a mixture of transparent epoxy resin and hardener, which required 24 h to fully harden at room temperature. Samples were subsequently grinded and polished with a Struers TegraPol-21 machine. Silicon carbide (SiC) sandpaper was used to grind the specimens. SiC sandpaper was selected by grit size in a sequence of 800, 1200, 2400, and 4000: grit is the number of grains of silicon carbide per square inch of abrasive paper. After grinding with the 4000 SiC sandpaper, the polishing process began with polycrystalline diamond suspension as the abrasive (particle size: 3.0 μm) on an MD-MOL polishing cloth. Final polishing was performed with an MD-CHEM polishing cloth using a colloidal silica suspension (particle size: 0.04 μm). After polishing, the specimen surface was thoroughly cleaned with distilled water and methyl alcohol and dried with a hot water blower to eliminate water spots and remove any remaining residue. A representative image of the prepared samples is shown in Figure 3.3. Subsequently, chemical etching was performed using a solution of 5 % hydrochloric acid/95 % ethanol. Disposable gloves were used during the samples preparation process to protect the hands from the chemicals.

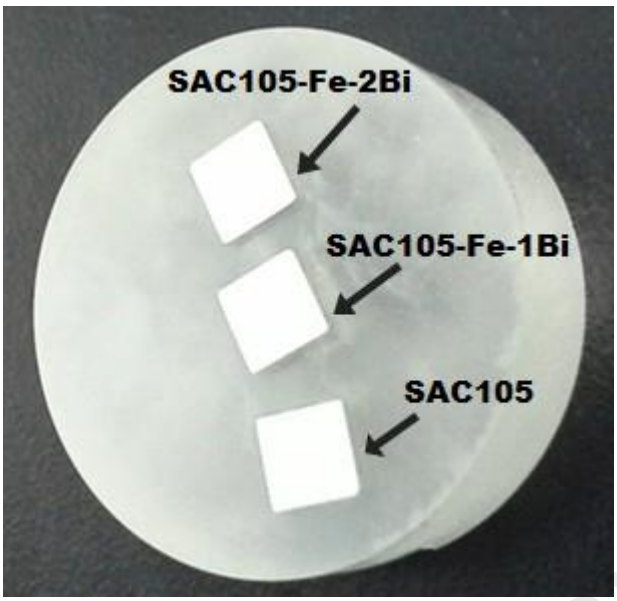

Figure 3.3: Prepared sample for microscopic study

Optical microscope with crossed polarized light was used to examine the change in grain size with the addition of Fe and Bi to SAC105 base alloy. Field Emission Scanning Electron Microscope (FESEM, FEG Quanta 450) with a backscattered electron detector was employed to study the microstructure of SAC105 and Fe/Bi bearing SAC105. Along with FESEM, the energy dispersive X-ray spectroscopy (EDX) analysis was performed to study the distribution of phases present in the alloy. Moreover, X-ray diffraction (XRD) analysis was carried out using PANalytical EMPYREAN X-ray diffractometer to determine the composition of the phases present in the alloy. The measurements were performed from 25° to 85° in 2θ mode, with steps of 0.02° and 1 s exposure time per step.

FESEM micrographs were further analyzed using ImageJ software (Figure 3.4) for quantitatively studying the microstructure. Here is how the software works: Open the file manager in imageJ and locate the image to be analyzed. Covert the image to bit format: Image > Type > 8-bit. Adjust the threshold: Image>Adjust>Threshold. To count the objects, use the Analyze menu: Analyze>Analyze Particles. In order to count only

particles above a certain number of pixels, enter a single value into the Size field. Particles smaller than that value will be ignored. Enter Size and Circularity into the dialog box, and check Display, Clear, Summarize, and Include Holes. The threshold of the image is adjusted such that the IMCs and matrix become clear and visible. This way the image is analyzed and the average particles size, circularity and solidity values are obtained. Circularity is a measure of how much circular the IMCs particles are. The circularity of a perfect circle is 1.0. Solidity is a measure of how much solid the IMCs particles are from inside. The more the IMCs particles are circular and solid, the better the properties would be.

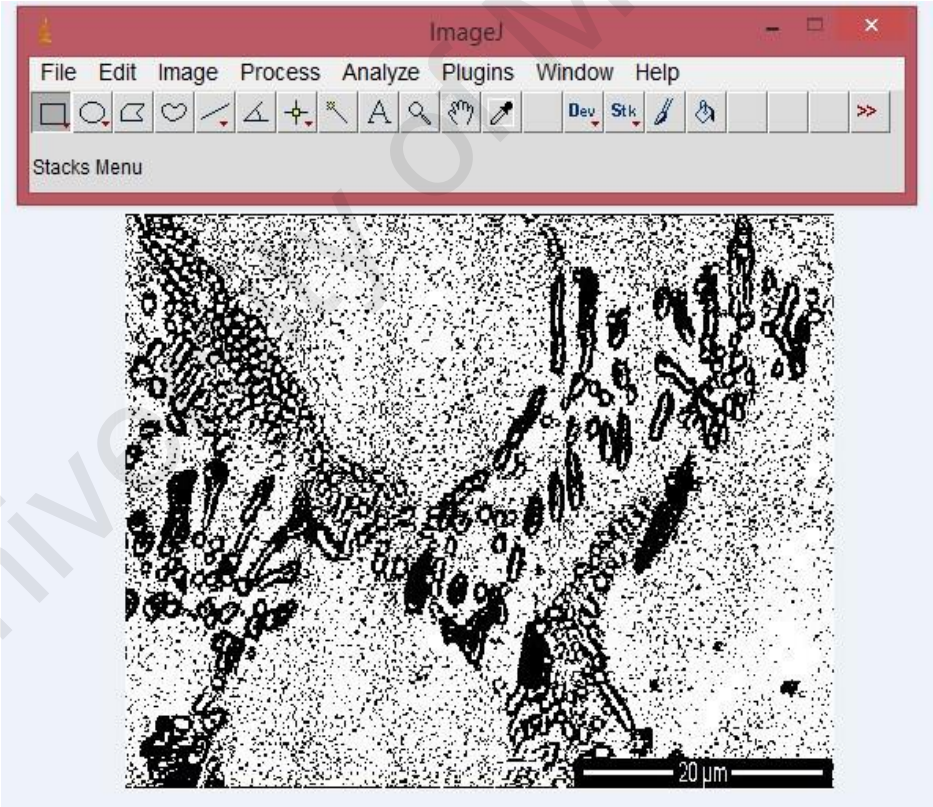

Figure 3.4: IMCs particles analysis through ImageJ software

3.5 Tensile testing of specimens

Instron 3369 universal testing machine, equipped with 50 kN load cell and interfaced with Bluehill 2 (version 2.19) software, was used to perform quasi-static tensile tests at a strain rate of 2×10^{-4} s^{-1} to investigate the tensile properties, including yield stress, ultimate tensile strength (UTS) and ductility, of SAC105 and Fe/Bi bearing SAC105 solder alloys. The yield stress of the solder alloy was considered as the stress value at which a 0.2 % plastic strain occurred. The UTS of the alloy was considered as the maximum stress in the stress-strain curve. Ductility was assessed through percent elongation and percent reduction of area. Both of these are good indicators of ductility. To determine the percent elongation, the gage length (L_o) of 20 mm was used and the samples were marked before the test. After the test, the fractured pieces were carefully joined together to determine the final gage length (L_f), as shown in Figure 3.5. Percent elongation was then calculated using percent change equation. Percent reduction of area was calculated by examining the original cross sectional areas (A_o) and final cross sectional areas (A_f), as shown in Figure 3.5, and applying the percent change equation. Tensile properties values for each solder specimen were the average of five repetitions of the test under the same testing conditions.

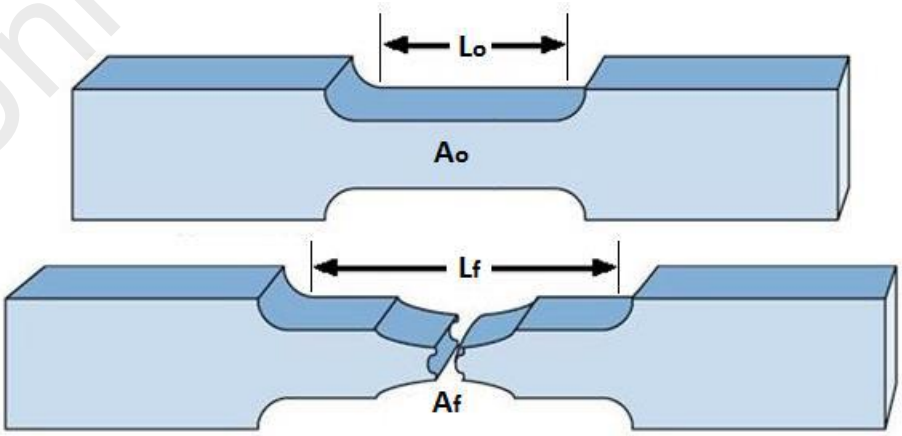

Figure 3.5: Schematic diagram for calculating the percent elongation and reduction in area

3.6 Charpy impact testing of specimens

Impact tests are conducted for measuring the resistance of a material to a suddenly applied force. The test measures the energy absorbed prior to failure or impact energy. The most common method of measuring impact energy is Charpy Impact test. The Charpy test is a widely used method for evaluating the impact toughness or relative toughness of materials, which is critically important for the impact reliability of materials. It is an economical and fast test. It is employed more as a comparative test of materials rather than a definitive test.

A pendulum-type Charpy impact testing machine, with a 5.4 m/s impact speed, was employed to conduct the impact tests. The effective weight of pendulum was 20.59 kg with an impact energy of 30 kg.m. The specimens' dimensions were 5 mm wide × 5 mm thick × 70 mm long. Figure 3.6 shows the schematic diagram of the setup and principle of Charpy impact testing machine. First, the pendulum was lifted to H height and as a result it gained an E_1 initial potential energy. The pendulum was then released. It hit the specimen and raised to h height with E_2 as final potential energy. During the process, the specimen absorbed some of the energy (E) during the impact, which was directly recorded from the reader. The impact absorbed energy for each sample composition was the average of five tests under the same testing conditions. Special care was taken to avoid any injury during lifting and releasing of the pendulum.

Impact toughness can also be assessed from a combination of strength and ductility (post-yield deformation). A material with higher strength and ductility possesses higher toughness. Instron 3369 universal testing machine was used to carry out tensile tests at a strain rate of $2 \times 10{-}4\ s^{-1}$ to determine yield stress, tensile strength and elongation to failure. The dimensions of the tested specimens are given in Figure 3.2. Approximate modulus of toughness was then calculated by using the following well-known equation:

$$U_t = \frac{1}{3}(\varepsilon)(\sigma_{yp} + 2\sigma_{ult}) \qquad (3.1)$$

Where,

U_t = Modulus of toughness,

ε = Strain to failure,

σ_{yp} = Yield stress,

σ_{ult} = Ultimate tensile strength.

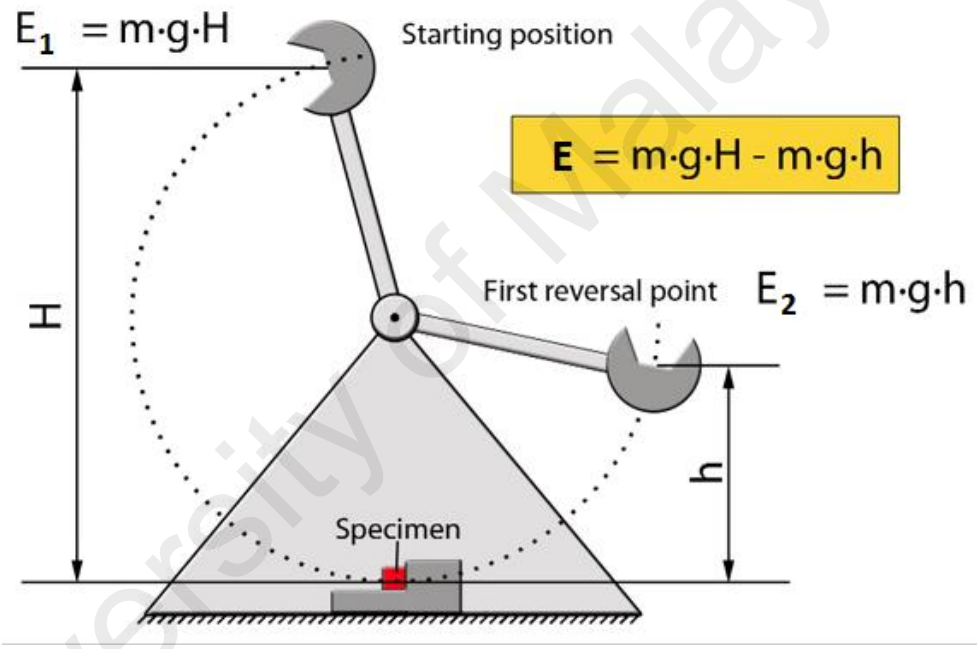

Figure 3.6: Schematic diagram showing the setup and principle of Charpy impact tester

3.7 Microhardness tests of specimens

Sample preparation for the microhardness test is important in order to make a small enough specimen to fit into the hardness tester. In addition, the sample preparation will smoothen the surface of the specimen to ensure a regular indentation shape and a good measurement as well as to make sure that the sample can be placed perpendicular to the

indenter. Therefore, the samples were prepared for microhardness test using the dicing, resin molding and grinding with four grads of SiC papers (Nos. 800, 1200, 2400 and 4000) as well as polishing with diamond suspension (3 μm) and colloidal silica suspension (0.04 μm). Hardness tests were carried out using HMV-G micro Vickers hardness tester. A load of 245.2 mN was applied for a dwell time of 10 s. The hardness test was repeated fifteen (15) times for each of the samples and the two-sample t-tests were performed using SPSS statistics software to statistically analyze the testing data. The following equation can be used to calculate the Vickers hardness values:

$$HV = \frac{1.854\ F}{d^2} \qquad (3.2)$$

Where,

d = mean diagonal of the indentation,

F = Applied load,

HV = Vickers hardness number.

3.8 Shear testing of specimens

Shear tests were carried out with a shear speed of 0.25 mm/min using a single shear holder attached with the upper and lower cross heads of Instron 3369 universal testing machine (UTM). Figure 3.7 shows a schematic diagram of the shear testing setup and principle. Shear strength was obtained by placing the specimen in the punch type shear fixture and the punch was pushed downward until the specimen failed in shear. Shear strength was calculated as the maximum shear force/ shear area. The shear cross-sectional area was 5 mm × 5 mm with a shear height of 5 mm. Shear strength was determined for Fe/Bi-bearing SAC105 and their results were compared with the base alloy SAC105. Five

samples were used for the tests under the same testing conditions for each solder specimen and the shear strength was obtained for that specimen by averaging the tests data.

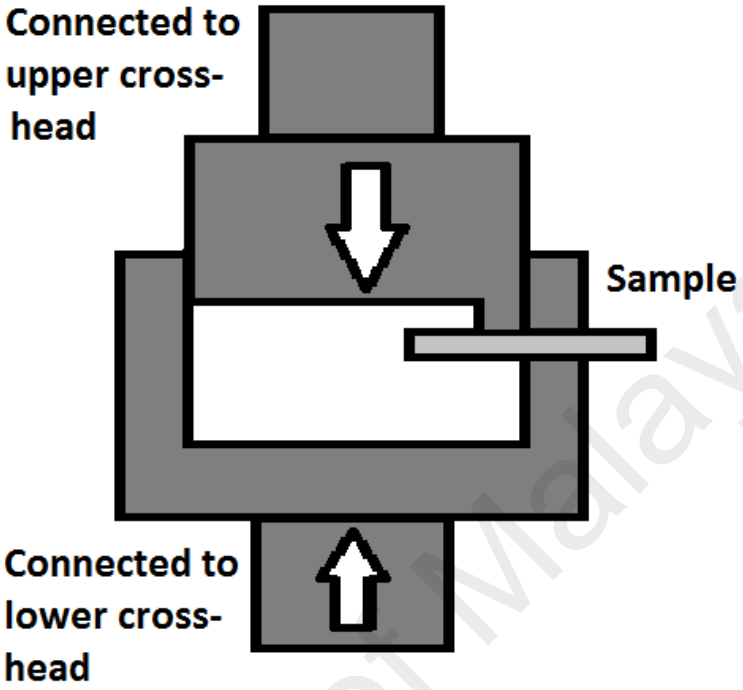

Figure 3.7: Schematic diagram showing the shear testing setup and principle

3.9 Summary

This chapter provides details about the samples fabrication, and experimental setups and equipment, as well as sample preparation and characterization. The overall casting process as well as the details about the prepared specimens are described. The thermal treatment conditions to which the samples were exposed before the analyses are also described. The samples preparation for microscopy, which includes dicing, resin molding and grinding with different grads of SiC papers as well as polishing processes are also presented. Moreover, microscopic techniques, including optical microscope, field emission scanning electron microscope, X-ray diffraction analysis, energy dispersive X-ray spectroscopy analysis are explained in detail. The mechanical properties

characterization techniques, like tensile testing, impact testing, shear testing and microhardness testing are also explained in detail in this chapter.

CHAPTER 4: RESULTS AND DISCUSSION

4.1 Qualitative microstructure study

The FESEM micrographs of base alloy SAC105 as well as Fe and Bi added SAC105-Fe-1Bi and SAC105-Fe-2Bi are shown in Figure 4.1. Microstructure of the SAC105 is comprised of large primary β-Sn grains/dendrites and the inter-dendritic region consists of eutectic Ag_3Sn and Cu_6Sn_5 IMCs. The microstructures of SAC105-Fe-1Bi and SAC105-Fe-2Bi are comprised of relatively smaller primary β-Sn grains surrounded by three distinct types of eutectic IMCs, namely Ag_3Sn, Cu_6Sn_5 and $FeSn_2$. The XRD analysis confirmed the existence of these three IMCs in the samples, while Bi addition to the alloys does not alter the IMCs type, as provided in Figure 4.2. The EDX elemental map, given in Figure 4.3, revealed that the concentration of Fe increases at the $FeSn_2$ location, while the rest of Fe are uniformly dispersed throughout the microstructure of Fe/Bi-bearing SAC105, whereas Bi is homogeneously distributed throughout the Sn matrix. $FeSn_2$ IMCs are very rarely seen in the microstructure of Fe/Bi added alloys, and thus has no significant effect on the mechanical properties. This is due to the Fe low concentration as well as its almost insolubility in Sn. Bi causes no significant influence on the chemical composition of IMCs phases (Hodúlová, Palcut, Lechovič, Šimeková, & Ulrich, 2011). The element Bi exists mostly in the solder bulk and strengthens the alloy by its solid solution strengthening mechanism (Hodúlová et al., 2011). Bi also curbs the formation of the IMCs phases, especially Cu_6Sn_5 IMCs (Hodúlová et al., 2011). As observed in Figure 4.1, the sizes of Ag_3Sn and Cu_6Sn_5 IMCs in Fe/Bi bearing SAC105 are much smaller than the base alloy SAC105. This is because of the Bi presence in the alloy, which restricts the formation of IMCs (Hodúlová et al., 2011) and thus the size of intermetallic compounds (IMCs) progressively decreases with increasing the Bi content

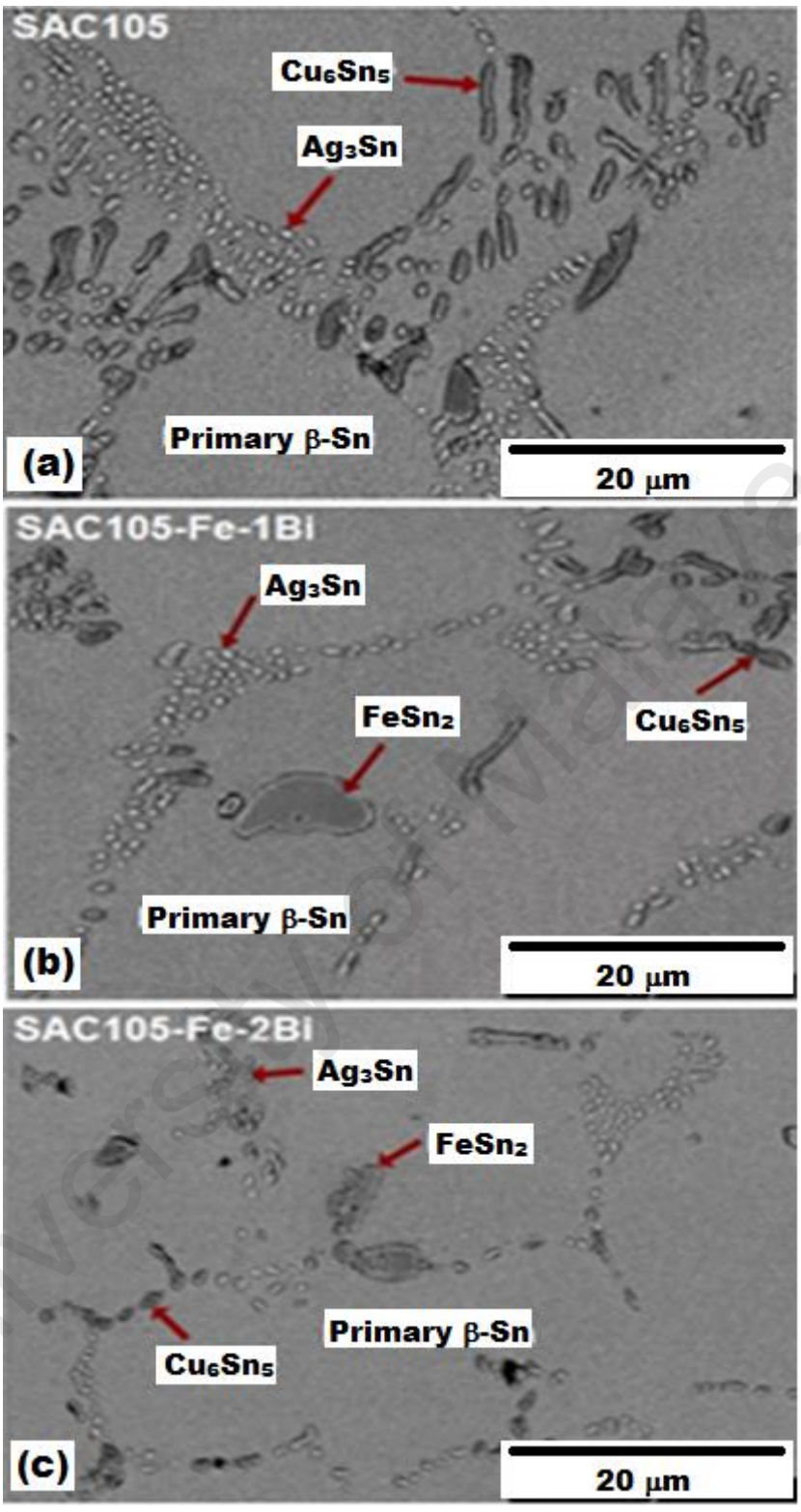

Figure 4.1: FESEM micrographs for as-cast samples of: (a) SAC105, (b) SAC105-Fe-1Bi, (c) SAC105-Fe-2Bi

in the alloy. The IMCs being rich in Ag and Cu, are strong and brittle in nature as compared to the soft Sn matrix, and influence the mechanical properties of the lead-free solder joints (Wu et al., 2004). The smaller IMCs place more obstacles per unit area to the slipping of dislocations and, as a result, produce strong strengthening effect in the solder.

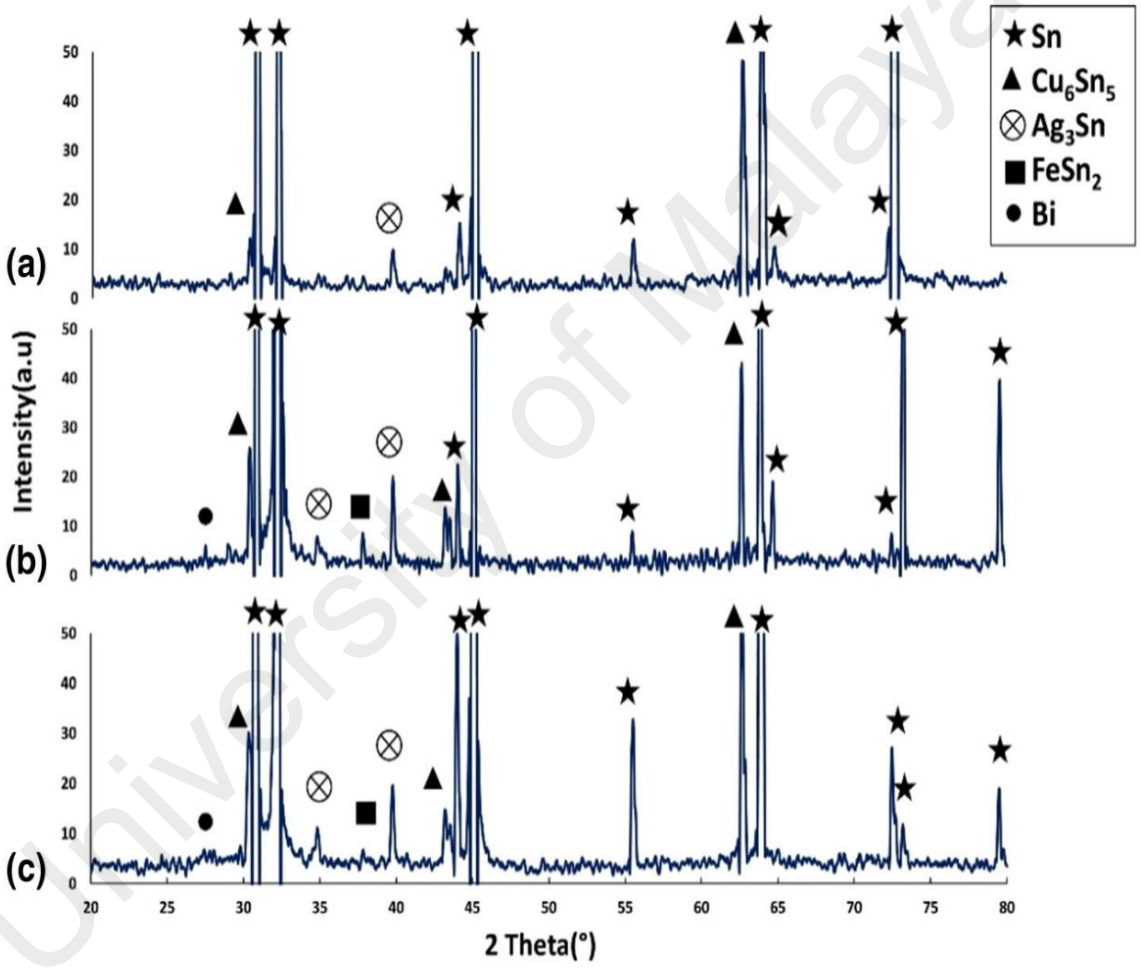

Figure 4.2: XRD analysis results for: (a) SAC105, (b) SAC105-Fe-1Bi and (c) SAC105-Fe-2Bi

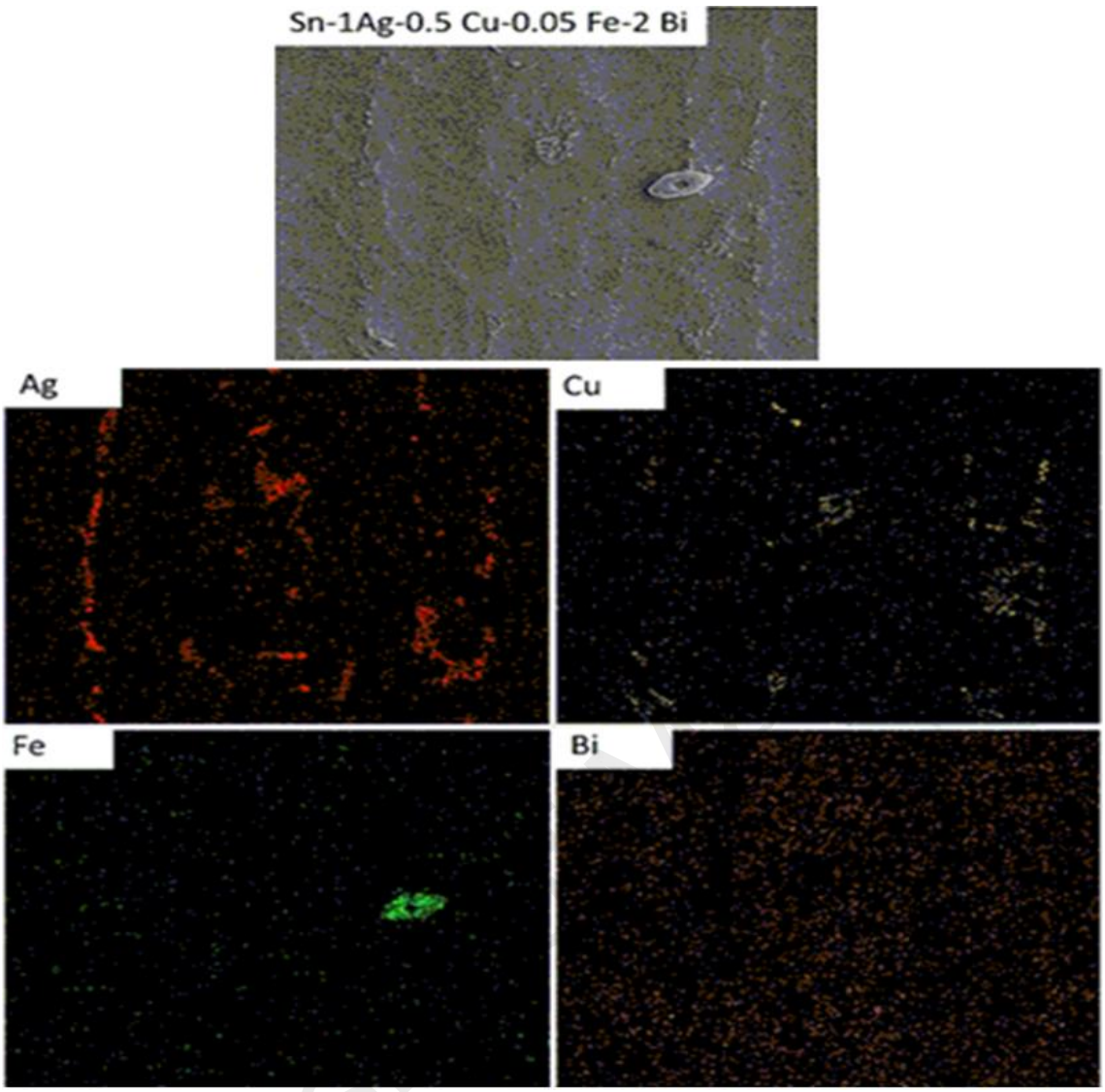

Figure 4.3: EDX elemental mapping analysis of SAC105-Fe-2Bi solder alloy

The influence of severe thermal aging at 200 °C for 100 h, 200 h and 300 h on the microstructure of SAC105 is shown in the FESEM micrographs in Figure 4.4. It can be clearly seen in the micrographs that severe thermal aging progressively leads to excessive coarsening of the eutectic regions and a loss in the definition of the primary β-Sn dendrites. As clear from the micrographs, the Cu_6Sn_5 and Ag_3Sn IMCs undergo Ostwald ripening during aging, and, consequently, the microstructure excessively coarsens. In an Ostwald ripening process, the larger crystals grow due to the dissolution of smaller crystals, which have a higher interfacial enthalpy than the larger crystals (Fix, Nüchter,

& Wilde, 2008). This phenomenon describes the large particles' growth through the small particles' dissolution. The change in particle size changes the free energy of the particle, which results in a change in solubility at the matrix/particle interface due to the Gibbs–Thomson effect (D. A. Shnawah et al., 2015). The matrix region surrounding smaller particles possesses more solute, as compared to the matrix region surrounding bigger particles. This sets up solute concentration gradients in the direction of the smaller particles to the bigger particles. As a result the bigger particles grow with time while the smaller particles shrink. So, the number of Cu_6Sn_5 and Ag_3Sn IMCs in the SAC105 solder alloy decrease acutely after aging as compared to the as-cast microstructures. The Cu_6Sn_5 IMCs grow even more intensely, particularly after 200 h aging, because of the higher diffusivity of Cu in Sn than that of Ag in Sn. (Fix, López, Brauer, Nüchter, & Mittemeijer, 2005; Seo et al., 2009). It is well established that coarsened IMC phases are less able to hinder the movement of dislocation, resulting in a loss of strength. Therefore, the coarsening of these IMCs after aging results in the SAC105 solder alloy with significantly decreased strength.

The FESEM micrographs of SAC105-Fe-1Bi and SAC105-Fe-2Bi aged at 200 °C are shown in Figure 4.5 and Figure 4.6, respectively. It can be observed in the micrographs that the microstructural coarsening is significantly suppressed for both of the alloy compositions. Moreover, the IMCs coarsening with aging is more suppressed in SAC105-Fe-2Bi than SAC105-Fe-1Bi showing that the Bi addition contributes to the suppression of the microstructure, which is consistent with the findings by Cai et al. (Cai et al., 2012). Cai et al. (Cai et al., 2012) also reported that the Bi solubility in Sn increases greatly with temperature. Therefore, the solid solution strengthening effect is even more significant at higher aging temperatures (Cai et al., 2012). Likewise, Fe addition also contributes to the suppression of microstructure coarsening with aging. The $FeSn_2$ IMCs particles do not undergo any noticeable growth. This is because of the low solubility and diffusivity of Fe

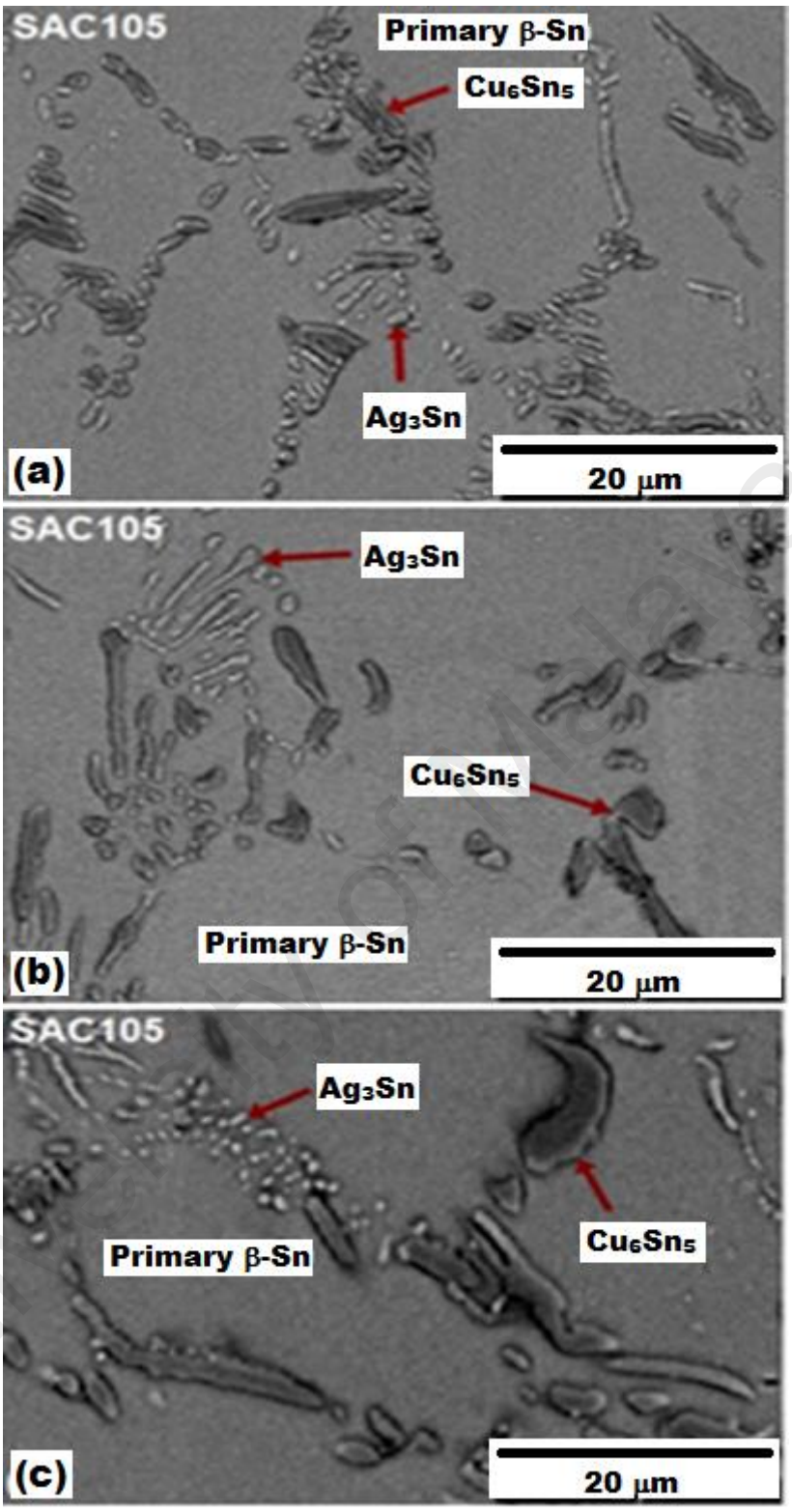

Figure 4.4: FESEM micrographs of SAC105 after thermal aging at 200 °C for: (a) 100 h, (b) 200 h, (c) 300 h

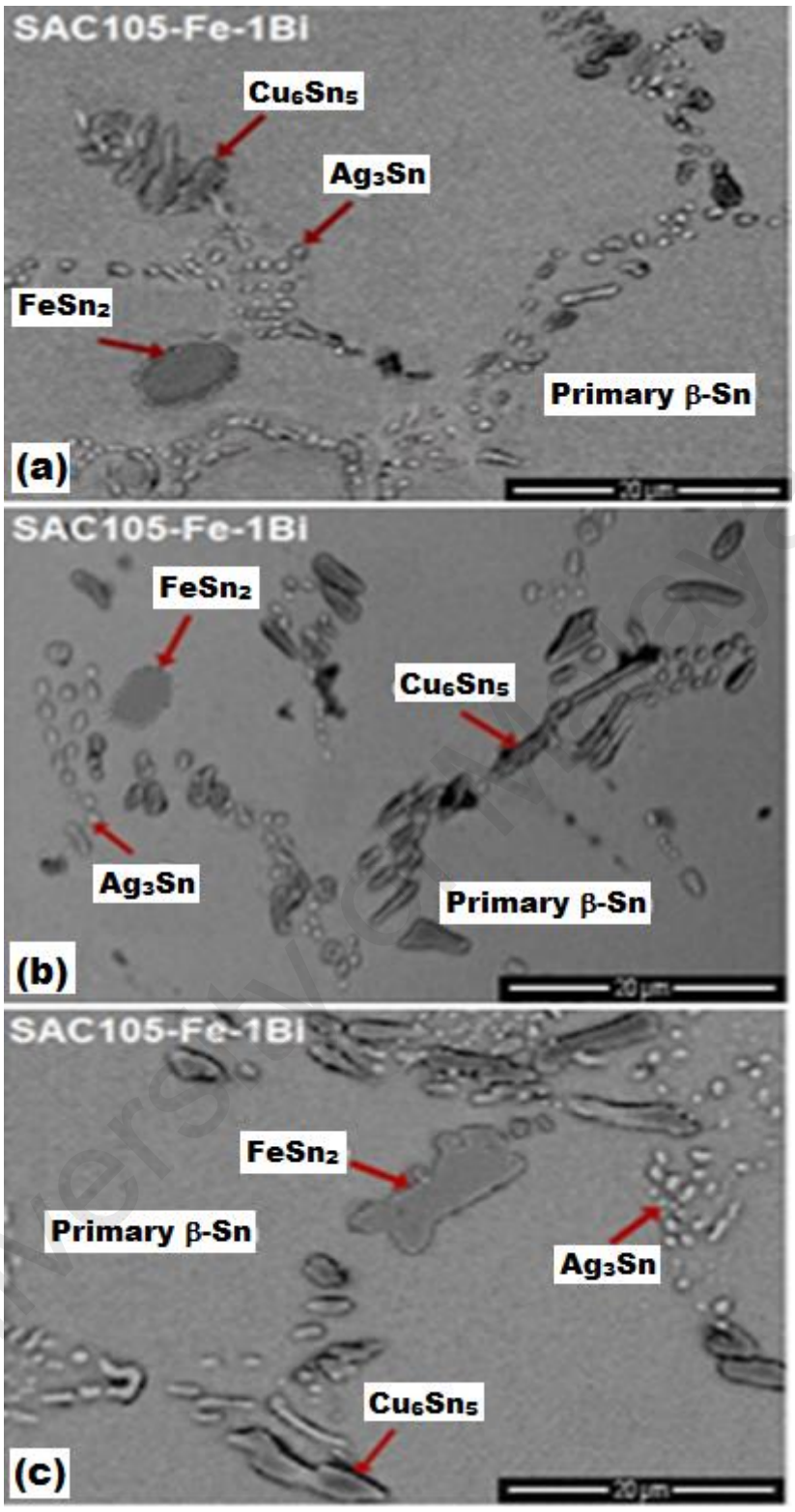

Figure 4.5: FESEM micrographs of SAC105-Fe-1Bi after thermal aging at 200 °C for: (a) 100 h, (b) 200 h, (c) 300 h

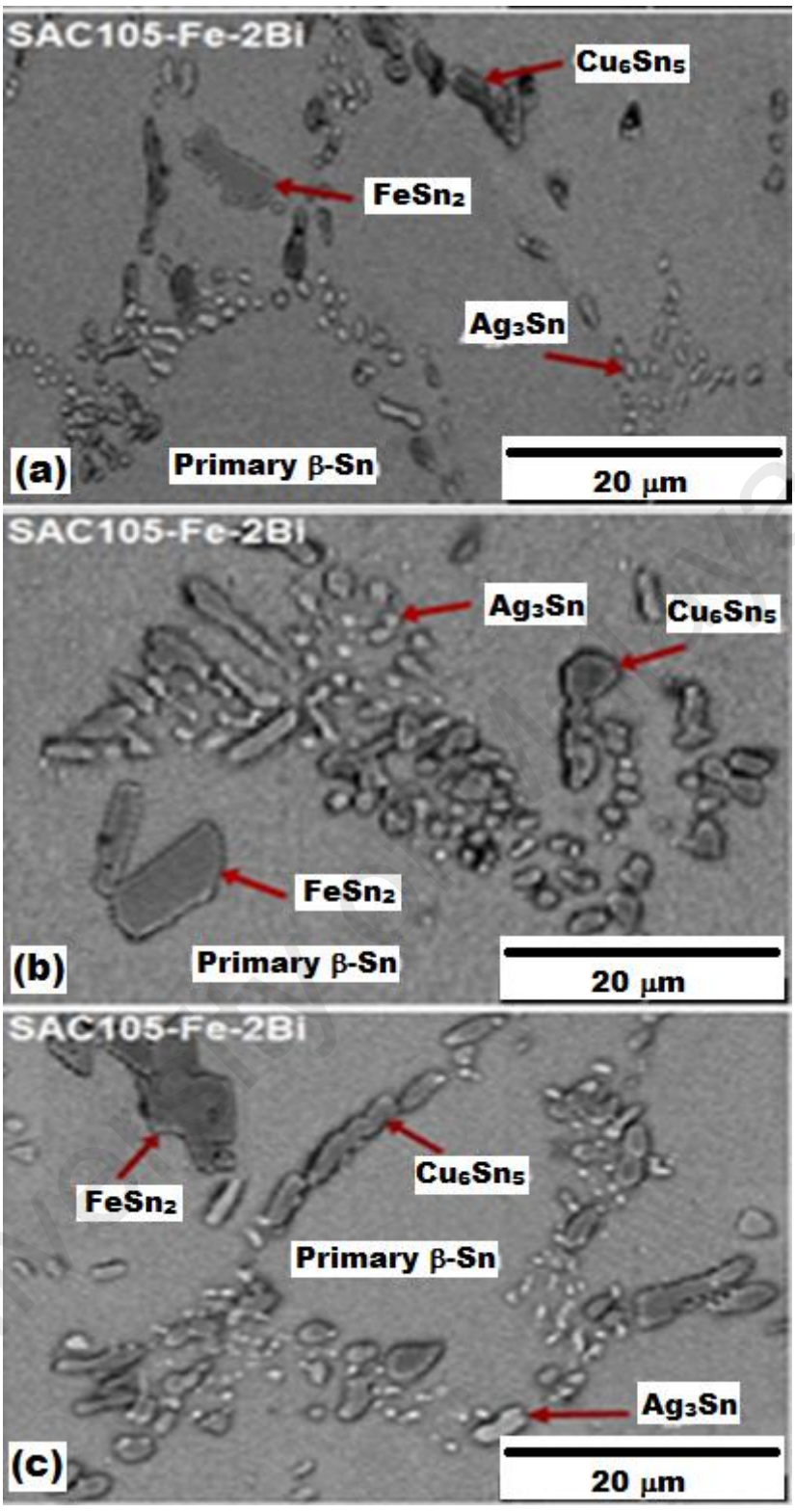

Figure 4.6: FESEM micrographs of SAC105-Fe-2Bi after thermal aging at 200 °C for: (a) 100 h, (b) 200 h, (c) 300 h

in Sn as well as its non-reactivity with Sn (D. A. Shnawah et al., 2012). Furthermore, small amount of Fe is incorporated in Ag_3Sn and Cu_6Sn_5 IMC particles, which reduces the vacancy diffusion rate-a crucial mechanism for IMCs coarsening with aging (D. A. Shnawah et al., 2012). Therefore, the Fe/Bi-bearing SAC105 solder alloys are more resistant to microstructural coarsening, which contributes to their mechanical stability during aging.

4.2 Grains size evaluation

Optical microscopy with crossed polarized light, was used for studying the primary β-Sn grains. Optical microscopy images were taken at 500 × magnification. A representative image for each composition is shown in Figure 4.7, in which grains can be clearly observed. The sizes of the majority of grains were 60-100 μm for SAC105, while with the addition of Fe/Bi to the alloy, the grain sizes reduced to 20-40 μm. This decrease in average grain size can be attributed to the presence of Fe/Bi in the alloy, which serves as additional nucleation sites for the formation of grains and thus decreases the grains size. It is well established theory that a material with smaller grains possesses better strength (Ali, 2015). The grain size and strength has been correlated by the Hall–Petch relationship (Armstrong, 2014). This can be explained as follows: The movement of dislocations results in plastic deformation. Thus, the strength, which is resistance to deformation, can be improved by hindering this dislocation movement, which will impede the onset of plasticity. Reducing the grain size is one of the best ways to improve the strength of the alloy as the smaller grains place more obstacles per unit area to the movement of dislocation. Moreover, (Vianco & Rejent, 1999a) showed that the Bi particles in solder pinned several grain boundaries. Grain boundary pinning would also contribute to the high mechanical strength of the modified solder alloys. The thermal aging caused literally no change in average grains size, as shown in Figure 4.7, due to

being solid-state aging of the same solidified alloys and having no further space to grow, as consistent with the other studies (Ali, 2015).

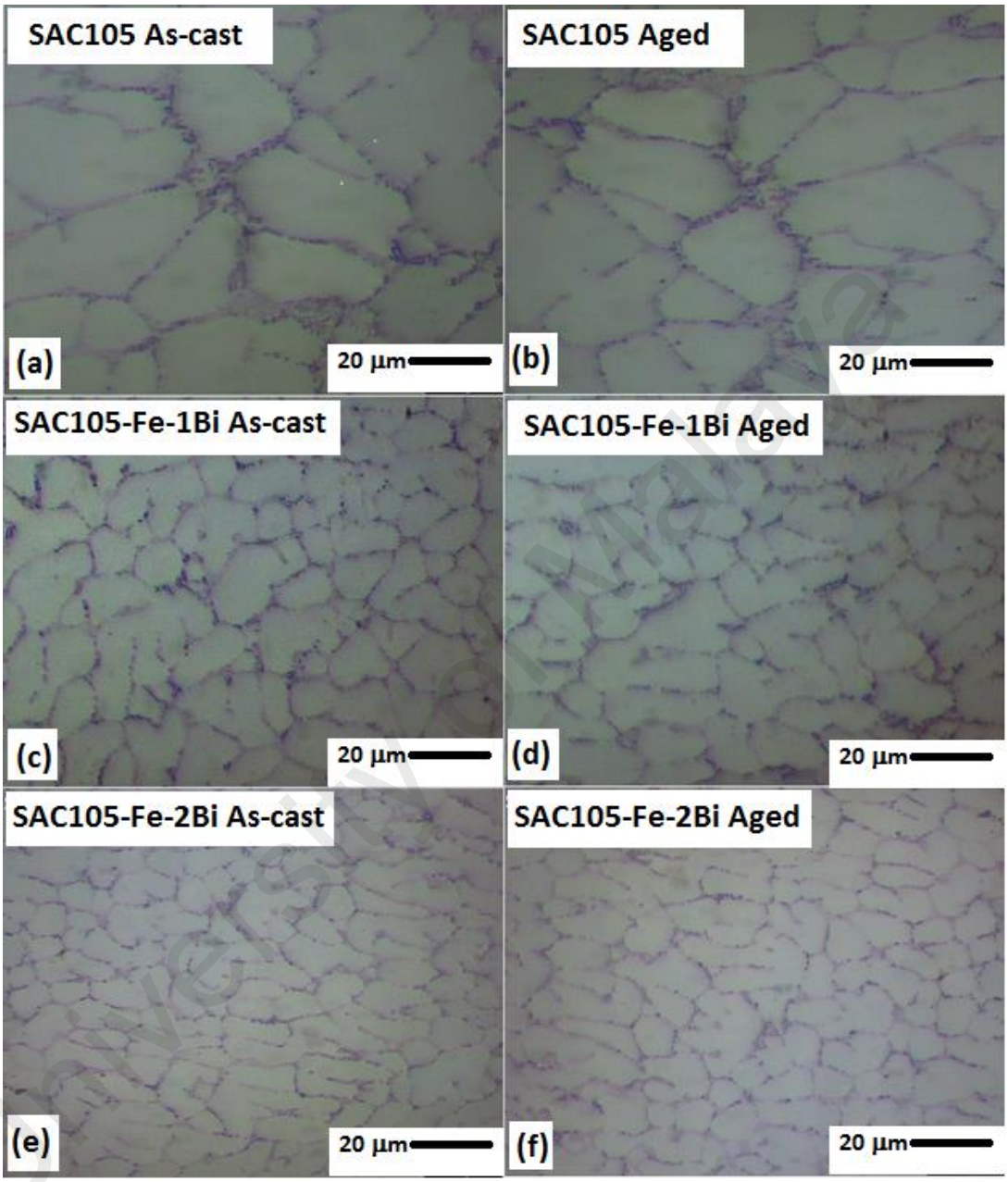

Figure 4.7: Grains size of as-cast samples and thermally aged samples at 200 °C for 300 h: (a) SAC105 as-cast, (b) SAC105 aged, (c) SAC105-Fe-1Bi as-cast, (d) SAC105-Fe-1Bi aged, (e) SAC105-Fe-2Bi as-cast, and (f) SAC105-Fe-2Bi aged

4.3 Quantitative microstructure study

The average particles (IMCs) size was quantitatively measured using ImageJ software. The data obtained is provided in Table 4.1 at 5,000 × image magnification. As seen in the table, the average IMCs size rapidly reduces with the addition of 0.05% Fe and 1% Bi to the base alloy SAC105. Increasing the Bi content in the alloy further reduces its average IMCs size. Table 4.1 also shows the respective circularity and solidity of the IMCs particles for all of the samples (on a one scale). It is observed that these parameters are also slightly improved with the Fe/Bi addition to SAC105 alloys. The circularity is a measure of how close the shape of the particle is to that of a circle. The circularity of a perfect circle is 1.0. Solidity is a measure of how much filled a particle is from inside. The solidity of hollow or porous objects is much less than 1.0. Improvement in both the circularity and solidity of the IMCs particles contributes to the mechanical strength of the alloy. The reduction in IMCs size can be ascribed to the addition of Bi to the alloy, which suppresses the formation of the IMCs phases (Hodúlová et al., 2011). Moreover, the data provided in Table 4.1 also show that the growth rates of these IMCs particles are more controlled for the Fe/Bi added SAC105 alloys under severe thermal aging. Also, the aging less affects the circularity and solidity of Fe/Bi bearing SAC105, as compared to base alloy SAC105. Both Fe and Bi contribute to limiting the growth of IMCs with aging for the Fe/Bi modified alloys (Cai et al., 2012; D. A. Shnawah et al., 2012), which then contributes to the stability in their mechanical properties with aging.

Table 4.1: Effect of thermal aging 200°C on the average IMCs particles size of SAC105, SAC105-Fe-1Bi and SAC105-Fe-2Bi

Aging time (h)	Sample	Count	Total area (pixels)	Average Area (pixels)	Circularity	Solidity
0	SAC105	2506	60514	24.2	0.726	0.764
	SAC105-Fe-1Bi	1850	32364	17.5	0.782	0.783
	SAC105-Fe-2Bi	1258	15913	12.6	0.839	0.792
100	SAC105	1917	72674	37.9	0.683	0.764
	SAC105-Fe-1Bi	1550	38628	26.9	0.765	0.772
	SAC105-Fe-2Bi	1080	19070	17.7	0.812	0.785
200	SAC105	1359	81102	59.6	0.657	0.738
	SAC105-Fe-1Bi	1271	42113	33.1	0.758	0.768
	SAC105-Fe-2Bi	896	22932	25.6	0.794	0.781
300	SAC105	989	86102	87.0	0.623	0.716
	SAC105-Fe-1Bi	917	44107	48.1	0.712	0.762
	SAC105-Fe-2Bi	715	25493	35.7	0.788	0.776

4.4 Tensile Properties

Solder joints behave as the weakest link in electronic packages owing to their relatively lower mechanical properties, as compared to the metalized substrates to which they are connected (Ali, 2015). Thus, the mechanical properties for a solder materials need special attention. Figure 4.8 provides the tensile testing data, i.e. yield stress, ultimate tensile strength (UTS), total percent elongation and percent reduction in area with a maximum relative standard error of 5 %, for all as-cast samples as well as thermally aged samples at 200 °C for 100 h, 200 h and 300 h. Referring to Figure 4.8, for the as-cast SAC105-Fe-

1Bi and SAC105-Fe-2Bi as compared to SAC105, the yield stress increased from 26.8 MPa to 41.7 MPa and 47.5 MPa, UTS increased from 30.9 MPa to 46.7 MPa and 54.5 MPa, while total percent elongation decreased from 60 % to 47 % and 35 %, and percent reduction in area decreased from 81.5 % to 52.5 % and 36.4 %, respectively. It is clear that the yield stress and tensile strength are much better for Fe/Bi-bearing SAC105 and progressively increase with increasing the Bi content in the alloy. This is due to the Bi solid solution strengthening mechanism (Huang & Wang, 2005), where Bi is dissolved in the matrix and strengthens the Sn matrix and ultimately improves the strength. Likewise, the ductility (total elongation and reduction in area) lowers with Fe/Bi addition to the base alloy. This decrease in ductility can be ascribed to the same solid solution strengthening mechanism (Huang & Wang, 2005). The dissolution of Bi in the bulk impedes the dislocation movement, which ultimately lowers the ductility. Shnawah et al. (D. A. Shnawah et al., 2012) reported that Fe addition to SAC105 actually reduces the strength and does not affect the ductility level. Therefore, the improvement in strength and decrease in ductility of the Fe/Bi modified alloys are merely due to the presence of Bi in the alloy.

The higher strength materials generally possess better creep and fatigue resistances than lower strength materials (Ali, 2015). The reason is that creep tests are performed under constant stress, while fatigue tests are performed at a certain cyclic stress. In both of these tests, applied stress is much less than the tensile strength. With an increase in tensile strength, the gap between applied stress and tensile strength increases and thus the creep and fatigue resistances of the material are expected to improve as well. Therefore, it is expected that Fe/Bi addition would also increase the creep and fatigue lives of SAC105 alloy.

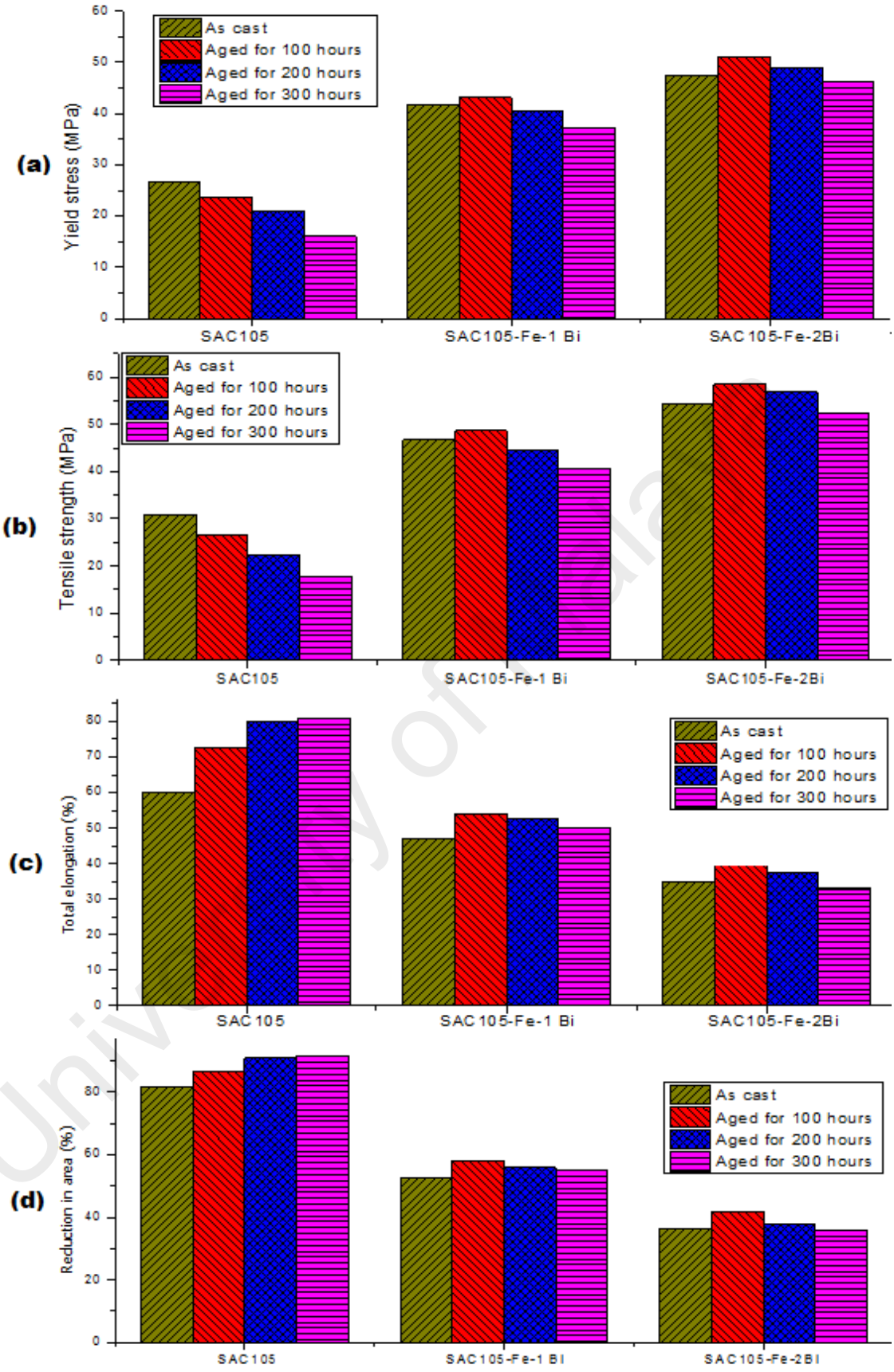

Figure 4.8: Effect of thermal aging at 200 °C of SAC105, SAC105-Fe-1Bi and SAC105-Fe-2Bi on the tensile properties: (a) yield stress, (b) tensile strength, (c) total percent elongation, (d) percent reduction in area

For the base alloy SAC105, as shown in Figure 4.8, with aging at 200 °C, the yield stress and UTS drastically decrease whereas the ductility (total elongation and reduction in area) increases, as compared to the as-cast alloy. Based on the microscopy of the SAC105, it is evident that the decrease in strength and increase in ductility of the alloy after aging is a consequence of particle coarsening with aging. The aging limits the load-sharing contribution of IMCs particles during deformation (Maleki, Cugnoni, & Botsis, 2016). The bigger particles place less obstacles per unit area to the slip of dislocations, resulting in decrease in strength and increase in ductility. These results are consistent with the findings by Shnawah et al. (D. A. Shnawah et al., 2012). For SAC105-Fe-1Bi and SAC105-Fe-2Bi, as shown in Figure 4.8, the tensile properties improve with initial thermal aging and start degrading with further aging. This trend can be explained as follows: The solubility of Bi in Sn increases dramatically with temperature (Cai et al., 2012). The impact is even more significant at higher aging temperatures, which improves the tensile properties with initial aging (Cai et al., 2012). With further aging, the particles' coarsening and degradation of microstructure becomes prominent and the tensile properties start degrading with further aging. After long term aging, Fe/Bi bearing SAC105 solder alloys were found to have much more stable mechanical behaviors than the base alloy SAC105. Witkin (Witkin, 2012) reported that the Bi addition to SAC solder alloys minimizes the loss in strength during aging. Moreover, the Fe addition also stabilizes mechanical properties with the aging (D. A. Shnawah et al., 2012). Thus, this mechanical stability under thermal aging can be attributed to the presence of both Fe and Bi in the Fe/Bi added SAC105 alloys, both of which stabilize the microstructure and thus mechanical properties with aging (Cai et al., 2012; D. A. Shnawah et al., 2012).

4.5 Impact performance

The materials which can absorb greater impact energy during impact tests have better impact reliability and the microstructure is of great importance in influencing the impact toughness of a solder joint (C.-Y. Yu, Lee, Chen, & Duh, 2014). Impact absorbed energy is useful in assessing the impact toughness, which is crucially important for the impact performance of a material. The no-notch Charpy impact test is considered as one of the most effective techniques to investigate the impact reliability of solder materials (N. Zhang, Shi, Guo, & Yang, 2010). Although the Charpy impact test specimens are much larger than the actual soldered interconnections, the strain rate of around 10^2/s is experienced by a solder ball in the board-level drop test, which is close to the strain rate during the Charpy impact test (Kobayashi, Lee, & Subramanian, 2009). Therefore, the Charpy impact test is a good determinant of the actual solder joint impact performance.

Figure 4.9 provides the experimental data of the impact absorbed energy determined during Charpy impact tests for the solder samples under severe thermal aging at 200 °C temperature for 100 h, 200 h and 300 h aging times with the standard deviation error bars. As shown in the Figure 4.9, the as-cast SAC105 base alloy absorbs 8.1 J impact energy in the impact tests. Addition of 0.05% Fe and 1% Bi to SAC105 solder increases its impact absorbed energy to 9.7 J, increasing it by about 20%. With the increase in the Bi-content to 2%, the impact absorbed energy of the alloy does not increase further.

Impact absorbed energy is comprised of crack initiation energy as well as crack propagation energy (N. Zhang et al., 2010). Crack initiation energy is mainly dependent on elastic/plastic deformation behaviors of the alloy until the initiation of crack, while the energy for the propagation of crack depends on the plastic dissipation energy, which originates at the tip of crack, as the crack further propagates. The energy absorbed during impact largely relies on the interfacial cohesive strengths and the plastic deformation

behaviors of the joint during the crack initiation and propagation under high speed impact tests (N. Zhang et al., 2010). Thus, the toughness is also assessed from a combination of material strength and its ductility level and a material with high strength and ductility level possesses high toughness, as represented by area enclosed by the stress-strain curve. Figure 4.10 shows the respective data of tensile strength, yield stress and total percent elongation as well as the toughness modulus, as calculated by using equation (3.1), for the three solder test compositions. As shown the figure, the Fe/Bi-bearing SAC105 solders have better combination of strength and percent elongation (ductility) which improves their impact toughness. To be more specific, the modulus of toughness, as shown in Figure 4.10(d), improves by around 20% and 15%, respectively, for SAC105-Fe-1Bi & SAC105-Fe-2Bi, as compared to SAC105, which is fairly consistent with the respective Charpy testing data.

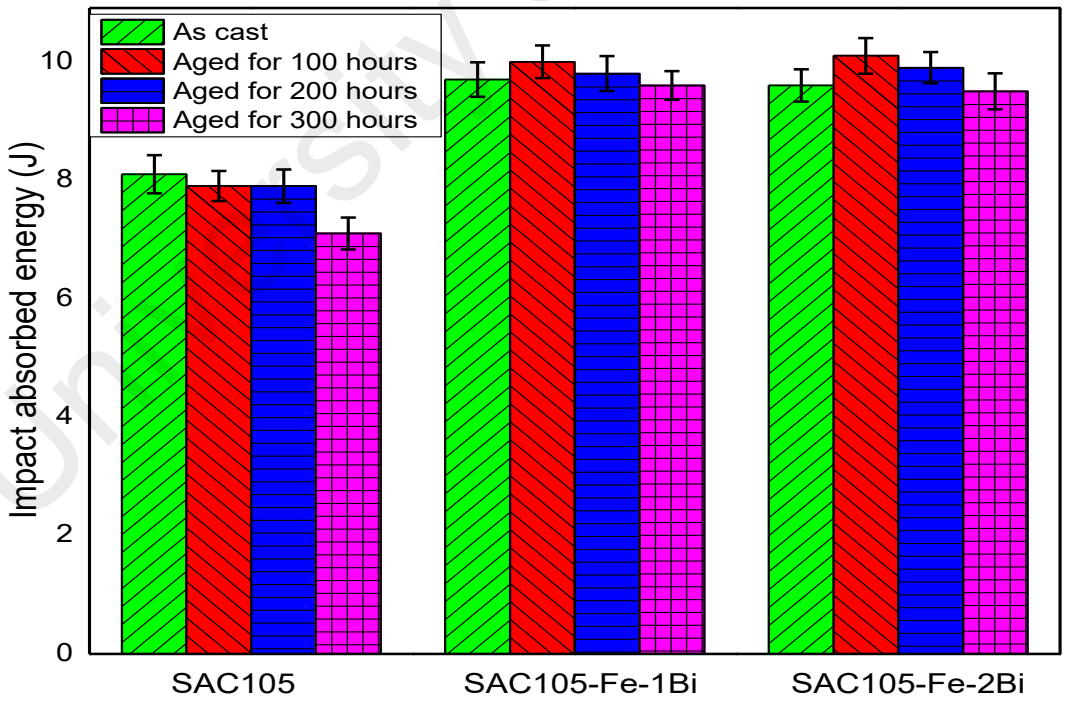

Figure 4.9: Impact absorbed energy of the solder specimens during Charpy impact tests under severe thermal aging at 200 °C

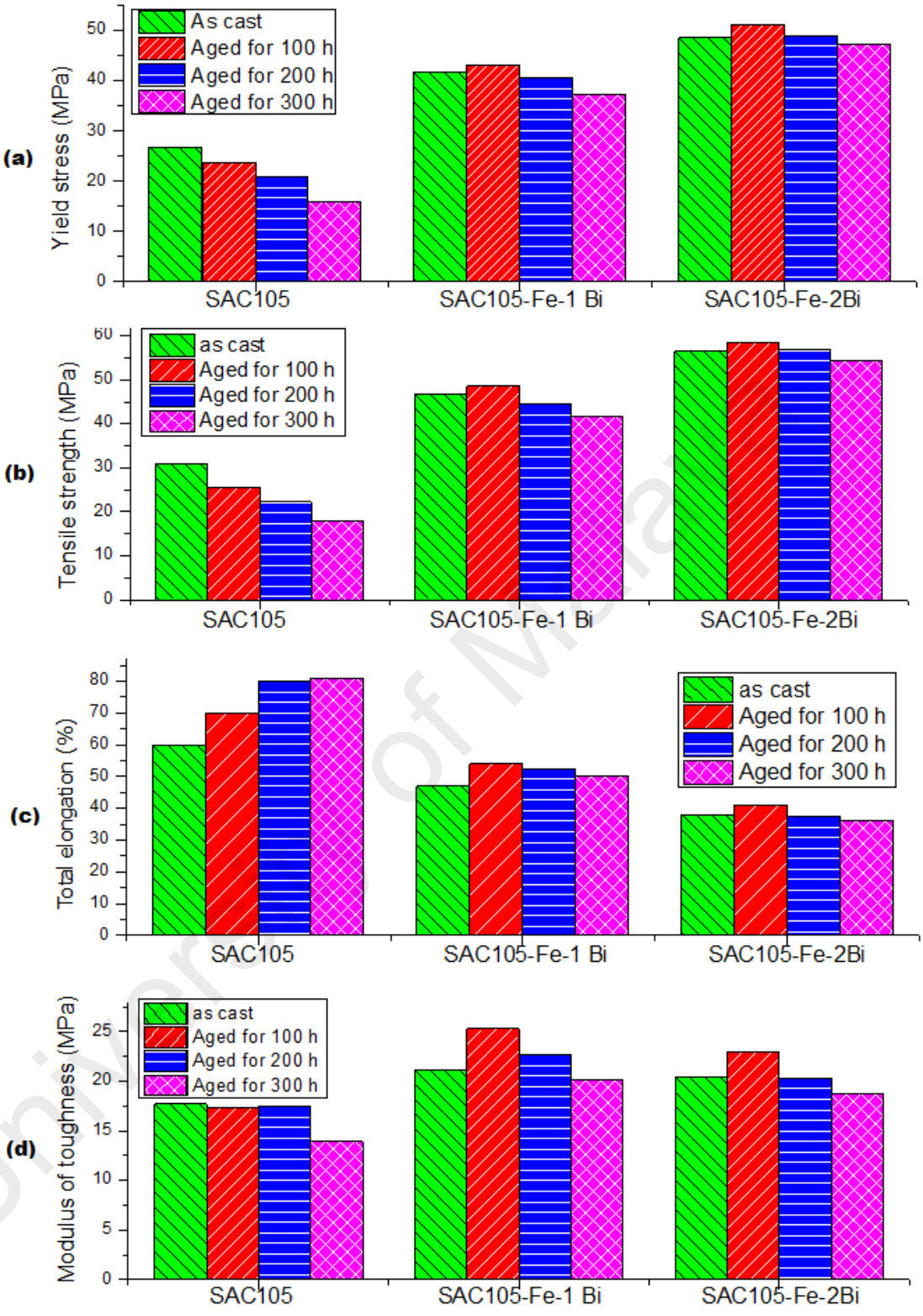

Figure 4.10: Effect of thermal aging at 200 °C of SAC105, SAC105-Fe-1Bi and SAC105-Fe-2Bi on: (a) yield stress, (b) tensile strength, (c) total percent elongation, (d) modulus of toughness

For SAC105, as shown in Figure 4.9, the impact absorbed energy remains nearly at the same level with severe thermal aging at 200 °C for up to 200 h and then drastically lowers with further aging. The tensile testing data, given in Figure 4.10, show consistency with this trend. As seen in the figure, with aging for up to 200 h, the yield stress and tensile strength decrease, while the total elongation (ductility) increases. As a result, the net area under the stress-strain curve would remain almost the same and thus the impact toughness would stay nearly at the same level. With further aging, the strength continues to decrease, whereas the ductility does not increase further, which would result in a decrease in net area under the stress-strain curve and, consequently, the impact toughness would decrease. The modulus of toughness values (Figure 4.10(d)), calculated using equation (3.1), show the same trend and corroborate the Charpy impact tests data for SAC105 under aging. For SAC105-Fe-1Bi and SAC105-Fe-2Bi, as presented in Figure 4.9, with thermal aging for up to 100 h, the impact absorbed energy increases and then progressively decreases with further aging. Yu et al. (C.-Y. Yu et al., 2014) reported that short term annealing at a higher temperature can improve the impact toughness of the solder alloys and ascribed the improvement in impact toughness to the evolution of microstructure of the alloy. The tensile testing data, given in Figure 4.10, show that with aging for 100 h, both the strength and ductility increase, which would increase the net area under the stress-strain curve and, as a result, the impact toughness would increase. With further aging, as shown in the figure, both the strength and ductility progressively degrade and thus the impact toughness would degrade as well. The modulus of toughness values (Figure 4.10(d)), calculated using equation (3.1), demonstrate the same trend and corroborate the Charpy impact tests data under thermal aging for Fe/Bi-bearing solder alloys.

4.6 Microhardness

The microhardness is useful for evaluating the wear and abrasion behavior of a solder material. It also helps in assessing the suitability of a solder alloy for various applications (Xiao Hu, Chan, Zhang, & Yung, 2013). The Vickers hardness (HV) test results, as analyzed via SPSS statistics software, are provided in Figure 4.11 and Table 4.2 for SAC105, SAC105-Fe-1Bi and SAC105-Fe-2Bi solder alloys compositions under high temperature aging at 200 °C for 100 h, 200 h and 300 h. In Figure 4.11, the mean hardness values with respective standard deviation error bars are presented. As shown in the figure, the SAC105 solder has a hardness number of 10.5. The addition of 0.05% Fe and 1% Bi to the base alloy SAC105 raises the hardness number to 18.2. Increasing the Bi content to 2% further increases the hardness number to 22.6. Figure 4.12 shows the indentation sizes left in the samples after removal of indenter during hardness test. It has been observed in the figure that the mean diagonal lengths of the indentation for SAC105-Fe-1Bi and SAC105-Fe-2Bi are about three-fourths and two-thirds of SAC105, respectively. Using equation (3.2), the hardness values, given in Figure 4.11, show consistency with the indentation sizes observed in Figure 4.12. Zhang et al. (P. Zhang, Li, & Zhang, 2011) reported that there is a direct relationship between the hardness and strength of a material. To be able to compare the hardness values of the samples with their corresponding strength values, the hardness in HV was converted to MPa unit using the following conversion relation: I HV = 9.807 MPa (Guillaume, Boschini, Rulmont, Ausloos, & Cloots, 2006). The tensile strength and hardness values for the three test samples are given in Table 4.3. It is clearly seen in the table that the hardness of the samples is in direct relationship with their corresponding strength, which is consistent with the findings by Zhang et al. (P. Zhang et al., 2011). Kamal et al. (Kamal, Gouda, & Marei, 2009) reported that Bi completely dissolves in the Sn matrix and, consequently, increases the hardness value due to its solid solution hardening mechanism.

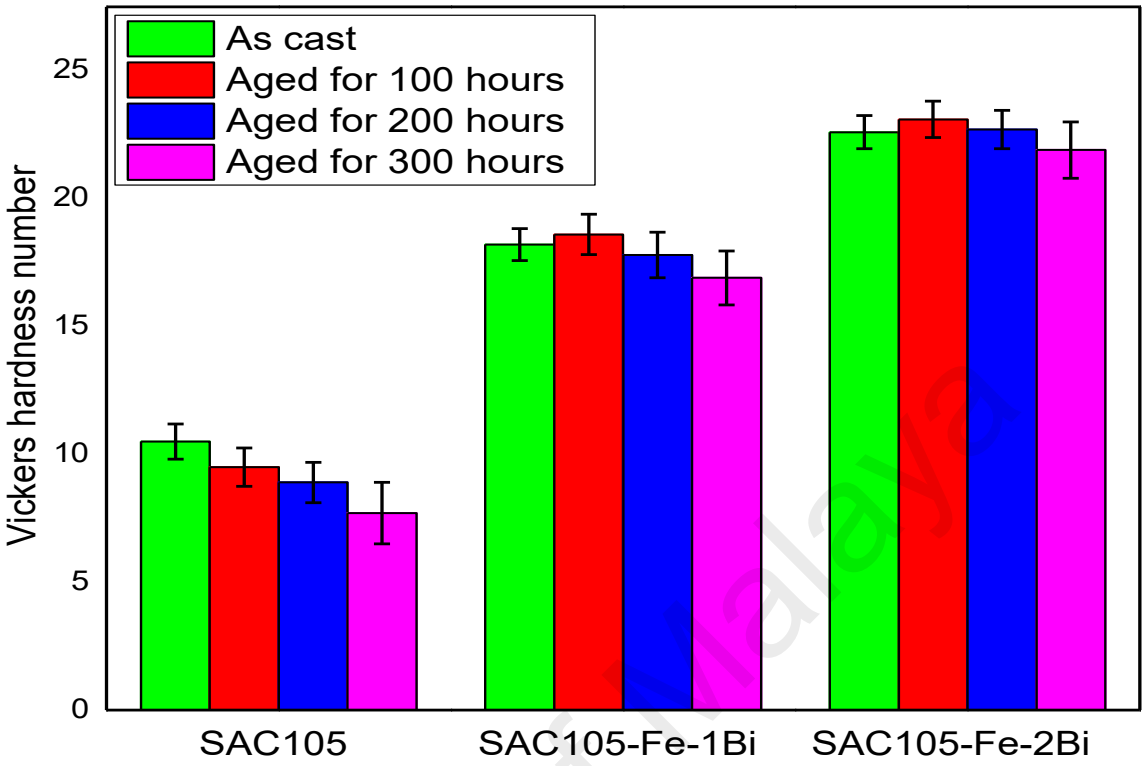

Figure 4.11: Effect of thermal aging at 200 °C on the hardness of SAC105, SAC105-Fe-1Bi and SAC105-Fe-2Bi

Moreover, (D. A.-A. Shnawah, Said, Sabri, Badruddin, & Che, 2012) found that Fe addition to SAC105 lowers the yield and tensile strengths of the alloy while does not affect its ductility level and, thus, softens the alloy and increases its bulk compliance. We can deduce that Fe addition has no contribution to the improvement in hardness of the modified alloy and the improvement in hardness is merely due to the presence of Bi in the alloy.

For the base alloy SAC105, as shown in Figure 4.11, with aging at 200 °C, the hardness progressively decreases, compared to the as-cast alloy i.e. hardness number of SAC105 decreases from 10.5 to 9.5, 8.9 and 7.7 with aging at 200 °C for 100 h, 200 h and 300 h,

respectively. For SAC105-Fe-1Bi, the hardness number first increases from 18.2 to 18.6 with initial aging for up to 100 h and then decreases to 17.8 and 16.9 with further aging

Table 4.2: Two-sample t-test results comparing various tested samples

	Sample	N	DF	t-value(2-tailed)	p-value
As-cast samples	SAC105	15			
	SAC105-Fe-1Bi	15	28	24.329	.00001
	SAC105-Fe-1Bi	15			
	SAC105-Fe-2Bi	15	28	11.927	.00001
SAC105	As-cast	15			
	Aged for 100	15	28	2.948	.00639
	Aged for 100 h	15			
	Aged for 200 h	15	28	1.813	.08057
	Aged for 200 h	15			
	Aged for 300 h	15	28	3.383	.00213
SAC105-Fe-1Bi	As-cast	15			
	Aged for 100 h	15	28	2.041	.05079
	Aged for 100 h	15			
	Aged for 200 h	15	28	3.332	.02430
	Aged for 200 h	15			
	Aged for 300 h	15	28	3.251	.02996
SAC105-Fe-2Bi	As-cast	15			
	Aged for 100 h	15	28	2.109	.04402
	Aged for 100 h	15			
	Aged for 200 h	15	28	2.021	.05294
	Aged for 200 h	15			
	Aged for 300 h	15	28	2.182	.03766

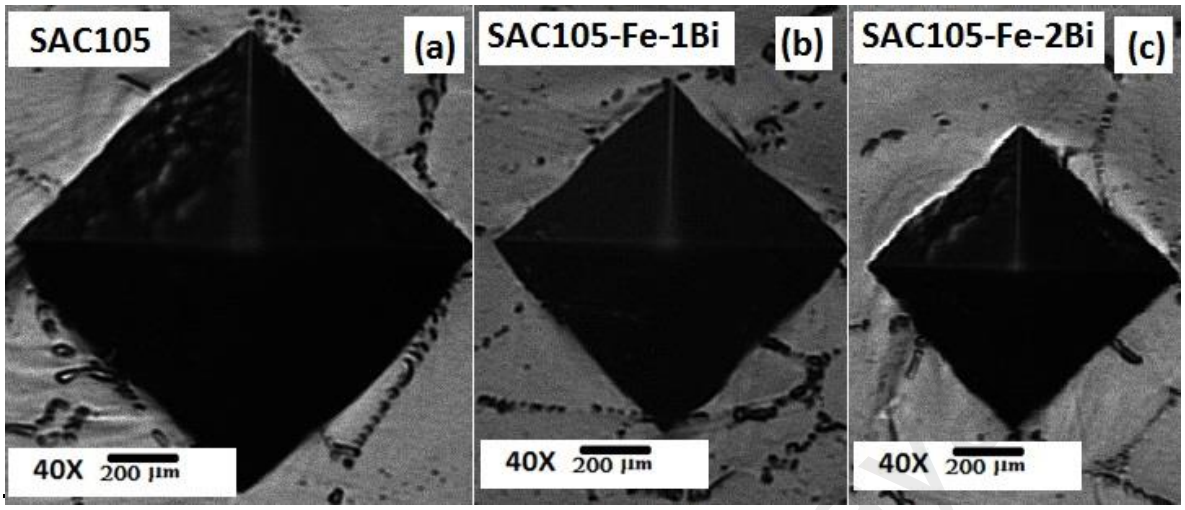

Figure 4.12: The indentations made during Vickers hardness test on the surface of: (a) SAC105, (b) SAC105-Fe-1Bi and (c) SAC105-Fe-2Bi

Table 4.3: Comparison of strength and hardness of SAC105, SAC105-Fe-1Bi and SAC105-Fe-2Bi

Sample	Tensile strength (MPa)	Hardness (MPa)
SAC105	30.879	102.974
SAC105-Fe-1Bi	46.683	178.487
SAC105-Fe-2Bi	56.440	221.638

for 200 h and 300 h, respectively. Likewise, for SAC105-Fe-2Bi, the hardness number increases from 22.6 to 23.1 with initial aging for up to 100 h and then decreases to 22.7 and 21.9 with further aging for 200 h and 300 h, respectively. We can observe that the hardness of SAC105-Fe-1Bi and SAC105-Fe-2Bi improves with initial thermal aging and progressively degrades with further aging.

In Table 4.2, the p-values, obtained via the two-sample t-test, are provided, along with the related statistical terms N (number of test repetitions), DF (degree of freedom) and two-tailed t-values. If the p-value is less than the pre-specified value (.05), we would conclude that means of the two compared samples are statistically significantly different from one another. This analysis is important due to the presence of various phases in the alloys, which may vary the hardness measured at different spots on the surface of the sample. As it can be seen in Table 4.2, the p-values are generally under .05, which implies that the HV data for various evaluated conditions are statistically different from each other. This means that the data points reported for hardness values in this study are the true representatives of the hardness of the three alloys under the mentioned conditions.

4.7 Shear performance

The transition from through-hole technology to surface mount technology increased the importance of shear strength as the solder joint must be able to withstand a shear force because of mechanical shock and thermal stress. The shear strength data for SAC105, SAC105-Fe-1Bi and SAC105-Fe-2Bi solder alloys compositions under high temperature aging at 200 °C for 100 h, 200 h and 300 h, with the respective standard deviation error bars, are provided in Figure 4.13. As shown in the figure, the SAC105 solder has a shear strength of 17.8 MPa. The addition of 0.05% Fe and 1% Bi to the base alloy SAC105 raises the shear strength to 25 MPa. Increasing the Bi content to 2% further increases the shear strength to 34.3 MPa. Liu et al. (Y. Liu, Sun, & Zou, 2011; Yang, Fenglian, & Miaosen, 2013) found that, due to the solid solution strengthening effect of Bi, the shear strength of the SAC solder alloy was improved with the addition of Bi to the alloy. Fallahi et al. (Fallahi, Nurulakmal, Arezodar, & Abdullah, 2012) reported that Sn3.6Ag0.9Cu solder alloy has a shear strength of 29 MPa, while we found in this study that the Fe/Bi modified SAC105 solder has a shear strength of 34.3 MPa. It is clearly seen that the Fe/Bi

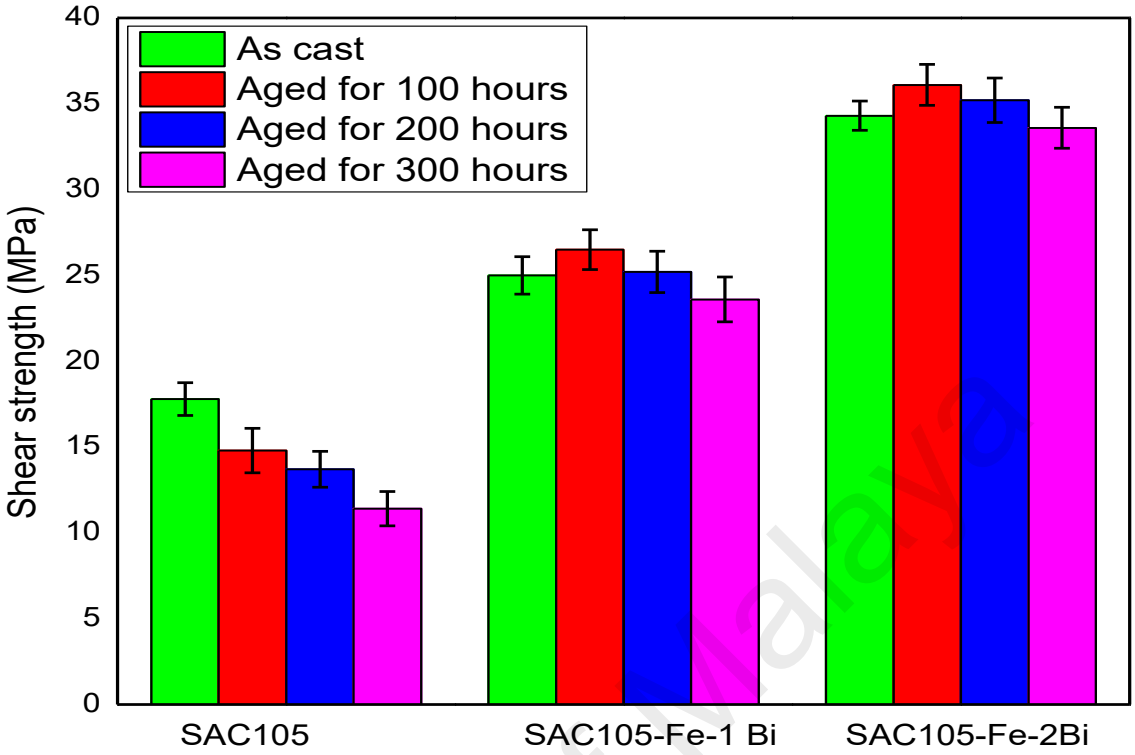

Figure 4.13: Effect of thermal aging at 200 °C on the shear strength of SAC105, SAC105-Fe-1Bi and SAC105-Fe-2Bi

addition to SAC105 can potentially result in an alloy with better shear performance than the high-Ag-content SAC solder alloys. Fallahi et al. (Fallahi et al., 2012) also reported that with the addition of 0.2 wt.% and 0.6 wt.% Fe, the shear strength of Sn3.6Ag0.9Cu increased to 40 MPa and 53 MPa, respectively. This means that Fe element can also effectively improve the shear strength of the SAC solder alloys. Therefore, the increase in shear strength for SAC105-Fe-1Bi and SAC105-Fe-2Bi is a combined effect of Fe and Bi to the alloy, as both contribute to the improvement in shear strength.

For the base alloy SAC105, as shown in Figure 4.13, with aging at 200 °C, the shear strength progressively decreases, compared to the as-cast alloy i.e. shear strength of SAC105 decreases from 17.8 MPa to 14.8 MPa, 13.7 MPa and 11.4 MPa with aging at

200 °C for 100 h, 200 h and 300 h, respectively. For SAC105-Fe-1Bi, the shear strength first increases from 25 MPa to 26.5 MPa with initial aging for up to 100 h and then decreases to 25.2 MPa and 23.6 MPa with further aging for 200 h and 300 h, respectively. Likewise, for SAC105-Fe-2Bi, the shear strength first increases from 34.3 MPa to 36.1 MPa with initial aging for up to 100 h and then decreases to 35.2 MPa and 33.6 MPa with further aging for 200 h and 300 h, respectively. We can observe that the shear strength of SAC105-Fe-1Bi and SAC105-Fe-2Bi improves with initial thermal aging and starts degrading with further aging.

4.8 Cost analysis

In the adoption of lead-free solders, the cost as well as reliability are two important factors for the practical applications. The cost of pure metals according to LME, Bloomberg and Shanghai Metals Market reported on 28th December 2016 are provided in Table 4.4. As shown in the table, the cost of the most popular lead-free solder alloys, namely SAC305 and SAC405 are about 2.5 and 3 times of that of the standard tin/lead (Sn-37Pb) solder alloy, respectively. The market prices for these metals vary in accordance with market trends. These prices impact the entire electronics industry supply chain. In the popular lead-free solders, the cost of silver at present accounts for the largest share of the total cost of raw metals and thus makes the differential in the cost even greater, as compared to Sn-37Pb. However, the cost of low-Ag-content SAC105 is about 1.8 times of that of lead-based Sn-37Pb solder alloy, which significantly reduces the overall cost of the materials. Such low-Ag SAC105 also improves the drop impact reliability of the solder joint and thus prolongs the life of the electronic product. In this study, the overall cost of solder is further reduced with the addition of Fe and Bi to low-Ag SAC105. The addition of Fe and Bi slightly reduces the overall cost of solder by about 1%. At the same time, the mechanical properties as well as the high temperature

performance of the modified solder alloys are better than the high-Ag-content lead-free solders.

Table 4.4: Cost analysis of various solder alloys

Cost/Metal	Sn	Ag	Cu	Fe	Bi	Pb	Raw materials cost, USD/kg
USD/MT	21225	513000	5482	72.25	9705	2185	-
USD/kg	21.225	513	5.482	0.07225	9.705	2.185	-
SAC105* (Wt.%)	20.90 (98.5)	5.13 (1)	0.02 (0.5)	-	-	-	26.05
SAC105-0.05Fe-1Bi* (Wt.%)	20.684 (97.45)	5.13 (1)	0.02 (0.5)	0.00003 (0.05)	0.097 (1)	-	25.93
SAC105-0.05Fe-2Bi* (Wt.%)	20.472 (96.45)	5.13 (1)	0.02 (0.5)	0.00003 (0.05)	0.194 (2)	-	25.82
SAC305 (Wt.%)	20.482 (96.5)	15.39 (3)	0.02 (0.5)	-	-	-	35.91
SAC405 (Wt.%)	20.270 (95.5)	20.52 (4)	0.02 (0.5)	-	-	-	40.81
Sn-37Pb (Wt.%)	13.38 (63)	-	-	-	-	0.80 (37)	14.18

*****Studied in this work

4.9 Summary

The key results of this work are presented in Table 4.5. As it can be seen, the addition of Fe and Bi significantly reduces the average IMCs size and improves the tensile strength, impact toughness, microhardness and shear strength, while reduces the percent elongation (ductility). This is due to the solid solution strengthening mechanism of Bi. The table also shows that severe thermal aging of SAC105 excessively coarsens the IMCs and deteriorates the mechanical properties of the alloy. The addition of Fe and Bi significantly suppresses the IMCs coarsening and degradation of mechanical properties. The presence of both Fe and Bi in the modified alloys contributes to the stability in their microstructure and mechanical properties.

Table 4.5: Summary of the key experimental findings

Aging time (h)	Sample	Average IMCs size (pixels)	Tensile Strength (MPa)	Total elongation (%)	Impact absorbed energy (J)	Microhardness Number	Shear strength (MPa)
0	SAC105	24.2	30.9	60	8.1	10.5	17.8
	SAC105-Fe-1Bi	17.5	46.7	47	9.7	18.2	25.0
	SAC105-Fe-2Bi	12.6	54.4	35	9.6	22.6	34.3
100	SAC105	37.9	26.5	72.5	7.9	9.50	14.8
	SAC105-Fe-1Bi	26.9	48.6	54	10	18.6	26.5
	SAC105-Fe-2Bi	17.7	58.5	41	10.1	23.1	36.1
200	SAC105	59.6	22.2	80	7.9	8.90	13.7
	SAC105-Fe-1Bi	33.1	44.4	52.5	9.8	17.8	25.2
	SAC105-Fe-2Bi	25.6	56.7	37.5	9.9	22.7	35.2
300	SAC105	87.0	17.8	81	7.1	7.70	11.4
	SAC105-Fe-1Bi	48.1	40.6	50	9.6	16.9	23.6
	SAC105-Fe-2Bi	35.7	52.3	33	9.5	21.9	33.6

CHAPTER 5: CONCLUSION AND RECOMMENDATIONS

5.1 Conclusion

An extensive study was carried out to investigate the effect of Fe and Bi addition to SAC105 solder alloy on the microstructure and mechanical properties under severe thermal aging at 200 °C for 100 h, 200 h and 300 h. The following conclusions were drawn:

- Bi is present mostly in the solder bulk and strengthens the alloys by solid solution strengthening mechanism. Bi also suppresses the formation of IMCs (Cu_6Sn_5 and Ag_3Sn) phases, especially Cu_6Sn_5 and refines the microstructure of the alloy. The sizes of both the intermetallic compounds (IMCs) and grains progressively decreases with increasing the Bi content, which contribute to the improvement in mechanical properties of the alloy. Fe makes $FeSn_2$ IMCs, which are very few in number and have no significant effect on the mechanical properties of the alloys.
- The addition of Fe and Bi significantly improves the tensile strength by about 75%, while lowers the percent elongation by about 40%. The impact toughness increases from 8.1 J to 9.7 J by about 20% with the addition of 0.05% Fe and 1% Bi to the base alloy SAC105. Increasing the Bi content from 1 to 2% does not improve the impact toughness further. Likewise, the addition of Fe and Bi to SAC105 increases the hardness of the alloy from 10.5 HV to 22.6 HV showing an increase of more than two fold. Moreover, shear strength almost doubles for the Fe/Bi added SAC105, as compared to the base alloy SAC105, increasing from 17.8 MPa to 34.3 MPa. These improvements in mechanical properties are due to

the Bi solid solution strengthening mechanism and the refinement in microstructure.

- Severe thermal aging of SAC105 progressively leads to excessive coarsening of the eutectic regions and a loss in the definition of the primary β-Sn dendrites. Due to the presence of both Fe and Bi in the alloys, the Fe/Bi-bearing SAC105 experienced far less coarsening of IMCs with severe thermal aging. The inclusion of Fe in the Cu_6Sn_5 and Ag_3Sn IMC particles of Fe/Bi-bearing SAC105 suppresses their IMC coarsening. The addition of Bi also contributes to the coarsening suppression of the microstructure of the alloy due to its solid solution strengthening mechanism. This coarsening suppression of the microstructure, due to the presence of Fe and Bi in the modified alloy, contributes to the stability in their mechanical properties, including the tensile properties, impact toughness, hardness and shear strength, under severe thermal aging.
- Due to having a low-Ag-content in the Fe/Bi-bearing SAC105 solder alloy, the cost of the solder would be significantly lower. At the same time, the reliability of this modified solder would be better than many expensive alternative solder alloys.

5.2 Recommendations

The future recommendations are outlined as follows:

1. The current study evaluates the bulk of solder and we know that solder joints are the most critical points of the printed circuit boards (PCBs). Therefore, the microstructure and mechanical properties of the Fe/Bi-bearing SAC solder joints need to be investigated in future.
2. The effect on Fe/Bi addition on the electrical properties and corrosion behavior of SAC105 needs to be investigated in future.
3. The β-Sn in eutectic SAC solder exhibits anisotropy in its elastic and thermal expansion properties that may induce a significant amount of stress at Sn-grain boundaries during thermal cycling. Therefore, a detailed investigation of failure in solder alloys under thermal cycling is required in future.
4. The electronic products may be subjected to high temperature in electronic industry for several years. Therefore, the long-term high temperature reliability needs to be investigated in future. For that, the thermal aging time may be extended to several months.
5. This current work focuses on the experimental results. Simulation studies can be performed in future to better understand the behavior of the alloy on atomic level.

REFERENCES

Abtew, M., & Selvaduray, G. (2000). Lead-free Solders in Microelectronics. *Materials Science and Engineering: R: Reports, 27*(5–6), 95-141.

Ali, B. (2015). Advancement in microstructure and mechanical properties of lanthanum-doped tin-silver-copper lead free solders by optimizing the lanthanum doping concentration. *Soldering & Surface Mount Technology, 27*(2), 69-75.

Allen, S. L., Notis, M. R., Chromik, R. R., Vinci, R. P. (2004). Microstructural Evolution in Lead-Free Solder Alloys: Part I Cast Sn–Ag–Cu Eutectic. *Journal of Material Research, 19*(5).

Allen, S. L., Notis, M.R., Chromik, R.R., Vinci, R.P. (2004). Microstructural evolution in lead-free solder alloys: Part II. Directionally solidified Sn-Ag-Cu, Sn-Cu and Sn-Ag. *Journal of Materials Research, 19*(5), 1425–1431.

Anderson, I. E., & Harringa, J. L. (2004). Elevated temperature aging of solder joints based on Sn-Ag-Cu: Effects on joint microstructure and shear strength. *Journal of Electronic Materials, 33*(12), 1485-1496.

Anderson, I. E., & Harringa, J. L. (2006). Suppression of void coalescence in thermal aging of tin-silver-copper-X solder joints. *Journal of Electronic Materials, 35*(1), 94-106.

Armstrong, R. W. (2014). Engineering science aspects of the Hall–Petch relation. *Acta Mechanica, 225*(4), 1013-1028.

Beyer, H., Sivasubramaniam, V., Hajas, D., Nanser, E., & Brem, F. (2014, 20-22 May 2014). *Reliability Improvement of Large Area Soldering Connections by Antimony Containing Lead-Free Solder.* Paper presented at the PCIM Europe 2014; International Exhibition and Conference for Power Electronics, Intelligent Motion, Renewable Energy and Energy Management.

Braun, T., Becker, K. F., Koch, M., Bader, V., Aschenbrenner, R., & Reichl, H. (2006). High-temperature reliability of Flip Chip assemblies. *Microelectronics Reliability, 46*(1), 144-154.

C-Mac-Technology. (2010). Product data sheet. www.cmac.com, accessed on April 2010.

Cai, Z., Suhling, J. C., Lall, P., & Bozack, M. J. (2012, May 30 2012-June 1 2012). *Mitigation of lead free solder aging effects using doped SAC-X alloys.* Paper presented at 13th IEEE Intersociety Conference.on the Thermal and Thermomechanical Phenomena in Electronic Systems (ITherm), 2012.

Callister. (1985). *Materials Science and Engineering: An Introduction, Wiley, New York.*

Chen, S.-W., Chen, C.-C., Gierlotka, W., Zi, A.-R., Chen, P.-Y., & Wu, H.-J. (2008). Phase Equilibria of the Sn-Sb Binary System. *Journal of Electronic Materials, 37*(7), 992-1002.

Chen, S.-w., Zi, A.-r., Chen, P.-y., Wu, H.-j., Chen, Y.-k., & Wang, C.-h. (2008). Interfacial reactions in the Sn–Sb/Ag and Sn–Sb/Cu couples. *Materials Chemistry and Physics, 111*(1), 17-19.

Chen, W. M., Kang, S. K., & Kao, C. R. (2012, May 29 2012-June 1 2012). *Systematic investigation of Sn-Ag and Sn-Cu modified by minor alloying element of titanium.* Paper presented at the 2012 IEEE 62nd Electronic Components and Technology Conference, 2012.

Choudhury, S. F., & Ladani, L. (2015). Single Crystal Plasticity Finite Element Analysis of Cu6Sn5 Intermetallic. *Metallurgical and Materials Transactions A, 46*(3), 1108-1118.

Chuang, C.-M., & Lin, K.-L. (2003). Effect of microelements addition on the interfacial reaction between Sn-Ag-Cu solders and the Cu substrate. *Journal of Electronic Materials, 32*(12), 1426-1431.

Chuang, T.-H., & Lin, H.-J. (2008). Inhibition of Whisker Growth on the Surface of Sn-3Ag-0.5Cu-0.5Ce Solder Alloyed with Zn. *Journal of Electronic Materials, 38*(3), 420.

Dutta, I., Kumar, P., & Subbarayan, G. (2009). Microstructural coarsening in Sn-Ag-based solders and its effects on mechanical properties. *JOM, 61*(6), 29-38.

Dutta, I., Park, C., & Choi, S. (2004). Impression creep characterization of rapidly cooled Sn–3.5Ag solders. *Materials Science and Engineering: A, 379*(1–2), 401-410.

El-Daly, A. A., Fawzy, A., Mansour, S. F., & Younis, M. J. (2013). Novel SiC nanoparticles-containing Sn–1.0Ag–0.5Cu solder with good drop impact performance. *Materials Science and Engineering: A, 578*, 62-71.

El-Daly, A. A., Fawzy, A., Mohamad, A. Z., & El-Taher, A. M. (2011). Microstructural evolution and tensile properties of Sn–5Sb solder alloy containing small amount of Ag and Cu. *Journal of Alloys and Compounds, 509*(13), 4574-4582.

El-Daly, A. A., Swilem, Y., & Hammad, A. E. (2009). Creep properties of Sn–Sb based lead-free solder alloys. *Journal of Alloys and Compounds, 471*(1–2), 98-104.

Fallahi, H., Nurulakmal, M. S., Arezodar, A. F., & Abdullah, J. (2012). Effect of iron and indium on IMC formation and mechanical properties of lead-free solder. *Materials Science and Engineering: A, 553*, 22-31.

Fawzy, A. (2007). Effect of Zn addition, strain rate and deformation temperature on the tensile properties of Sn–3.3 wt.% Ag solder alloy. *Materials Characterization, 58*(4), 323-331.

Fix, A. R., López, G. A., Brauer, I., Nüchter, W., & Mittemeijer, E. J. (2005). Microstructural development of Sn-Ag-Cu solder joints. *Journal of Electronic Materials, 34*(2), 137-142.

Fix, A. R., Nüchter, W., & Wilde, J. (2008). Microstructural changes of lead-free solder joints during long-term ageing, thermal cycling and vibration fatigue. *Soldering & Surface Mount Technology, 20*(1), 13-21.

Gao, F., Takemoto, T., Nishikawa, H., & Komatsu, A. (2006). Microstructure and mechanical properties evolution of intermetallics between Cu and Sn-3.5Ag solder doped by Ni-Co additives. *Journal of Electronic Materials, 35*(5), 905-911.

Geranmayeh, A. R., Mahmudi, R., & Kangooie, M. (2011). High-temperature shear strength of lead-free Sn–Sb–Ag/Al2O3 composite solder. *Materials Science and Engineering: A, 528*(12), 3967-3972.

Gibson, A. W., Choi, S. L., Subramanian, K. N., Bieler, T. R. . (1997). Issues regarding microstructural coarsening due to aging of eutectic tin-silver solder. *Proceedings of the TMS Annual Meeting - Orlando, FL, USA*, 97- 103.

Guillaume, B., Boschini, F., Rulmont, A., Ausloos, M., & Cloots, R. (2006). Influence of the shaping effect on hardness homogeneity by Vickers indentation analysis. *Journal of the European Ceramic Society, 26*(15), 3191-3196.

Hammad, A. E., El-Daly, A. A, Swilem, Y. (2008). Influences Of Ag And Au Additions On Structure And Tensile Strength Of Sn-5Sb Lead Free Solder Alloy. *JOURNAL OF MATERIALS SCIENCE \& TECHNOLOGY, 24*, 921-925.

Harry Schoeller, S. B., Aaron Knobloch, David Shaddock, Junghyun Cho. (2008). Effects of Microstructure Evolution on High-Temperature Mechanical Deformation of 95Sn-5Sb. *ASME International Mechanical Engineering Congress and Exposition*, 25-32.

Hodúlová, E., Palcut, M., Lechovič, E., Šimeková, B., & Ulrich, K. (2011). Kinetics of intermetallic phase formation at the interface of Sn–Ag–Cu–X (X = Bi, In) solders with Cu substrate. *Journal of Alloys and Compounds, 509*(25), 7052-7059.

Hu, X., Chan, Y. C., Zhang, K., & Yung, K. C. (2013). Effect of graphene doping on microstructural and mechanical properties of Sn–8Zn–3Bi solder joints together with electromigration analysis. *Journal of Alloys and Compounds, 580*, 162-171.

Hu, X., Li, Y., Liu, Y., & Min, Z. (2015). Developments of high strength Bi-containing Sn0.7Cu lead-free solder alloys prepared by directional solidification. *Journal of Alloys and Compounds, 625*, 241-250.

Huang, M. L., & Wang, L. (2005). Effects of Cu, Bi, and In on microstructure and tensile properties of Sn-Ag-X(Cu, Bi, In) solders. *Metallurgical and Materials Transactions A, 36*(6), 1439-1446.

Intel-Corporation. (2010). Product data sheet. www.intel.com, accessed on April 2010.

Jee-Hwan Bae, K. S., Joon-Hwan Lee, Mi-Yang Kim, Cheol-Woong Yang. (2015). Development of High-Temperature Solders: Contribution of Transmission Electron Microscopy. *Applied Microscopy, 45*, 89-94.

Jong Hoon Kim, S. W. J., Hyuck Mo Lee. (2002). Thermodynamics-Aided Alloy Design and Evaluation of Pb-free Solders for High-Temperature Applications. *Materials Transactions, 43*(8), 1873-1878.

Juergen Wolf, M., Engelmann, G., Dietrich, L., & Reichl, H. (2006). Flip chip bumping technology—Status and update. *Nuclear Instruments and Methods in Physics Research Section A: Accelerators, Spectrometers, Detectors and Associated Equipment, 565*(1), 290-295.

Kamal, M., Gouda, E. S., & Marei, L. K. (2009). Effect of Bi-content on hardness and micro-creep behavior of Sn-3.5Ag rapidly solidified alloy. *Crystal Research and Technology, 44*(12), 1308-1312.

Kang, N., Na, H. S., Kim, S. J., & Kang, C. Y. (2009). Alloy design of Zn–Al–Cu solder for ultra high temperatures. *Journal of Alloys and Compounds, 467*(1–2), 246-250.

Kariya, Y., Hosoi, T., Terashima, S., Tanaka, M., & Otsuka, M. (2004). Effect of silver content on the shear fatigue properties of Sn-Ag-Cu flip-chip interconnects. *Journal of Electronic Materials, 33*(4), 321-328.

Kim, D., Suh, D., Millard, T., Kim, H., Kumar, C., Zhu, M., & Xu, Y. (2007, May 29 2007-June 1 2007). *Evaluation of High Compliant Low Ag Solder Alloys on OSP as a Drop Solution for the 2nd Level Pb-Free Interconnection.* Paper presented at the 57th Electronic Components and Technology Conference, 2007.

Kim, H., Zhang, M., Kumar, C. M., Suh, D., Liu, P., Kim, D., . . . Wang, Z. (2007, May 29 2007-June 1 2007). *Improved Drop Reliability Performance with Lead Free Solders of Low Ag Content and Their Failure Modes.* Paper presented at the 2007 57th Electronic Components and Technology Conference, 2007.

Kim, K. S., Huh, S. H., & Suganuma, K. (2002). Effects of cooling speed on microstructure and tensile properties of Sn–Ag–Cu alloys. *Materials Science and Engineering: A, 333*(1–2), 106-114.

Kim, K. S., Huh, S. H., & Suganuma, K. (2003). Effects of fourth alloying additive on microstructures and tensile properties of Sn–Ag–Cu alloy and joints with Cu. *Microelectronics Reliability, 43*(2), 259-267.

Kim, S., Kim, K.-S., Kim, S.-S., Suganuma, K., & Izuta, G. (2009). Improving the Reliability of Si Die Attachment with Zn-Sn-Based High-Temperature Pb-Free Solder Using a TiN Diffusion Barrier. *Journal of Electronic Materials, 38*(12), 2668.

Kobayashi, T., Lee, A., & Subramanian, K. N. (2009). Impact Behavior of Thermomechanically Fatigued Sn-Based Solder Joints. *Journal of Electronic Materials, 38*(12), 2659-2667.

Lee, C., Lin, C.-Y., & Yen, Y.-W. (2007). The 260 °C phase equilibria of the Sn–Sb–Cu ternary system and interfacial reactions at the Sn–Sb/Cu joints. *Intermetallics, 15*(8), 1027-1037.

Lee, Y. W., Kim, I. H., Kim, E. S., Lee, J. H., & Moon, J. T. (2010, 8-10 Dec. 2010). *Improvement of wettability and drop impact reliability by Al addition in SnAgCu solder.* Paper presented at the 12th Electronics Packaging Technology Conference, 2010.

Li, B., Shi, Y., Lei, Y., Guo, F., Xia, Z., & Zong, B. (2005). Effect of rare earth element addition on the microstructure of Sn-Ag-Cu solder joint. *Journal of Electronic Materials, 34*(3), 217-224.

Li, G.-y., & Shi, X.-q. (2006). Effects of bismuth on growth of intermetallic compounds in Sn-Ag-Cu Pb-free solder joints. *Transactions of Nonferrous Metals Society of China, 16*, s739-s743.

Lifshitz, I. M., & Slyozov, V. V. (1961). The kinetics of precipitation from supersaturated solid solutions. *Journal of Physics and Chemistry of Solids, 19*(1), 35-50.

Lin, L.-W., Song, J.-M., Lai, Y.-S., Chiu, Y.-T., Lee, N.-C., & Uan, J.-Y. (2009). Alloying modification of Sn–Ag–Cu solders by manganese and titanium. *Microelectronics Reliability, 49*(3), 235-241.

Liu, C.-Y., Hon, M.-H., Wang, M.-C., Chen, Y.-R., Chang, K.-M., & Li, W.-L. (2014). Effects of aging time on the mechanical properties of Sn–9Zn–1.5Ag–xBi lead-free solder alloys. *Journal of Alloys and Compounds, 582*, 229-235.

Liu, Y., Sun, F., & Zou, P. (2011, 25-28 Oct. 2011). *Shear strength and interfacial microstructures of low-Ag SAC/Cu and SAC-Bi-Ni/Cu solder joints.* Paper presented at the International Symposium on Advanced Packaging Materials (APM), 2011.

Liu, Y., Sun, F. L., Yan, T. L., & Hu, W. G. (2008, 28-31 July 2008). *Effects of Bi and Ni addition on wettability and melting point of Sn-0.3Ag-0.7Cu Low-Ag Pb-free solder.* Paper presented at the 2008 International Conference on Electronic Packaging Technology & High Density Packaging.

Ma, H., & Suhling, J. C. (2009). A review of mechanical properties of lead-free solders for electronic packaging. *Journal of Materials Science, 44*(5), 1141-1158.

Mahmudi, R., Geranmayeh, A. R., Bakherad, M., & Allami, M. (2007). Indentation creep study of lead-free Sn–5%Sb solder alloy. *Materials Science and Engineering: A, 457*(1–2), 173-179.

Maleki, M., Cugnoni, J., & Botsis, J. (2016). Multi-scale modeling of elasto-plastic response of SnAgCu lead-free solder alloys at different ageing conditions: Effect of microstructure evolution, particle size effects and interfacial failure. *Materials Science and Engineering: A, 661*, 132-144.

McCormack, M., Jin, S., Kammlott, G. W., & Chen, H. S. (1993). New Pb-free solder alloy with superior mechanical properties. *Applied Physics Letters, 63*(1), 15-17.

Miller, C. M., Anderson, I. E., & Smith, J. F. (1994). A viable tin-lead solder substitute: Sn-Ag-Cu. *Journal of Electronic Materials, 23*(7), 595-601.

Ogunseitan, O. A. (2007). Public Health and Environmental Benefits of Adopting Lead-Free Solders. *JOM, 59*(7), 12-17.

Palomar-Technologies. (2010). Product data sheet. www.palomar.com, accessed on April, 2010.

Pei, M., & Qu, J. (2008). Effect of Lanthanum Doping on the Microstructure of Tin-Silver Solder Alloys. *Journal of Electronic Materials, 37*(3), 331-338.

Ratke, L., Voorhees, Peter W. (2002). Growth and Coarsening. *Engineering materials*.

Rettenmayr, M., Lambracht, P., Kempf, B., & Graff, M. (2005). High Melting Pb-Free Solder Alloys for Die-Attach Applications. *Advanced Engineering Materials, 7*(10), 965-969.

Sadiq, M., Pesci, R., & Cherkaoui, M. (2013). Impact of Thermal Aging on the Microstructure Evolution and Mechanical Properties of Lanthanum-Doped Tin-Silver-Copper Lead-Free Solders. *Journal of Electronic Materials, 42*(3), 492-501.

Senkov, O. N., & Myshlyaev, M. M. (1986). Grain growth in a superplastic Zn-22% Al alloy. *Acta Metallurgica, 34*(1), 97-106.

Seo, S.-K., Kang, S. K., Shih, D.-Y., & Lee, H. M. (2009). The evolution of microstructure and microhardness of Sn–Ag and Sn–Cu solders during high temperature aging. *Microelectronics Reliability, 49*(3), 288-295.

Shalaby, R. M. (2009). Influence of indium addition on structure, mechanical, thermal and electrical properties of tin–antimony based metallic alloys quenched from melt. *Journal of Alloys and Compounds, 480*(2), 334-339.

Shen, J., Pu, Y., Yin, H., Luo, D., & Chen, J. (2014). Effects of minor Cu and Zn additions on the thermal, microstructure and tensile properties of Sn–Bi-based solder alloys. *Journal of Alloys and Compounds, 614*, 63-70.

Shih, P.-C., & Lin, K.-L. (2006). Interfacial microstructure and shear behavior of Sn–Ag–Cu solder balls joined with Sn–Zn–Bi paste. *Journal of Alloys and Compounds, 422*(1–2), 153-163.

Shnawah, D. A.-A., Said, S. B. M., Sabri, M. F. M., Badruddin, I. A., & Che, F. X. (2012). Novel Fe-containing Sn–1Ag–0.5Cu lead-free solder alloy with further enhanced elastic compliance and plastic energy dissipation ability for mobile products. *Microelectronics Reliability, 52*(11), 2701-2708.

Shnawah, D. A., Sabri, M. F. M., Badruddin, I. A., Said, S. B. M., Ariga, T., & Che, F. X. (2012). Effect of Ag Content and the Minor Alloying Element Fe on the Mechanical Properties and Microstructural Stability of Sn-Ag-Cu Solder Alloy Under High-Temperature Annealing. *Journal of Electronic Materials, 42*(3), 470-484.

Shnawah, D. A., Sabri, M. F. M., Badruddin, I. A., Said, S. B. M., Bashir, M. B. A., Sharif, N. M., & Elsheikh, M. H. (2015). Study on coarsening of Ag3Sn

intermetallic compound in the Fe-modified Sn–1Ag–0.5Cu solder alloys. *Journal of Alloys and Compounds, 622*, 184-188.

Song, H. Y., Zhu, Q. S., Wang, Z. G., Shang, J. K., & Lu, M. (2010). Effects of Zn addition on microstructure and tensile properties of Sn–1Ag–0.5Cu alloy. *Materials Science and Engineering: A, 527*(6), 1343-1350.

Song, J.-M., Wu, Z.-M., & Huang, D.-A. (2007). Two-stage nonequilibrium eutectic transformation in a Sn–3.5Ag–3In solder. *Scripta Materialia, 56*(5), 413-416.

Suganuma, K., Kim, S.-J., & Kim, K.-S. (2009). High-temperature lead-free solders: Properties and possibilities. *JOM, 61*(1), 64-71.

Suh, D., Kim, D. W., Liu, P., Kim, H., Weninger, J. A., Kumar, C. M., . . . Tejada, H. B. (2007). Effects of Ag content on fracture resistance of Sn–Ag–Cu lead-free solders under high-strain rate conditions. *Materials Science and Engineering: A, 460–461*, 595-603.

Syed, A., Kim, T. S., Cho, Y. M., Kim, C. W., & Yoo, M. (2006, 6-8 Dec. 2006). *Alloying effect of Ni, Co, and Sb in SAC solder for improved drop performance of chip scale packages with Cu OSP pad finish.* Paper presented at the 8th Electronics Packaging Technology Conference, 2006.

Terashima, S., Kariya, Y., Hosoi, T., & Tanaka, M. (2003). Effect of silver content on thermal fatigue life of Sn-xAg-0.5Cu flip-chip interconnects. *Journal of Electronic Materials, 32*(12), 1527-1533.

Tu, K. N., Gusak, A. M., & Li, M. (2003). Physics and materials challenges for lead-free solders. *Journal of Applied Physics, 93*(3), 1335-1353.

Vianco, P. T., & Rejent, J. A. (1999a). Properties of ternary Sn-Ag-Bi solder alloys: Part I—Thermal properties and microstructural analysis. *Journal of Electronic Materials, 28*(10), 1127-1137.

Vianco, P. T., & Rejent, J. A. (1999b). Properties of ternary Sn-Ag-Bi solder alloys: Part II—Wettability and mechanical properties analyses. *Journal of Electronic Materials, 28*(10), 1138-1143.

Wang, F.-J., Gao, F., Ma, X., & Qian, Y.-Y. (2006). Depressing effect of 0.2wt.%Zn addition into Sn-3.0Ag-0.5Cu solder alloy on the intermetallic growth with Cu substrate during isothermal aging. *Journal of Electronic Materials, 35*(10), 1818-1824.

Wang, H., Fang, J., Xu, Z., & Zhang, X. (2015). Improvement of Ga and Zn alloyed Sn–0.7Cu solder alloys and joints. *Journal of Materials Science: Materials in Electronics, 26*(6), 3589-3595.

Weiping, L., Bachorik, P., & Ning-Cheng, L. (2008, 4-6 Nov. 2008). *The superior drop test performance of SAC-Ti solders and its mechanism.* Paper presented at the 33rd IEEE/CPMT International Electronics Manufacturing Technology Conference (IEMT), 2008.

Witkin, D. B. (2012). Influence of microstructure on quasi-static and dynamic mechanical properties of bismuth-containing lead-free solder alloys. *Materials Science and Engineering: A, 532*, 212-220.

Wu, C. M. L., Yu, D. Q., Law, C. M. T., & Wang, L. (2002). Microstructure and mechanical properties of new lead-free Sn-Cu-RE solder alloys. *Journal of Electronic Materials, 31*(9), 928-932.

Wu, C. M. L., Yu, D. Q., Law, C. M. T., & Wang, L. (2004). Properties of lead-free solder alloys with rare earth element additions. *Materials Science and Engineering: R: Reports, 44*(1), 1-44.

Yamada, Y., Takaku, Y., Yagi, Y., Nishibe, Y., Ohnuma, I., Sutou, Y., . . . Ishida, K. (2006). Pb-free high temperature solders for power device packaging. *Microelectronics Reliability, 46*(9), 1932-1937.

Yang, L., Fenglian, S., & Miaosen, Y. (2013, 11-14 Aug. 2013). *Shear strength and brittle failure of low-Ag SAC-Bi-Ni solder joints during ball shear test.* Paper presented at the14th International Conference on Electronic Packaging Technology (ICEPT), 2013.

Yu, A. M., Kim, J.-K., Lee, J.-H., & Kim, M.-S. (2010). Pd-doped Sn–Ag–Cu–In solder material for high drop/shock reliability. *Materials Research Bulletin, 45*(3), 359-361.

Yu, C.-Y., Lee, J., Chen, W.-L., & Duh, J.-G. (2014). Enhancement of the impact toughness in Sn–Ag–Cu/Cu solder joints via modifying the microstructure of solder alloy. *Materials Letters, 119*, 20-23.

Zhang, N., Shi, Y., Guo, F., & Yang, F. (2010). Study of the Impact Performance of Solder Joints by High-Velocity Impact Tests. *Journal of Electronic Materials, 39*(12), 2536-2543.

Zhang, P., Li, S. X., & Zhang, Z. F. (2011). General relationship between strength and hardness. *Materials Science and Engineering: A, 529*, 62-73.

LIST OF PUBLICATIONS

1. Bakhtiar Ali, Mohd Faizul Mohd Sabri, Iswadi Jauhari, Nazatul Liana Sukiman, (2016). Impact toughness, hardness and shear strength of Fe and Bi added Sn-1Ag-0.5Cu lead-free solders. *Microelectronics Reliability,* Vol. 63, pp. 224-230.

2. Bakhtiar Ali, Mohd Faizul Mohd Sabri, & Iswadi Jauhari, (2016). Microstructural behavior of iron and bismuth added Sn-1Ag-Cu solder under elevated temperature aging. *AIP Conference Proceedings*, *1756*(1), 030002 doi: 10.1063/1.4958754.

3. Bakhtiar Ali, Mohd Faizul Mohd Sabri, Nazatul Liana Sukiman, Iswadi Jauhari, (2017). Microhardness and shear performance of Fe/Bi-bearing SAC105 solder alloys under high temperature aging. *Journal of Materials Science: Materials in Electronics*, Vol. 28, pp. 197-206.

4. Bakhtiar Ali, Mohd Faizul Mohd Sabri, Suhana Mohd Said, Nazatul Liana Sukiman, Iswadi Jauhari, Norhayati Soin, (2017). High impact reliability and high temperature performance of Fe and Bi added Sn-1Ag-0.5Cu solder alloys. *Journal of Materials Science: Materials in Electronics*, Vol. 28, pp. 7277-7285.

5. Bakhtiar Ali, Mohd Faizul Mohd Sabri, Suhana Mohd Said, Mohammad Hossein Mahdavifard, Nazatul Liana Sukiman, Iswadi Jauhari, (2017). Microstructural modification of Sn-0.7Cu solder alloys by Fe/Bi-addition for achieving high mechanical performance. *Journal of Electronic Materials*, Vol. 46, pp. 4755-4764.

6. Bakhtiar Ali, Mohd Faizul Mohd Sabri, Suhana Mohd Said, Nazatul Liana Sukiman, Iswadi Jauhari, (2017). Effect of high temperature aging on the microstructural and mechanical properties of Fe and Bi added Sn-1Ag-0.5Cu lead-free solder alloy. *Microelectronics Reliability* (submitted)

7. Book Chapter
   Mohd Faizul Mohd Sabri, Bakhtiar Ali, Suhana Mohd Said, High Temperature Lead-free Solder Materials and Applications, In Interconnect Materials for Harsh Environments and High Temperature. IGI Global, 2017 (Submitted)